Mechanistic Investigations in Ultrasound-Assisted Food Processing

A
Thesis
Submitted in
Fulfillment of the
Requirements for the Degree of

DOCTOR OF PHILOSOPHY

Amit H. Batghare

DEPARTMENT OF CHEMICAL ENGINEERING
Indian Institute of Technology Guwahati
Guwahati – 781 039, Assam, India

June 2020

Dedicated

to

My Parents,

My Lovely Wife Trupti

and Son Nirmit

INDIAN INSTITUTE OF TECHNOLOGY GUWAHATI

DEPARTMENT OF CHEMICAL ENGINEERING

STATEMENT

I do hereby declare that the content embodied in this thesis entitled "**MECHANISTIC INVESTIGATIONS IN ULTRASOUND-ASSISTED FOOD PROCESSING**" is the result of investigations carried out by me at Department of Chemical Engineering, Indian Institute of Technology Guwahati, Guwahati, India, under the guidance of Prof. Vijayanand S. Moholkar.

In keeping with the general practice of reporting scientific observations, due acknowledgements have been made wherever the work described is based on the findings of other investigators.

June 2020

Amit H. Batghare

(Roll No.: 146107019)

INDIAN INSTITUTE OF TECHNOLOGY GUWAHATI

DEPARTMENT OF CHEMICAL ENGINEERING

CERTIFICATE

It is certify that the work contained in the thesis entitled "**MECHANISTIC INVESTIGATIONS IN ULTRASOUND-ASSISTED FOOD PROCESSING**", by **Amit H. Batghare** (Roll No: 146107019), has been carried out under my supervision and that this work has not been submitted elsewhere for a degree

June 2020

Prof. Vijayanand S. Moholkar
Professor
Department of Chemical Engineering
Indian Institute of Technology, Guwahati
Guwahati – 781 039
Assam, India

ACKNOWLEDGEMENTS

I owe my deepest gratitude to all those who made this thesis possible. The first and foremost appreciation goes to my thesis supervisor **Prof. Vijayanand S. Moholkar** for his valuable suggestions, encouragement and constant support throughout my research work. He has been a true source of inspiration and spending his precious time for discussion by which I have gained immense skill of knowledge in terms of research.

I would like to acknowledge my sincere gratitude to my doctoral committee members, Prof. Ramgopal Uppaluri, Prof. Chandan Das, and Dr. S. Senthilkumar (Department of Biosciences and Bioengineering) for their insightful advices and suggestions throughput the research.

I am thankful to the Chemical Engineering Department and also to the faculty members for their constant support. The kind and constant help of the staff members of Department of Chemical Engineering, IIT Guwahati. I am also thankful to the **Indian Institute of Technology Guwahati** for providing me with the state of the art infrastructure for advance level of research.

I am thankful to my seniors Dr. Shuchi Singh, Dr. Sankar Chakma, Dr. Maneesh Poddar and Dr. Pritam Dikshit for their valuable guidance. I also extend my thanks to my colleagues and friends, Dr. Jaykumar, Dr. Shyamali, Kuldeep, Bhaskar, Niharika, Neha, Philip, Kajal, Udangshree, Abhik, Dr. Saptak, Dr. Rahul, Karan, Kaustubh, for their constant help and enthusiastic company.

Finally, yet importantly, I would like to express my heartfelt thanks to GOD, my wife Mrs. Trupti Batghare and son Nirmit for their support, care and encouragement. At last but not the least, I am highly indebted to my parents for all the sacrifices they made for my better future and giving me freedom to take my own decision. My Ph.D. endeavor could not be completed without their endless love and blessing.

ABSTRACT

This thesis has addressed important fundamental issues in ultrasound-assisted food processing of liquid systems. An attempt has been made for intensification of product yield by application of sonication to the conventional food processing techniques. Three food processes, viz. extraction (astaxanthin from *Phaffia rhodozyma*), fermentation (riboflavin from *Debaryomyces hansenii var. hansenii*) and crystallization (lactose monohydrate) were studied in this thesis work. Previous literature has already reported beneficial action of ultrasound on these processes for increasing product yield or faster kinetics. However, the missing link was the physical mechanism of the process, i.e. the connections between basic mechanics of the process and physics of sonication. An attempt has been made in this thesis to fulfill this research gap with basic approach of coupling experimental results to simulations. The results of this thesis research have shed light on intricate links between physics of ultrasound and cavitation, and the physics of the basic process. A peculiar feature of this thesis is that in all studies, the natural strains and isolates of microbial strains have been used. This is in view of their stability and sturdiness in open natural environment. An important outcome of this thesis is the strong influence of mass transfer on the process. Thus, the key to intensification of these processes is enhancement mass transfer characteristics of the system. Looking at the prevalent mechanics for all processes that has become evident from this thesis; the physical effects of sonication – i.e. generation of intense microconvection - are relevant for enhancing efficiencies of food processes. This microconvection is able to enhance mass transfer in microscale systems (bacterial cultures or lactose crystals etc.), which is manifested in terms of faster kinetics with higher yield. A key revelation of the thesis (which has not been reported in previous literature) is the intra-cell influence of sonication in terms of overexpressions of genes corresponding to different enzymes in metabolic pathway. This effect is underlying the enhanced productivity of natural isolates of bacterial cultures – at par with genetically modified strains.

Keywords: Astaxanthin extraction, Riboflavin fermentation, Lactose crystallization, Ultrasonication

CONTENTS

LIST OF TABLES

LIST OF FIGURES

Chapter 4

Chapter 5

Nomenclature

Acronyms

AcaT	Acetoacetyl Co-A thiolase
ADE12	Adenylosuccinate synthase
AMP	Adenosine monophosphate
ARP	5-Amino-6-ribitylamino-2, 4 (1H, 3H)-pyrimidine
DBP	4-Dihydroxy-2-butanone-4-phosphate
DCW	Dry cell weight
DMAPP	Dimethylallyl pyrophosphate
DMRL	6, 7-Dimethyl-8-ribityllumazine
DMSO	Dimethyl sulphoxide
DRTP	2, 5-Diamino-6-ribosylamino-4 (3H)-pyrimidinedione 5-phosphate
DSC	Differential scanning calorimetry
FE-SEM	Field emission scanning electron microscope
FPP	Farnesyl-diphosphate
FSC	Forward scatter
GMP	Guanosine monophosphate
GPP	Geranyl diphosphate
GTP	Guanosine triphosphate
HMG	3-Hydroxy-3-methylglutaryl-CoA
HmgR	HMG-CoA reductase
HmgS	HMG-CoA synthase
HPLC	High performance liquid chromatography

IMP	Inosine monophosphate
IPP	Isopentenyl pyrophosphate
MS	Mean of squares
MS	Mechanical shaking
MSMPR	Mixed suspension mixed product removal
MTCC	Microbial type culture collection
NADPH	Nicotinamide adenine dinucleotide phosphate hydrogen
ODE	Ordinary differential equation
Ribu-5P	Ribulose-5-phosphate
SDS-PAGE	Sodium dodecyl sulfate polyacrylamide gel electrophoresis
SS	Sum of squares
SSC	Side scatter
UNIFAC	Universal Quasi-Chemical Functional-Group Activity Coefficients
US	Ultrasound
XMP	Xanthosine monophosphate

Parametric symbols

B	Nucleation rate
C_S	Substrate concentration
C_X	Biomass concentration
c	Sonic speed in bulk liquid

Nomenclature

ΔC_p	Specific heat difference between liquid and solid
dR/dt	Velocity of bubble wall
f_{pure2}^{L}	Fugacity of pure (subcooled) liquid 2 at system temperature
G	Crystal growth rate
Δh_f	Enthalpy of fusion
kDa	Kilo dalton
K_S	Monod saturation constant
L	Crystal size or length
n	Crystal population density
n_o	Nuclei population density
N	Total number of crystals
P_0	Ambient or static pressure in bulk liquid
$P(t)$	Time variant pressure of the acoustic wave
$p(R,t)$	Pressure inside the cavitation bubble
$P_s(r,t)$	Pressure amplitude of the shock waves
R	Radius of the bubble at any time
r	Distance from bubble centre
T_m	Melting temperature of pure substance 2
T	Temperature of the system
$u(r,t)$	Velocity of the microturbulence

Greek symbols

γ_2	Activity coefficient of solute
ρ	Density of bulk liquid
μ	Viscosity of the bulk liquid
μ_{max}	Maximum specific growth rate
σ	Surface tension of bulk liquid

Introduction and Literature Review

1.1 INTRODUCTION

Food is a basic requirement of our body to generate energy, to repair and build cells, and to prevent against the sickness and heal from it. Food can be categorized based on plant or animal origin. When food is consumed inside the body, it gets converted to energy by oxygen and the waste product remained is carbon dioxide which is then breathed out. A balanced diet helps to maintain strength and fitness which promotes to have a healthy immune system which helps to fight against infections.

$$\text{Food} + O_2 \longrightarrow \text{Energy} + CO_2$$

Food security concerns have grown in recent years due to the rise in food prices and world food demand. According to United Nations population prospects, the population will grow from 6.9 billion (2010) to 9.3 billion (2050) which is a 35% rise

and nearly all population growth is forecast to occur in developing countries (United Nations, 2011). The World Bank estimates an increase of global economy at average annual rate of 2.9% from 2005 to 2050 and it also shows substantial increase in the shares by developing countries from 20% (2005) to 55% (2050) (van der Mensbrugghe et al., 2009). According to Food and Agricultural Organization (FAO), the global food demand may rise by 77% (higher than in 2007) by 2050 in concurrence with the rising consumer incomes (Linehan et al., 2012). In accordance with the rise in population, agricultural food production has to increase at an annual rate of 0.8%.

Food can be classified based on shelf life, nutrients and, extent and purpose of processing (Amit et al., 2017). Based on shelf life, they can be classified as perishable, semi-perishable and non-perishable (Doyle, 2009). Based on nutrients, they can be classified as carbohydrate rich foods, fat rich foods, protein rich foods and, vitamins and mineral rich foods. Based on extent and purpose of processing, they can be classified as, unprocessed foods, processed foods and ultra-processed food products (Carlos et al., 2010). Food or food products are seasonal and also they undergo spoilage due to chemical, physical or microbial actions. Therefore, they are required to be preserved (in terms of quality) for a longer time so that they can be available throughout the year (Amit et al., 2017). To avoid spoilage, various food processing techniques being used to maintain food quality in terms of shelf life, nutritional values, flavor, texture and color.

1.2 CLASSIFICATION OF FOOD PROCESSING TECHNIQUES

Food processing techniques can be broadly classified as: chemical processing, biological processing and physical processing. Chemical processing techniques

involves the addition of chemical preservatives and controlled pH method. Biological processing involves fermentation of carbohydrates to value added products. Physical processing involves various thermal and non-thermal processing techniques (Ohlsson and Bengtsson, 2002; Karel and Lund, 2003; Drake et al., 2008). Chemical processing techniques are being used with the addition of chemical preservatives or food additives (Michael et al., 2005). They help to increase the shelf life of food products by retarding the degradation caused by the micro-organisms. However, use of these chemical compounds may cause serious health issues. The use of chemical preservatives may cause asthma, gastric irritation, diarrhea, nausea, skin rashes, cancer, migraines and many more. Biological or fermentation process uses micro-organisms which decomposes carbohydrates into value added products. Fermentation enriches nutritional value and converts food into digestible form. This process is a healthy alternative over chemical processes which involve toxic preservatives (Lewin, 2012). Physical processes involve cutting, emulsification/homogenization, sterilization/pasteurization, meat tenderization, degassing, drying, extraction, freezing, crystallization, oxidation, thawing, filtration, brining, etc. (Tao and Sun, 2015).

These conventional food processing techniques have disadvantages such as more processing time, lower shelf life, low quality and high energy requirements (Chemat et al., 2011). Various novel food processing techniques have emerged due to the modernization of society as the consumers became more health conscious and they need good quality food products (Jasim et al., 2009). Novel food processing techniques involves high hyperbaric treatment, pulsed electric field, commercial cool-plasma, ultrasonics, magnetic fields, ultraviolet and microwave heating (Vanga et al., 2017).

The present thesis is focused on the application of one of the modern

technique of ultrasound to the conventional food processing techniques of extraction, fermentation and crystallization. Extraction is a two step process viz. breakage of cells with the application of physical and/or chemical method and use of organic solvent to leach out the product. Fermentation is a method of breakage of carbohydrates into simpler and more digestible form with the use of micro-organisms. Crystallization is a two step process viz. generation of nuclei in the magma and its growth into crystals. The details of these studies can be seen from the later sections of this thesis.

1.3 FOOD PROCESSES OF PRESENT THESIS RESEARCH

The present thesis has addressed the fundamental issues of establishing the physical mechanism of ultrasound-assisted food processing. The basics of ultrasound, its physical and chemical effects can be obtained in greater details in the later sections of this thesis. As mentioned in the earlier section, food processing is a broad umbrella but in this thesis research three food processes have been addressed viz. extraction, fermentation and crystallization. Three model systems (one of each) have been selected to observe the effect of ultrasound towards the intensification of these food processes viz. extraction of astaxanthin (nutraceutical) from yeast *Phaffia rhodozyma*, fermentative production of riboflavin (vitamin B_2) using yeast *Debaryomyces hansenii var. hansenii* and crystallization of lactose monohydrate.

1.3.1 ASTAXANTHIN

Astaxanthin (3,3'−dihydroxy−β,β'−carotene−4,4'−ketone) is a versatile nutraceutical (or carotene pigment) having widespread application ranging from animal nutrition to human health. Astaxanthin has been widely used in aquaculture industry for pigmentation of salmon, trout and shrimps. It is also used as antioxidant

in pharmaceutical industry (Bhosale and Bernstein 2005). In addition, astaxanthin finds applications in cosmetics and food industry for its skin care and anti−aging properties and fortification of foods or beverages (Nakano et al., 1995; Mayne, 1996). Large scale production of astaxanthin is based on chemical synthesis. The conventional chemical routes to astaxanthin manufacture include: (1) Wittig reaction of two equivalents of C_{15} phosphonium salt with a central C_{10}−dialdehyde, or (2) hydroxylation of canthaxanthin, and (3) isomerization of lutein (extract product of marigold) to zeaxanthin followed by oxidation to astaxanthin. The natural producers of astaxanthin include the microalga *Haematococcus pluvialis* and the red−pigmented heterobasidiomycetous yeast *Xanthophyllomyces dendrorhous*, which is also known as *Phaffia rhodozyma* (Barredo et al., 2017). The yeast *Phaffia rhodozyma* contains around 90% of astaxanthin out of total carotenoids content in it. However, production of astaxanthin from *Phaffia rhodozyma* fermentation suffers from low productivity and yield, as compared to chemical synthesis route, and this has been the hurdle in commercial implementation of this process. Genetically improved strains, which show high yields in laboratory scale experiments, suffer from instability in large scale systems (Xiao et al., 2015). Astaxanthin yield can be improved by two ways viz. (a) Optimization of nutrient sources (fermentation media) and fermentation/process parameters and (b) use of proper cell disruption technique to extract majority of astaxanthin formed within the cells.

1.3.1.1 Astaxanthin biosynthetic pathway in *Phaffia rhodozyma*

Figure 1.1 shows astaxanthin biosynthetic pathway from *Phaffia rhodozyma (Xanthophyllomyces dendrorhous)* containing glucose as a carbon source (Hara et al., 2014). The pathway consists of four parts viz. mevalonate synthesis, terpene

synthesis, *β*-carotene synthesis and astaxanthin synthesis. Mevalonate synthesis pathway utilizes acetyl Co-A (which is formed by glycolysis of glucose) to form mevalonic acid which is a primary precursor in the metabolic pathway. The mevalonic acid was utilized to produce terpenes through the formation of carbon building blocks isopentenyl pyrophosphate (IPP) and dimethylallyl pyrophosphate (DMAPP) which are utilized to develop isoprenoids. Terpene synthesis pathway produces farnesyl-diphosphate (FPP) by utilization of geranyl diphosphate (GPP). *β*-carotene synthesis pathway utilizes FPP to produce geranylgeranyl-diphosphate (GGPP) with the secretion of *β*-carotene synthetic pathway gene (*crtE*) to produce *β*-carotene. Finally astaxanthin is formed from *β*-carotene by astaxanthin synthetic pathway gene (*crtS*).

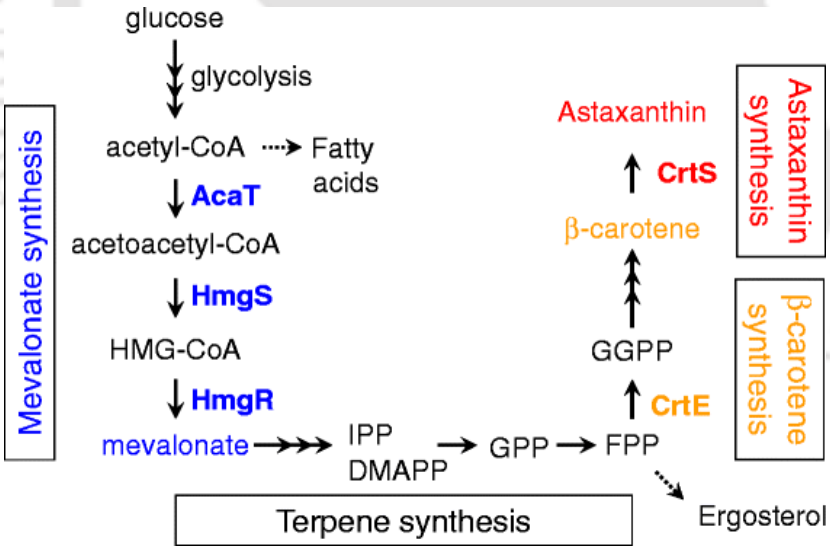

Figure 1.1: Astaxanthin biosynthetic pathway in *Phaffia rhodozyma* (Adopted from Hara et al., 2014). Abbreviations: AcaT, acetoacetyl Co-A thiolase; HMG, 3-hydroxy-3-methylglutaryl-CoA; HmgS, HMG-CoA synthase; HmgR, HMG-CoA reductase.

1.3.1.2 Methods of cell disruption and extraction of astaxanthin

The microbial cells of *Phaffia rhodozyma* have a rigid cell wall, which creates difficulties in extraction of total content formed within the cells (Lim et al., 2002). Astaxanthin production from micro-organisms not only depends on fermentation conditions (medium composition and process parameters) but also it greatly depends on the extent of cell disruption and extraction using various chemical, mechanical and enzymatic techniques or a combination of two or more.

Mechanical techniques include abrasion with celite, abrasion with glass pearls, supercritical fluid extraction, immersion in liquid nitrogen, ultrasound treatment and microwave assisted extraction. In abrasion with celite, the cells were triturated with celite using pestle in a mortar and solvent was added after a specified time to extract astaxanthin (da Fonseca et al., 2011; Michelon et al., 2012). The astaxanthin yield from this method is lowest compared to other techniques of cell disruption which can be viewed from Table 1.1. Another similar method to this is abrasion with glass pearls (Medeiros et al., 2008; da Fonseca et al., 2011; Michelon et al., 2012). In this method, cells along with glass pearls and solvent were put in a vortex agitator and agitated for some time. The astaxanthin content was recovered as a supernatant after centrifugation. The net yield of astaxanthin form this method was much more compared to that obtained using celite. Supercritical fluid extraction is another technique in which supercritical fluids such as CO_2 was used directly as a solvent to extract the extractant (here astaxanthin). Extraction conditions used are above critical temperature of 31°C and pressure above 74 bar (Lim et al., 2002). This method is rarely used due to the involvement of high temperature and pressure conditions which may degrade the astaxanthin formed within the cells. In immersion in liquid nitrogen technique (Michelon et al., 2012), the cells were added to a solvent and the mixture

was placed in liquid nitrogen. The frozen mixture was then macerated using a pestle in a mortar for 1-2 min, centrifuged and supernatant containing astaxanthin was collected. Ultrasonic techniques being used greatly as an emerging technique in extraction of value added products such as astaxanthin (Medeiros et al., 2008; da Fonseca et al., 2011; Michelon et al., 2012; Bhatt et al., 2013; Gogate and Nadar, 2015). Ultrasound of different power, pressure amplitude and frequency was used to disrupt the cells with or without the addition of external cell disrupting agent. Broken cells was then added by solvent and agitated thoroughly which were then centrifuged to get astaxanthin as a supernatant. Microwave assisted extraction technique was used by Choi et al. (2007). The yeast culture suspension was treated with microwave to destroy the cell wall (by optimizing microwave operation conditions) and then they are dried and extracted using a solvent. This method does not look that much feasible though astaxanthin content was more as high temperature of microwave may degrade the astaxanthin formed within the cells.

Chemical techniques of cell disruption involve use of chemicals such as DMSO (dimethyl sulphoxide), sodium bicarbonate or acid treatments. DMSO method was first used by Sedmak et al. (1990) to disrupt *Phaffia rhodozyma* cells. But it was then used consistently by many authors (Persike et al., 2002; Cannizzaro et al., 2003; Hu et al., 2006; Zheng et al., 2006; Ni et al., 2007; Liu et al., 2008; Ni et al., 2008; Liu and Wu, 2008; Wang and Yu, 2009; Bhatt et al, 2013; Xie et al., 2014; Gogate and Nadar, 2015; Xiao et al., 2015; Pan et al., 2017; Schewe et al., 2017) as it binds properly to the cell and penetrates inside the cell by breaking the rigid cell wall. A standing time has to be provided so as to get near to complete cell breakage after addition. DMSO method generally uses hot DMSO (temperature between 50-60°C) as it gives faster cell breakage compared to room temperature conditions. Another rarely

used chemical method for cell disruption is by using sodium bicarbonate (Sabaj, 1979; da Fonseca et al., 2011; Michelon et al., 2012). Sodium bicarbonate was added to the cells and the mixture was kept in a bath at 40-45°C for around one day which was then centrifuged and astaxanthin was recovered. This method was used for other yeasts but was not as effective for *Phaffia rhodozyma* due to the rigidity of cell wall. Acid treatment was also used effectively in disruption of *Phaffia rhodozyma* cells (Ni et al., 2008; Michelon et al., 2012). Acids generally used in this method are hydrochloric acid, lactic acid or acetic acid. The cell biomass was mixed with acid solution and the mixture was agitated in a bath (maintained at a temperature slightly higher than room temperature) which was then centrifuged and astaxanthin was recovered. Few authors have also applied combination of two or more techniques such as sonication with DMSO treatment or acid treatment with sonication or lactic acid treatment with sonication (Gogate and Nadar, 2015). Enzymatic technique was also used but the major drawback of this technique is the activity of the lysing enzymes. Once an enzyme loses its activity it will be no more of use and the cost of commercial enzymes is not economically feasible. A sodium acetate buffer (with acidic pH) and enzyme was added to the *Phaffia rhodozyma* cells so as to match the initial activity of enzyme (Bjerkeng et al., 2007; Michelon et al., 2012). The mixture was then incubated at 50-60°C for half an hour, centrifuged and astaxanthin was recovered.

1.3.1.3 Importance of fermentation conditions in intracellular astaxanthin accumulation

Fermentation conditions (media and process parameters) plays a dominating role over extraction techniques as extraction techniques are useful to extract the

amount of astaxanthin formed within the cells but to increase intracellular astaxanthin content, a proper or optimized fermentation conditions are required. Mutant strains may give high astaxanthin yield but they are less stable compared to wild strains so if the fermentation conditions are optimized it can give a comparable yield as that from mutant strains. Carbon and nitrogen sources play a major role in the metabolic pathway towards synthesis of a desired product. Also an optimized ratio of carbon to nitrogen (C/N) helps to accumulate more intracellular astaxanthin (Pan et al., 2017). Process/fermentation parameters such as initial pH of fermentation media, fermentation temperature, inoculum/ seeding, speed of agitation, aeration rate, etc. are also important to provide feasible conditions for cell growth and product synthesis (An et al., 1999; Ramirez et al., 2001; Moriel et al., 2004; Ni et al., 2007; Ni et al., 2008; Bhatt et al., 2013; Xie et al., 2014; Schewe et al., 2017). pH influences cell growth and accumulation of product but it differs with the strains and fermentation conditions. Temperature is very important parameter as particular strain grows at a particular temperature range towards product synthesis. Rate of agitation and aeration improves the oxygen transfer rate which increases the dispersion of cells and nutrients and in turn boosts the cell growth and product formation. Literature reviews (Tables 1.1 and 1.2) for wild and mutant strains of *Phaffia rhodozyma* shows how the fermentation conditions (media + process parameters) and various cell disruption and extraction techniques affect final astaxanthin yield. Conditions at shake flask level may differ when it is applied to large scale system as they involve more parameters which are important for product maximization. Hence fermentation conditions at large scale need to be optimized separately.

Table 1.1: Effect of fermentation conditions and cell disruption techniques on astaxanthin yield from wild strains of *Phaffia rhodozyma*

Strain	Fermentation media (g/L)	Fermentation/process parameters	Cell biomass (g)	Cell disruption method	Solvent for extraction	Astaxanthin yield (µg/g DCW)	Reference
67–385	Glucose = 10 yeast extract = 3.0 malt extract = 3.0 peptone = 5.0	pH = 4.0–6.0 temperature (°C) = 22 agitation (rpm) = 150	~0.01 (2 mL broth)	DMSO	Any organic solvent or soybean oil	332*	Sedmak et al., 1990
ATCC 24228	Enzymatic eucalyptus wood hydrolysates KNO_3 = 0.1 Nutrients	pH = 6.0 temperature (°C) = 22	10@	DMSO	Hexane	214	Cruz and Parajo, 1998
NRRL Y–17268	Hemicellulosic hydrolysates of Enzymatic eucalyptus Peptone = 3.0 KNO_3 = 0.2	temperature (°C) = 22 aeration (vvm) = 3.0 agitation (rpm) = 400	23.2@	DMSO	Hexane	448	Parajo et al.,1998
Jeil–Bio Korea	NM	NM	NM	Supercritical CO_2	–	90#	Lim et al., 2002
ATCC 24202	Sugar cane juice: total carbohydrates = 20 Urea = 1	pH = 6.0 temperature (°C) = 24 aeration (vvm) = 1.0 inoculum (% v/v) = 3.0–4.0	19.3@	DMSO	Acetone	383.7	Moriel et al., 2005
ATCC 96594	Glucose = 10 Peptone = 5.0 Yeast extract = 3.0 Malt extract = 3.0	temperature (°C) = 22 agitation (rpm) = 270–300	10	Microwave irradiation	Ethanol	3650	Choi et al., 2007

Table 1.1 (continued….)

Strain	Fermentation media (g/L)	Fermentation/process parameters	Cell biomass (g)	Cell disruption method	Solvent for extraction	Astaxanthin yield (µg/g DCW)	Reference
NRRL–Y 17268	Glucose = 10 yeast extract = 3.0 malt extract = 3.0 peptone = 5.0 KNO_3 = 0.2	temperature (°C) = 25 inoculum (% v/v) = 10 agitation (rpm) = 150	0.5	Abrasion with celite Abrasion with glass pearls Ultrasonic waves (20 kHz) DMSO	Acetone	138.1 305.3 2198.4 1645.3	da Fonseca et al., 2011
NRRL–Y 17268	Sucrose = 15 malt extract = 16.25 peptone = 8.75 rice parboilization waste water = 87.5	pH = 5.0 temperature (°C) = 25 inoculum (mL)= 17 agitation (rpm) = 150	0.5	Abrasion with celite Abrasion with glass pearls Ultrasonic waves (40 kHz) Immersion in liquid nitrogen DMSO Acid treatment Enzymatic technique Enzymatic technique + Ultrasonic waves Sodium bicarbonate	Acetone –	93.1* 75.4* 88.4* 84.7* 155.7* 65.4* 156.9* 163.1* 36.9*	Michelon et al., 2012
Past–1	Glucose = 20 $(NH_4)_2SO_4$ = 2.0 KH_2PO_4 = 1.0 $MgSO_4 \cdot 7H_2O$ = 0.5 $CaCl_2$ = 0.1 Yeast extract = 2.0	pH = 6.0 temperature (°C) = 22 aeration (vvm) = 1.5–3.6 agitation (rpm) = 290	NM	Acid treatment (lactic acid)	Ethanol	1294.7	Ni et al., 2008

Table 1.1 (continued….)

Strain	Fermentation media (g/L)	Fermentation/process parameters	Cell biomass (g)	Cell disruption method	Solvent for extraction	Astaxanthin yield (µg/g DCW)	Reference
MTCC 7536	Mixture of *C. officinalis*, *Z. mays, T. aestivum and P. glaucum* (2 g each) Glucose = 20 $(NH_4)_2SO_4$ = 1.0 KH_2PO_4 = 1.0 $MgSO_4 \cdot 7H_2O$ = 0.5 $CaCl_2$ = 0.1 $MnSO_4$ = 0.5 $ZnCl_2$ = 0.14 $FeCl_3$ = 0.27 $CuSO_4$ = 1.25	pH = 5.8 ± 0.2 temperature (°C) = 22 agitation (rpm) = 200 aeration (vvm) = 0.5 inoculum (% v/v) = 10	~0.05 (10 mL broth)	DMSO + Ultrasound	Acetone	1448.4	Bhatt et al., 2013
UV3−721	Glucose = 20 $(NH_4)_2SO_4$ = 0.5 KH_2PO_4 = 1.0 $MgSO_4 \cdot 7H_2O$ = 0.5 $CaCl_2 \cdot 2H_2O$ = 0.1 NaCl = 0.1 Yeast extract = 0.2	pH = 6.0 temperature (°C) = 22 agitation (rpm) = 200	1.3[@]	DMSO	Acetone	1026	Pan et al., 2017
MTCC 7536	Glucose = 10 yeast extract = 3.0 malt extract = 3.0 peptone = 5.0	temperature (°C) = 18 agitation (rpm) = 150	0.05	Acid treatment (lactic acid) + Ultrasound (20 kHz)	Ethanol	~120	Gogate and Nadar, 2015

[*] – Total carotenoids, [#] – % Astaxanthin, DCW – dry cell weight, [@] – cell biomass in g/L, NM = Not mentioned

Table 1.2: Effect of fermentation conditions and cell disruption techniques on astaxanthin yield from mutant strains of *Phaffia rhodozyma*

Strain	Fermentation media (g/L)	Fermentation/process parameters	Cell biomass (g)	Cell disruption method	Solvent for extraction	Astaxanthin yield (µg/g DCW)	Reference
ZJUT003	Glucose = 120 yeast extract = 8.0 $(NH_4)_2SO_4$ = 8.0 $MgSO_4 \cdot 7H_2O$ = 0.1 KNO_3 = 0.3 K_2HPO_4 = 0.5 Polyethylene glycol = 0.1 mL/L	pH = 5.0 temperature (°C) = 20 aeration (vvm) = 0.5–1.2 agitation (rpm) = 300–500 inoculum (% v/v) = 5.0	NM	DMSO	Hexane + 0.01 M Sodium phosphate	2770	Zheng et al., 2006
ZJUT46	Glucose = 80 yeast extract = 8.0 $(NH_4)_2SO_4$ = 6.0 $MgSO_4 \cdot 7H_2O$ = 0.1 KNO_3 = 0.3 K_2HPO_4 = 0.5	pH = 4.0 temperature (°C) = 20–22 aeration (vvm) = 0.5–1.2 agitation (rpm) = 200–400 inoculum (% v/v) = 5.0	NM	DMSO	Hexane + 0.01 M Sodium phosphate	1740	Hu et al., 2006
AXJ–20	Glucose = 31.5 $(NH_4)_2SO_4$ = 2.45 KH_2PO_4 = 14.25 $MgSO_4 \cdot 7H_2O$ = 2.1 $CaCl_2 \cdot H_2O$ = 0.865 $FeSO_4 \cdot 7H_2O$ = 0.28 Trace elements and vitamins	pH = 5.5 temperature (°C) = 21 aeration (vvm) = 6.0 agitation (rpm) = 300–1000 inoculum (% v/v) = 10	0.5	DMSO	Diethyl ether	9700	Schewe et al., 2017

Table 1.2 (continued….)

Strain	Fermentation media (g/L)	Fermentation/process parameters	Cell biomass (g)	Cell disruption method	Solvent for extraction	Astaxanthin yield (µg/g DCW)	Reference
AS 2.1557 N9	Glucose = 50 yeast extract = 10 KH_2PO_4 = 2.0 Na_2HPO_4 = 1.0 $MgSO_4 \cdot 7H_2O$ = 2.0	pH = 5.0 temperature (°C) = 22 aeration (vvm) = 1.0 agitation (rpm) = 100–400	NM	DMSO	Acetone	830	Wang and Yu, 2009
E 5042	Glucose = 80 yeast extract = 8.0 K_2HPO_4 = 0.5 $(NH_4)_2SO_4$ = 6.0 $MgSO_4 \cdot 7H_2O$ = 0.1 KNO_3 = 0.3	pH = 6.0 temperature (°C) = 22 aeration (vvm) = 2.0 agitation (rpm) = 350 inoculum (% v/v) = 10	38[@]	DMSO	Acetone	2512	Liu et al., 2008
ENM5	Glucose = 50 $(NH_4)_2SO_4$ = 3.0 KH_2PO_4 = 1.5 $MgSO_4 \cdot 7H_2O$ = 1.5 yeast extract = 1.5 corn steep liquor = 10	pH = 5.0 temperature (°C) = 20 aeration (vvm) = 1.0 agitation (rpm) = 300–1200 inoculum (% v/v) = 6.0	16.8[@]	DMSO	Hexane/ ethyl acetate (50:50)	918	Liu and Wu, 2008
JMU–MVP14	Glucose = 20 $(NH_4)_2SO_4$ = 5.0 KH_2PO_4 = 2.0 $MgSO_4 \cdot 7H_2O$ = 1.0 $CaCl_2 \cdot H_2O$ = 1.0 Trace elements	pH = 6.0 temperature (°C) = 22 agitation (rpm) = 190 inoculum (% v/v) = 3.0	NM	DMSO	Ethanol	6800	Xiao et al., 2015

Table 1.2 (continued….)

Strain	Fermentation media (g/L)	Fermentation/process parameters	Cell biomass (g)	Cell disruption method	Solvent for extraction	Astaxanthin yield (µg/g DCW)	Reference
J4-3	Glucose = 20 $(NH_4)_2SO_4$ = 5.0 KH_2PO_4 = 3.0 $MgSO_4 \cdot 7H_2O$ = 0.5 Trace elements and vitamins	pH = 5.0 temperature (°C) = 22 aeration (vvm) = 15 agitation (rpm) = 800	9[@]	DMSO	Tetrahydra-furan (THF)	720	Cannizzaro et al., 2003
7B12	Glucose = 20 $(NH_4)_2SO_4$ = 1.0 KH_2PO_4 = 1.0 $MgSO_4 \cdot 7H_2O$ = 0.5 $CaCl_2 \cdot H_2O$ = 0.1 Trace elements	pH = 6.0 temperature (°C) = 22 agitation (rpm) = 200 inoculum (% v/v) = 1.0	7.71[@]	DMSO	Acetone	1000	Ni et al., 2007
YZUXHONG686	Glucose = 35 $(NH_4)_2SO_4$ = 3.0 KH_2PO_4 = 1.5 $MgSO_4 \cdot 7H_2O$ = 1.5 Yeast extract = 1.5 Calcium stearoyl lactylate = 10	pH = 5.25 temperature (°C) = 23 agitation (rpm) = 170 inoculum (% v/v) = 10	0.02	DMSO	Acetone	2560	Xie et al., 2014
SK984	Sucrose = 50 Bacto peptone = 10 Yeast extract = 10 Malt extract = 3.0 KH_2PO_4 = 3 mM Oak leaf extract = 5 % (v/v)	pH = 5.0 temperature (°C) = 22 agitation (rpm) = 190	8.7[@]	DMSO	Acetone	1980	Kothari et al., 2019

DCW – dry cell mass, [@] – cell biomass in g/L, NM = Not mentioned

1.3.1.4 Analysis from literature review on astaxanthin and scope for research

Table 1.1 and 1.2 shows astaxanthin production from mutant and wild strains of *Phaffia rhodozyma*. Table 1.1 (mutant strains) shows minimum astaxanthin yield (720 µg/g DCW) when a mutant strain JM−3 was used (Cannizzaro et al., 2003). The cell disruption was performed using hot DMSO (55°C) and tetrahydrafuran (THF) was used as a solvent. Highest astaxanthin yield of 9700 µg/g DCW was obtained from AXJ−20 when DMSO was used for cell disruption and diethyl ether as an extracting solvent (Schewe et al., 2017). Both of these strains were cultivated at nearly same process conditions but optimized medium composition and trace elements played a major role in enhancing intracellular astaxanthin content as in both cases cell disruption was performed using DMSO method only. Also it creates scope for use of appropriate solvent in order to extract maximum astaxanthin released after breakage of cell wall.

Table 1.2 (wild strains) shows astaxanthin yields from wild strains of *Phaffia rhodozyma*. The lowest astaxanthin yield (36.9 µg/g DCW total carotenoids) was obtained when sodium bicarbonate was used for cell disruption and extraction of astaxanthin. The medium composition for fermentation of yeast contained sucrose as a carbon source (Michelon et al., 2012). Same strain (NRRL−Y 17268) was used by da Fonseca et al. (2012) but he got better yield by using glucose as carbon source. The cell disruption technique using sodium bicarbonate was used for other yeasts but not found much effective for *Phaffia rhodozyma* due to rigidity of its cell wall. Hence this method was discarded to use as a sole technique but it can be used in combination to other techniques. The highest astaxanthin yield (2198.4 µg/g DCW) of their (da Fonseca et al., 2012) study was obtained using ultrasonic waves of 20 kHz frequency compared to other techniques.

Acid treatment technique also showed lower astaxanthin yields when performed by Michelon et al. (2012) and, Gogate and Nadar (2015). However, Ni et al. (2008) got the highest astaxanthin yield (1294.7 µg/g DCW) compared to above two authors. Gogate and Nadar (2015) has used simple yeast malt (YM) media for fermentation which may not fulfill the nutrient requirement by yeast although he used acid treatment along with ultrasound for cell disruption but which is of no use when intracellular content is less. Maximum astaxanthin yield (3650 µg/g DCW) of all wild strains reported in literature was obtained by Choi et al. (2007) when microwave irradiation technique at optimized conditions was used for cell disruption. This technique is not much popular due to the disadvantage of using high temperature which may degrade astaxanthin and reduce its quality. Also, the power requirement is another issue to restrict it using at large scale.

Wild strain (MTCC 7536) of Indian origin was used by Bhatt et al. (2013) and Gogate and Nadar (2015). This wild strain gave good astaxanthin yield (reports of Bhatt et al. (2013)) which is comparable to yields obtained from mutant strains JM−3 (Cannizzaro et al., 2003), ZJUT46 (Hu et al., 2006), 7B12 (Ni et al., 2007), ENM5 (Liu and Wu, 2008), AS 2.1557 N9 (Wang and Yu, 2009) and SK984 (Kothari et al., 2019). Bhatt et al. (2013) used mixture of various flowers (*C. officinalis*, *Z. mays, T. aestivum and P. glaucum*) and glucose as a carbon source and, optimized medium composition (containing nitrogen source and nutrients). The cell disruption was performed using combination of DMSO method and ultrasonic waves. Maximum astaxanthin yield obtained in the study was 1448.4 µg/g DCW. The same strain gave less yield (~120 µg/g DCW) when simple yeast malt (YM) media was used although cell disruption was done using a combination of acid treatment and ultrasonic waves (Gogate and Nadar, 2015). The same strain, when used in our study (can be seen in

upcoming chapters), gave an increased astaxanthin yield of 1728 µg/g DCW. Fermentation experiments were performed at optimized conditions of medium composition and process parameters, and DMSO method was used for cell disruption. The rise in the yield may be due to induction of sonication during fermentation which may increase intracellular astaxanthin content. In another study, this yield was reduced to 1536 µg/g DCW although cell disruption was done using combination of DMSO method and ultrasonic probe technique, and fermentation was performed using un-optimized fermentation conditions (media + process parameters).

All above studies (mentioned in literature) created scope for research as: (1) Use of appropriate carbon and nitrogen sources (and maintained C/N ratio) which are the major factors in media to enhance astaxanthin yield, (2) use of statistical optimization techniques to optimize medium composition and process parameters, (3) use of appropriate cell disruption techniques to keep the quality and reduce the loss due to degradation of astaxanthin formed within the cells, (4) use of appropriate solvent with great solubility of astaxanthin in it, (5) as most of the authors used DMSO as a cell disruption technique which gave good yield which can be further enhanced when used in combination to modern techniques and (6) use of optimized ratios of DMSO and extracting solvent can enhance astaxanthin extraction yield and also it may reduce the cost of solvents required and their separation.

1.3.2 RIBOFLAVIN (VITAMIN B_2)

Riboflavin or vitamin B_2 is an important water-soluble vitamin that has crucial role in human health. It helps human body in assimilation and digestion of carbohydrates, proteins, and fats for energy production. Essentially, riboflavin is a metabolic precursor of flavin nucleotides, viz. mononucleotide (FMN) and flavin adenine dinucleotide (FAD) (Chaudhuri et al., 2014; Xin et al., 2017). These nucleotides are involved mostly in oxidative metabolism and various enzymatic reactions. The natural food sources for vitamin B_2 are eggs, green vegetables, milk, meat, mushrooms etc. (Stahmann et al., 2000; Survase et al., 2006; Abbas and Sibirny, 2011). Commercial-scale riboflavin production (as dietary supplement) is based on fermentation route employing filamentous fungi such as *Eremothecium gossypii* (or *Ashbya gossypii*), *Candida famata* or *Candida flareri* (Lim et al., 2001; Jimenez et al., 2005; Mateos et al., 2006; Wei et al., 2012; Kato and Park, 2012; Dmytruk et al., 2014; Aguiar et al., 2015; Ledesma-Amaro et al., 2015; Aguiar et al., 2017; Silva et al., 2019). Some bacterial species such as *Cornebacterium* or *Bacillus subtilis* have also been used for commercial riboflavin production (Wu et al., 2007; Zhu et al., 2007; Wang et al., 2011; Oraei et al., 2018). Industrial-scale riboflavin production often involves genetically engineered strains (Dmytruk et al., 2014), which have high productivity. Based on phylogenetic data, *Debaryomyces hansenii* was misidentified as other yeast species but after advanced genomic studies it was confirmed that *Debaryomyces hansenii* and *Candida famata* are not different. However, it has shown that *Debaryomyces hansenii* is a telemorph of *Candida famata var. famata* and then *Candida famata* renamed as *Debaryomyces hansenii* (Voronovsky et al., 2004; Kurtzman and Robnett, 2013; National Collection of Yeast Cultures, 2017). There are two varieties of *Debaryomyces hansenii* viz. *D. hansenii*

var. fabryii and *var. hansenii* but later *D. hansenii var. fabryii* was renamed as *Debaryomyces fabryii* (Yaguchi et al., 2017). Some author's called *Candida famata* as *Candida flareri* (Dmytruk et al., 2012; Dmytruk et al., 2014). In this thesis, *Debaryomyces hansenii* refers to *Debaryomyces hansenii var. hansenii. Debaryomyces hansenii* was isolated in saline environment of seawater and concentrated brines (Bruer and Harms, 2006). Due to halotolerant nature, it adapts to conditions of higher salinity, and can grow in marine environment. However, wild strains of *Debaryomyces hansenii* strains have relatively low productivity and yield of riboflavin as compared to genetically engineered strains.

1.3.2.1 Synthetic vs. microbial fermentation route for riboflavin synthesis

After being used for several decades, chemical synthesis route is now being replaced with fermentation route due to the fact that it saves cost, reduces the waste and energy required and use of renewable sources as carbon source (Stahmann et al., 2000). The chemical synthesis route starts with glucose which is then converted to D-ribose. This ribose was reacted with xylidine to form riboside which was then hydrogenated to give ribamine. This ribamine was coupled with phenyl diazonium halogenide to produce an azo compound which reacts to barbituric acid to produce riboflavin (Stahmann et al., 2000). The major disadvantages of chemical route are: (1) It only gives 60% product yield and generate lot of waste; (2) it needs organic solvents and (3) requirement of 25% more energy compared to microbial route (Stahmann et al., 2000). Chemical process has just one advantage of less separation cost as it produces riboflavin of nearly 96 % purity.

Fermentation routes for riboflavin synthesis from microbial strains of *Ashbya gossypii*, *Bacillus subtillis* and *Candida famata* (*Debaryomyces hansenii*) have been

started to overcome the disadvantages caused by chemical synthesis route. A commercial fermentative production of riboflavin from *Ashbya gossypii* was started by BASF (Germany) in 1990 using mutant strain which gave very good yield and forced them to shut down chemical process finally in 1996 (BASF 1996). Similarly in 2000, La Roche Ltd replaced their chemical process with fermentation process from *Bacillus subtillis* which saved their 50% cost compared to chemical process. *Candida famata* (*Debaryomyces hansenii*) is still under research to get a comparative yield as other two microbes by the developments in the fermentation techniques and metabolic engineering. Fermentation process has many advantages of low cost, low energy requirement and non toxic product synthesis but has a major disadvantage of purity of final product. In case of riboflavin, fermentation route gives nearly 80% product purity and hence the purification cost is higher compared to chemical synthesis route.

1.3.2.2 Riboflavin biosynthetic pathway in *Debaryomyces hansenii (Candida famata)*

Microbial production of riboflavin from *Debaryomyces hansenii* (*Candida famata*) has the simplest pathway in terms of guanosine triphosphate (GTP) formation compared to that from *Ashbya gossypii* and *Bacillus subtillis* which requires several steps (Lim et al., 2001; Survase et al., 2006). GTP is an important energy source for the translocation of ribosome towards the formation of mRNA. As stated by previous authors (Dmytruk et al., 2004; Voronovsky et al., 2004), riboflavin synthesis pathway from *Debaryomyces hansenii* shows involvement of five major enzymes viz. GTP cyclohydrolase II (*RIB1* gene), HTP reductase (*RIB2* gene), dimethylribityllumazine synthase (*RIB5* gene), dihydroxybutanone phosphate synthase (*RIB6* gene) and riboflavin synthase (*RIB7* gene). Figure 1.2 shows the metabolic pathway of

riboflavin synthesis from *Debaryomyces hansenii* (adopted from Lim et al., 2001).

Riboflavin metabolic pathway from glucose consists of three major parts viz. pentose phosphate pathway, purine pathway and riboflavin biosynthesis pathway. Glucose supplied in the media utilized in pentose phosphate pathway for the generation of NADPH (nicotinamide adenine dinucleotide phosphate hydrogen), glucose 6-phosphate and ribulose-5-phosphate (Ribu-5P). NADPH is required to form other molecules such as fatty acids and ribulose-5-phosphate helps to make DNA's and RNA's. Guanosine triphosphate (GTP) and dihydroxy butanone phosphate (DBP) are the metabolic precursors of riboflavin synthesis and are synthesized from ribulose 5-phospahte. Purine pathway from ribulose 5-phosphate produces GTP (via. Formations of IMP, inosine monophosphate; AMP, adenosine monophosphate; XMP, xanthosine monophosphate and GMP, guanosine monophosphate), which is an important molecule needed for synthesis of RNA during transcription process. Increase in the flux towards the formation of GTP enhances riboflavin production. Riboflavin biosynthesis pathway from GTP involves major enzymes for riboflavin synthesis as *RIB1*, *RIB2*, *RIB5, RIB6* and *RIB7*. Overexpression of these enzymes helps to boost riboflavin yield.

1.3.2.3 Riboflavin biosynthesis from *Debaryomyces hansenii (Candida famata)*

Riboflavin biosynthesis from *Candida famata* (*Candida flareri*) which is an anamorph of *Debaryomyces hansenii*, is still a part of research as it gives lower riboflavin yield compared to other commercial microbes such as *Ashbya gossypii* and *Bacillus subtillis*. Being the simplest pathway for riboflavin synthesis in *Debaryomyces hansenii,* attract researchers for further study. In the present thesis, only wild microbial strains have considered for biotechnological production of value

added products such as astaxanthin and riboflavin.

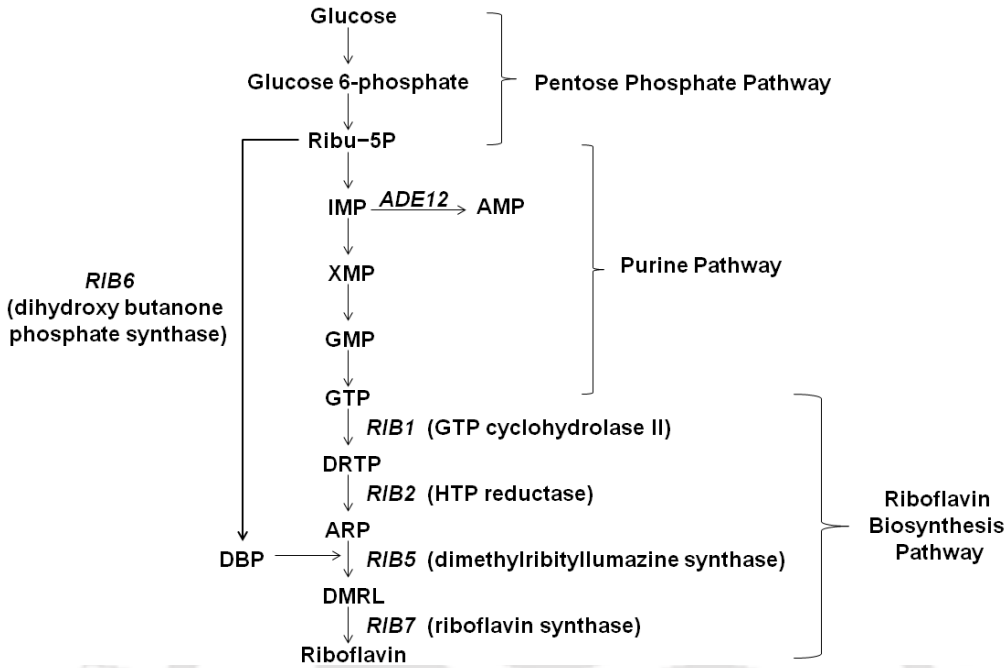

Figure 1.2: Metabolic pathway of riboflavin production from *Candida famata* (*Debaryomyces hansenii*) (Adopted from Lim et al., 2001). Abbreviations: Ribu-5P, Ribulose-5-phosphate; IMP, inosine monophosphate; *ADE12*, adenylosuccinate synthase; AMP, adenosine monophosphate; XMP, xanthosine monophosphate; GMP, guanosine monophosphate; GTP, Guanosine triphosphate; DRTP, 2, 5-diamino-6-ribosylamino-4 (3H)-pyrimidinedione 5-phosphate; ARP, 5-amino-6-ribitylamino-2, 4 (1H, 3H)-pyrimidine; DBP, L-3, 4-dihydroxy-2-butanone-4-phosphate; DMRL, 6, 7-dimethyl-8-ribityllumazine.

Wild strains may give lower product yield, but are the most stable forms than mutant strains. Although, the product yield from wild strains can be enhanced by proper fermentation medium composition (including additives or trace elements) and fermentation parameters. As per the pathway of riboflavin synthesis in *Debaryomyces*

hansenii, it is clear that purine pathway is the most important which produces GTP (important precursor for riboflavin synthesis). In order to increase riboflavin production, the metabolic flux for GTP has to be increased with the appropriate and optimized carbon source, nitrogen source and important additives. Importance of carbon and nitrogen sources and their ratios in the fermentation media has already addressed in literature review on astaxanthin. Also addition of yeast extract (source of micronutrients and vitamins), metal ions and additives (such as glycine, butin or asparagine) along with basal medium is important to follow proper pathway for desired product synthesis and enhanced yield. Metal ions such as cobalt, zinc, manganese, copper etc. binds with enzymes to form metalloenzymes with higher metabolic activity. Some metal ions such as ferrous, being a part of haemoproteins assists intracellular oxygen transport (Palmer and Bonner, 2008). Additives such as glycine, butin or asparagine plays important role in purine pathway. Glycine nitrogen was distributed in riboflavin leading to metabolic makeup of purine, which enhances availability of GTP resulting in improvement of riboflavin production (Plaut, 1954).

Table 1.3: Riboflavin synthesis from wild microbial strains

Strain	Feeding method	Fermentation media	Fermentation parameters	Riboflavin (mg/g of cells)	Riboflavin (mg/L)	Reference
Debaryomyces hansenii J26	Shake flask	Synthetic dextrose media: Dextrose = 2.0 % yeast nitrogen base without amino acids = 0.67 % selected amino acid mix without uracil = 0.02 % sorbitol = 1.0 mol/L Additive: $CoSO_4 \cdot 5H_2O$ = 0.5 mmol/L	Temperature = 30°C Shaking speed = 200 rpm Inoculum = 1.25×10^6 cells	–	0.0016	Seda-Miro et al., 2007
Candida sp. LEB 130	Shake flask	Sucrose = 30 g/L KH_2PO_4 = 2.0 g/L $MgSO_4$ = 1.0 g/L $ZnSO_4$ = 0.5 mL/L	Temperature = 30°C Shaking speed = 100 rpm	–	12.5	Suzuki et al., 2011
Candida sp. LEB 130	Shake flask	Sucrose = 40 g/L KH_2PO_4 = 2.0 g/L $ZnSO_4$ = 1.5 mL/L Flaxseed oil = 45 g/L	Temperature = 30°C Shaking speed = 100 rpm	–	105.7	Suzuki et al., 2012
Candida famata AF–4	7 L Bioreactor	Glucose = 2.0 % yeast nitrogen base without amino acids = 0.67 % peptone = 1.0 % yeast extract = 0.5 %	pH = 5.5 Temperature = 28 °C Aeration rate = 1.2 vvm Agitation = 1200 rpm % inoculum = 10–25 %	52.2 ± 2.8	260	Dmytruk et al., 2014
Candida famata AF–4/SEF1/RIB1/RIB7*				337.9 ± 15.1	1450	
Pichia guilliermondii R–66	Shake flask	Sucrose = 20 g/L Peptone = 20 g/L Yeast extract = 10 g/L	Shaking speed = 200 rpm Temperature = 30 °C	4.45×10^{-6}	–	Boretsky et al., 2011

Table 1.3 (continued….)

Strain	Feeding method	Fermentation media	Fermentation parameters	Riboflavin (mg/g of cells)	Riboflavin (mg/L)	Reference
Candida famata ATCC 20849 (dep8) *Candida famata* AF-4 *Candida famata* AF-4/RIB1/RIB7*	–	Glucose = 2.0 % yeast nitrogen base without amino acids = 0.67 % peptone = 1.0 % yeast extract = 0.5 %	–	53.5 ± 2.6 48.1 ± 2.3 67.6 ± 3.3	284 ± 14 250 ± 12 345 ± 17	Dmytruk et al., 2011
Bacillus subtilis 1012	6 L Bioreactor	Glucose = 3.6 g/L $(NH_4)_2SO_4$ = 2.0 g/L $MgSO_4 \cdot 7H_2O$ = 0.2 g/L K_2HPO_4 = 4.0 g/L Trace elements	Agitation = 1500 rpm Aeration rate = 2 liters/min % inoculum = 5 % Temperature = 37 °C pH = 6.60 ± 0.05	–	80	Sauer et al., 1996
Bacillus subtilis ATCC 6051	Shake flask	Fructose = 38.1 g/L $MgSO_4$ = 0.85 g/L K_2HPO_4 = 2.27 g/L $FeSO_4$ = 0.02 g/L Yeast extract = 4.37 g/L	Shaking speed = 200 rpm % inoculum = 5 % Temperature = 30 °C	–	12.08	Oraei et al., 2018
Bacillus subtilis	6 L Bioreactor	Glucose = 20 g/L $(NH_4)_2SO_4$ = 8.0 g/L $MgSO_4 \cdot 7H_2O$ = 0.2 g/L $K_2HPO_4 \cdot 3\ H_2O$ = 15 g/L KH_2PO_4 = 6.0 g/L Trace elements	Agitation = 800 rpm Aeration rate = 2 vvm % inoculum = 2 % Temperature = 37 °C pH = 7.2	–	620	Hu et al., 2017

Table 1.3 (continued….)

Strain	Feeding method	Fermentation media	Fermentation parameters	Riboflavin (mg/g of cells)	Riboflavin (mg/L)	Reference
Ashbya gossypii ATCC 10895	Shake flask	Glucose = 10 g/L Peptone = 20 g/L Yeast extract = 2.0 g/L *myo*-inositol = 0.6 g/L	pH = 6.8 Temperature = 28°C Shaking speed = 120 rpm	–	28	Jiménez et al., 2005
Ashbya gossypii ATCC 10895	Shake flask	Glucose = 1.0 g/L NH_4Cl = 1.5 g/L NaCl = 0.2 g/L Asparagine = 0.5 g/L $MgSO_4 \cdot 7H_2O$ = 0.4 g/L $MnSO_4 \cdot H_2O$ = 0.05 g/L $CaCl_2 \cdot 2\ H_2O$ = 0.04 g/L Yeast extract = 0.05 g/L *myo*-inositol = 0.1 g/L	pH = 6.8 Temperature = 28°C Shaking speed = 120 rpm	–	96	Ledesma-Amaro et al., 2015
Ashbya gossypii ATCC 10895	Shake flask	Glucose = 10 g/L Peptone = 20 g/L Yeast extract = 2.0 g/L *myo*-inositol = 0.6 g/L	pH = 6.8 Temperature = 28°C Shaking speed = 120 rpm Inoculum = 1×10^6 spores/L	2.58 ± 0.13	–	Mateos et al., 2006

* – mutant strain

1.3.2.4 Analysis from literature review on riboflavin from wild microbial strains and scope for research

Table 1.3 shows literature review on riboflavin synthesis from various microbial strains of wild type. The present thesis is focused on the use of wild strains (considered as a stable form) and enhancement in the product yield with the modifications in the fermentation process. Literature review shows minimum riboflavin yield (titer 0.0016 mg/L) from *Debaryomyces hansenii* J26 (Seda-Miro et al., 2007) and maximum yield of 53.5 mg/g of cells (titer 284 mg/L) from *Candida famata* ATCC 20849 (dep8) when only wild strains of *Debaryomyces hansenii* (*Candida famata*) were considered. Although, mutagenesis of *Candida famata* AF-4 enhanced riboflavin yield to 337.9 mg/g of cells. Enzymatic activity of *RIB1* gene (GTP cyclohydrolase II) and *RIB7* gene (riboflavin synthase) has been triggered through mutations which ultimately improved final riboflavin yield. These enzymes are very important to start (by *RIB1* gene) and end (by *RIB7* gene) riboflavin biosynthesis pathway after purine pathway.

Riboflavin titer in *Candida sp.* LEB 130 shows increment from 12.5 mg/L (Suzuki et al., 2011) to 105.7 mg/L (Suzuki et al., 2012) when flaxseed oil was supplied in the fermentation media along with basal medium. Flaxseed oil contains important fatty acids such as α-linolenic acid, linolenic acid, oleic acid, stearic acid and palmitric acid and majority is by α-linolenic acid. Flaxseed oil thus becomes a good source of nutrients to boost biosynthetic riboflavin yield. This shows importance of the contents of fermentation medium even when exactly same microbial strain is used for production of a particular product.

Other microbial strains such as *Pichia guilliermondii* (Boretsky et al., 2011), *Bacillus subtilis* (Sauer et al., 1996; Hu et al., 2017; Oraei et al., 2018) and *Ashbya*

gossypii (Jiménez et al., 2005; Mateos et al., 2006; Ledesma-Amaro et al., 2015) were shown just to have a review on riboflavin yield from wild microbial strains in comparison to that from *Debaryomyces hansenii* (*Candida famata*). Strains of *Debaryomyces hansenii* are still a part of research so as to use at commercial level like *Ashbya gossypii* and *Bacillus subtilis*. Although researchers are working on mutagenesis with the modifications in metabolic pathway to enhance activity of intracellular enzymes. Literature review also shows a wild strain from Indian origin i.e. *Debaryomyces hansenii var. hansenii* MTCC 3574. This strain achieved improved riboflavin yield with the modifications in conventional fermentation process. Riboflavin titer (240 mg/L) was found many fold higher than that from the strain *Debaryomyces hansenii* J26 which gave only 0.0016 mg/L of riboflavin.

Above studies on riboflavin yield from microbial strains of *Debaryomyces hansenii* (*Candida famata*) shows a scope for further research as: (1) Use of significant fermentation media with rich source of micronutrients and vitamins (like Suzuki et al., 2012), (2) Optimization of medium components and fermentation parameters by statistical optimization techniques over one variable at a time (OVAT) method which has several disadvantages, (3) Supplementation of additives such as glycine, butin or asparagines which helps for betterment of purine pathway (by enhancing metabolic flux towards GTP) and final riboflavin yield, (4) Supplementation of transition metal ions which binds with enzymes to form metalloenzymes of higher metabolic activity and (5) Assistance of modern techniques with fermentation to help in overexpression of intracellular enzymes which ultimately increases the product yield.

1.3.3 LACTOSE

Lactose ($C_{12}H_{22}O_{11}$) is a disaccharide consisting of galactose and glucose subunits. When lactose is fed to a mammal (in the form of milk), lactase enzyme is secreted inside the intestine which divides lactose molecule into glucose and galactose so that it can be absorbed. Being a sugar (energy source) it is used in day to day life in the form of food and pharmaceutical products (Wong et al., 2012). Solid form of lactose may be amorphous or crystalline. Crystalline lactose is generally α-lactose, β-lactose or mixture of both which depends on the techniques of their production or recovery. Existence of α-lactose and β-lactose is due to the phenomenon called mutarotation (Haase and Nickerson, 1966; Raghavan et al., 2001). Addition of water to the lactose creates mutarotation reaction due to which one form of lactose changes to another. Mutarotation means the rotation of hydroxyl group available on the C-1 carbon of the glucose molecule which allows the opening of the ring available on number one carbon molecule and spatial arrangement of hydroxyl group gives either α-lactose or β-lactose (Jawad et al., 2012; Pawar et al., 2018). Industrially, lactose is produced from the whey (by product) remained after processing of milk to milk products. Whey or whey permeate was concentrated, crystallized and separated from other impurity to get pure lactose (Wong and Hartel, 2014; Pandalaneni et al., 2018).

1.3.3.1 Lactose crystallization

Crystallization is the formation of solid crystals from the crystal magma when supersaturation is reached. Supersaturation is when the concentration of the solute reaches above the saturation solubility at the reaction temperature. Supersaturation can be achieved by cooling, evaporation or by the addition of a substance which reduces the solubility of solute in a solvent (Bund and Pandit, 2007a; Pawar et al.,

2018; MacFhionnghaile et al., 2017). This substance can also termed as "antisolvent". The supersaturation leads to two phenomenon viz. nucleation and crystal growth. ***Nucleation:*** Nucleation relates to the birth of small nuclei which then grows to form crystals. Nucleation in a homogeneous solution controls number, size and morphology of crystals. An allowable supersaturation level is created during crystallization called as metastable zone and supersaturation concentration between solubility and super-solubility is called metastable zone width (MSZW) (Ulrich and Strege, 2002). Superstauration driving force above super-solubility curve induces spontaneous primary nucleation. Addition of crystalline components (such as lactose crystals) creates homogeneous nucleation whereas the presence of foreign substances or roughness of the wall or surface creates heterogeneous nucleation. A dominant crystal growth with an extent of secondary nucleation is observed when supersaturation concentration stays in MSZW (Wong et al., 2011). Secondary nucleation occurs due to the presence of lactose seed crystals or due to agitation or collision to the reactor wall (Pandalaneni and Amamcharla, 2016).

Crystal growth: Crystals are formed from the nuclei with continuous diffusion of lactose onto formed crystal lattice. Temperature and supersaturation driving force are the major factors responsible for crystal growth. Crystal growth is a three step process viz. liquid to solid phase mass transport, surface integration and reversal of latent heat from growing crystals (Wong and Hartel, 2014). Presence of additives or impurities greatly influences the crystal growth. Their presence may boost or retard the crystal growth. Rate of nucleation and crystal growth also depends on various process parameters in a particular crystallization technique.

Lactose is being crystallized by cooling crystallization, seeded cooling crystallization

and antisolvent crystallization (Figura., 1993). Cooling crystallization has its disadvantage as induction time for nucleation ranges from days to weeks but not in the case of seeded cooling crystallization. Moreover, seeded cooling crystallization provides the stability of crystals at ambient temperatures. But the issue with seeded cooling crystallization is that it gives fines and varied crystal morphology which can affect downstream processing and final product properties (Zeng et al., 2000; Omar et al., 2015). These issues can be solved using antisolvent crystallization which gives better control over nucleation, growth rate and morphology (MacFhionnghaile et al., 2017).

1.3.3.2 Factors affecting lactose crystallization

There are various factors which affect nucleation, crystal growth, size, shape and morphology. These include supersaturation, solution/reaction temperature, initial lactose concentration, pH, rate of agitation or mixing and presence of additives or impurities.

Supersaturation: Supersaturation, being a driving force in crystallization, plays a dominant role in crystal growth rate. Crystal growth rate increases when a concentration reaches to a certain limit. At higher supersaturation, molecular mobility reduces which ultimately results in decrease of crystal growth rate (Wong et al., 2012). Also an interlinkage between supersaturation and mutarotation affects final form of the crystal in terms of its shape. At low supersaturation level, large size crystals with well developed faces are formed compared to those formed at high supersaturation level (Wong et al., 2012; Parimaladevi and Srinivasan, 2014).

Temperature: Temperature is an important factor in lactose crystallization. Increase in temperature increases rate of crystallization but within an optimal crystallization

range. Optimal temperature range for lactose crystallization without the addition of additives or impurities is between 20°C to 30°C (Ribeiro et al., 2006; Bund and Pandit, 2007a). There is no point in going below 20°C which results in decreased crystallization rate. Also mutarotation is dependent on temperature. Change in temperature affects mutarotation which results in α-lactose, β-lactose or a combination of both (Thomsen et al., 2005).

Initial lactose concentration: Solution concentration and temperature are interdependent factors towards the solubility of a solute into the solvent (water in case of lactose solution). At lower temperature and high concentration, the viscosity increases which results in decreased nucleation rate (Hartel, 2001). The solution concentration needs to be optimized for a particular temperature in order to get increased nucleation and growth rate and generation of crystals of uniform shape and size. In case of antisolvent crystallization, increased viscosity of lactose solution creates barrier for interactions between antisolvent and water (from aqueous lactose solution) which ultimately reduces the rate of crystallization (Bund and Pandit, 2007a; Gajendragadkar and Gogate, 2017).

pH of lactose solution: pH of lactose solution plays an important role in crystallization. Studies have shown that pH in the range of 3 to 7 gives better growth rate in presence or absence of additives like whey protein, lactic acid or any impurities (Bund and Pandit, 2007a; Bund and Pandit, 2007b; Pisponen et al., 2013; Sánchez-García et al., 2018). Induction time for crystallization increases with an increase in pH of the lactose solution (Raghavan et al., 2001). In order to keep better control over mutarotation, pH of the solution must be kept within the specified range.

Agitation: Agitation creates seeding effect inside the lactose solution which brings the nuclei formed in one part of the reaction volume to other which promotes secondary

nucleation. Increased agitation rate increases frequency for activated molecular collisions which is a result of the movement of active centres to the surface (Mcleod et al., 2016). Nucleation increases more rapidly in presence of seed crystals than in the absence which ultimately increases crystal growth rate (Wong et al., 2012). Also rate of agitation determines the size and uniformity of the crystals in the crystal magma.

Additives: Nucleation is affected by the addition of ingredients such as proteins, lactic acid, salts, flavor additives, starches etc. Each of these additives may accelerate or hinder nucleation (Gänzle et al., 2008). Addition of insoluble materials creates catalytic sites to help heterogeneous nucleation while soluble components prevent the molecules to come together and hinders nuclei formation (Hartel, 2001). Addition of whey protein helps to increase lactose recovery due to the seeding effect (Bund and Pandit, 2007a). Addition of lower content of lactic acid (0.2% w/v) gives higher yield (77%) while higher content (1% w/v) decrease it to just 59% (Chandrapala et al., 2016). Vegetable and marine gums act as inhibitors and suppress nucleation whereas gelatin supports nucleation (Gänzle et al., 2008). Presence of glycerol in the solution obstructs primary nucleation process (Vu et al., 2009).

1.3.3.3 Antisolvent lactose crystallization

Antisolvent crystallization is the method of crystallization by the addition of solvent to the aqueous sugar solution. Antisolvent added to aqueous lactose solution is generally miscible with the water and reduces the lactose solubility in the new mixture of solvents (water + antisolvent) which results in crystal formation (Bund and Pandit, 2007a; Kougoulos et al., 2010; Gajendragadkar and Gogate, 2017; Pawar et al., 2018). Antisolvent crystallization greatly depends on the choice of solvent and its

concentration. Antisolvent concentration is an additional factor responsible for nucleation and crystal growth along with other factors discussed in earlier section. Antisolvent crystallization technique is preferred for lactose crystallization over other methods of cooling or evaporative crystallization (Parimaladevi and Srinivasan, 2014). Cooling crystallization requires days to weeks for completion of crystallization whereas in evaporative crystallization, there is no great control over the shape, size and morphology and also existence of evaporative losses from crystal magma. Cooling or evaporative crystallization gives limited information in engineering point of view based on crystal size and shape (Pawar et al., 2018). Antisolvent crystallization is known to produce crystals of various size, phase (α and β) composition and morphology (Kougoulos et al., 2010; Crisp et al., 2011). Also time of crystallization or induction time reduces from hours or days to minutes in antisolvent crystallization compared to cooling crystallization (MacFhionnghaile et al., 2017). Generation of agglomerates may be one of the disadvantage of anisolvent crystallization which can be reduced with the assistance of some modern techniques (Pawar et al., 2018). Another disadvantage may be the cost for separation for the removal of the antisolvent from the final product.

Table 1.4: Literature review on antisolvent lactose crystallization

Initial lactose concentration	Additives	Antisolvent	Experimental conditions	Results	Reference
22–27 % w/w	–	Acetone	Heating (°C) = 70 Cooling (°C) = 20 Agitation (rpm) = 350	Lactose yield = 92.63 %. Mean crystal size = 51.37 µm. Crystal growth rate = 0.0055 µm/s.	Brito and Giulietti, 2007
3.6–5.0 % w/v	Paneer whey (0.13–0.28 % w/v)	Ethanol (85 % v/v)	pH = 3.6–5.0 Temperature (°C) = 7 ± 2 Agitation (rpm) = 750–1000	Lactose recovery = >90 %. Lactose purity = 97–99 %. Mean crystal size = 4.19 µm. Crystal growth rate = 4.33×10^{-4} µm/s.	Bund and Pandit, 2007a
30 % w/v and 60 % w/v	–	Ethanol:butanol @ 5 mL/min	Temperature (°C) = 55 Agitation (rpm) = 200	Lactose yield = 100 % @ 30 % w/v lactose solution and 20:60 (mL) of antisolvent. Volume mean diameter = 82.6 µm and span = 0.83.	Kaialy and Nokhodchi, 2012
25 % w/w	–	Acetone (60 % w/w) @ 5 mL/min	Temperature (°C) = 6 Agitation (rpm) = 400	Lactose yield = 90 %. Volume mean diameter = 102 µm. α-lactose = 60 % & β-lactose = 40 %.	Simone et al., 2019
NM (α–lactose monohydrate)	–	DMSO and ethanol Each = 5–85 % v/v	Temperature (°C) = 33	5–45 % ethanol addition gave α–LM. 65–85 % ethanol addition gave β–LM. No nucleation for 10–85 % DMSO addition upto 7 days. DMSO + gas phase diffusion decreased induction time.	Vinodhini and Srinivasan, 2018
12–18 % w/v	–	Acetone (80 % v/v)	Temperature (°C) = 30 ± 3 Agitation (rpm) = 500 rpm US power (W) = 120	Sonicated lactose recovery = 80–92% (w/w) @4 min of sonication. Non-sonicated lactose recovery = 75.2% (w/w) @32 min of stirring.	Patel and Murthy, 2009

Table 1.4 (continued….)

Initial lactose concentration	Additives	Antisolvent	Experimental conditions	Results	Reference
5–15 % w/w	–	Acetone (80 % v/v)	pH = 2.5–6.5 Temperature (°C) = 30 ± 3 Sonication time (min) = 5–15 US power (W) = 120	Narrower crystal size distribution was observed for sonicated samples. More β lactose (rod/needle shape) formed with sonication.	Patel and Murthy, 2011a
0.25–0.45 kg/kg of solution	–	Ethanol (0.1–0.5 mL/s)	Temperature (°C) = 40 Sonication time (min) = 5–15 US frequency (kHz) = 20 & 40	More β lactose formed with increased antisolvent addition rate and increased lactose concentration. Smaller size crystals were obtained with the application of ultrasound.	Pawar et al., 2018
11.5–17.5% w/v	Bovine serum albumin (0–0.8 % w/v)	Ethanol (85 % v/v)	pH = 2.8–4.2 Temperature (°C) = 30 ± 2 Agitation (rpm) = 500 Sonication time (min) = 1–15 US frequency (kHz) = 22	Lactose recovery of 91.48 % and 14.63 % was obtained for 5 min sonication and stirring respectively. Optimum concentration and pH was 17.5 % w/v and 4.2 respectively.	Bund and Pandit, 2007b
20–30 % w/w	–	Ethanol (0.4–6 mL/min)	Heating (°C) = 60 Cooling (°C) = 25 US power (W) = 10–30	Maximum lactose yield of 88 % was obtained for 30 % w/w lactose solution at 1 mL/min ethanol addition rate	Kougoulos et al., 2010
0.131–0.214 g/g water	–	Acetone and isopropanol	Concentric capillary mixer Temperature (°C) = 21 ± 2	Maximum lactose yield of ~90 % obtained by acetone (75 % v/v) and isopropanol (90 % v/v). Acetone as an antisolvent gave best results in terms of morphology.	MacFhionnghaile et al., 2017

Table 1.4 (continued….)

Initial lactose concentration	Additives	Antisolvent	Experimental conditions	Results	Reference
17.3–21.7 % w/v	Protein (0.075–0.105 % w/v)	n-propanol (85 % v/v)	Agitation (rpm) = 325 ± 25 US frequency (kHz) = 22 & 33 US irradiation (min) = 10 & 20	Maximum lactose recovery and purity was ~98 % and ~97 % respectively using ultrasonic horn. Particle size decreased with increase in sonication time and US frequency.	Gajendragadkar and Gogate, 2017
16 % w/v	Protein (0.2–0.8% w/v)	n-propanol (85 % v/v)	pH = 2.9 & 4.2 Temperature (°C) = 30 ± 3 Sonication time (min) = 2–8 US frequency (kHz) = 20	Maximum lactose yield of 85 % w/w was obtained for 4 min of sonication. Span of crystal size distribution decreased with increase in sonication time.	Patel and Murthy, 2011b
70 % w/w	Organic acids, salts, galactose and proteins	–	Heating (°C) = 70 Cooling (°C) = 30 Agitation (rpm) = 600 ± 5	Supplementation of organic acids (lactate, citrate) boosted crystallization while presence of whey proteins slowed down crystal growth.	Gernigon et al., 2013[#]
25 % w/v	κ-carrageenan (150 & 300 mg/L) whey proteins (0.64 %)	–	pH = 7 Heating (°C) = 60 ± 2 Cooling (°C) = 30 Agitation (rpm) = 3500 US frequency (kHz) = 20	The combination of additives gave smallest crystals (6 μm), narrowed crystal size distribution and reduced the generation of amorphous lactose in presence of ultrasound.	Sánchez-García et al., 2018[#]
0.55–0.80 g/g water	α-LM seed crystal (0.1 g/g water)	–	Heating (°C) = 90 Cooling (°C) = 30 Agitation (rpm) = 500 ± 100	A kinetic model accounting for mutarotation, nucleation and crystal growth was presented. Variations in operating temperature, presence of additives (other than lactose) and impurities create an impact on lactose solubility and kinetics.	Mimouni et al., 2009[#]

Table 1.4 (continued….)

Initial lactose concentration	Additives	Antisolvent	Experimental conditions	Results	Reference
33 % w/w	–	–	Oscillatory baffled crystallizer US frequency (Hz) = 4 US amplitude (mm) = 1 Sonication time (h) = 4 Cooling rate = 0.18 °C/min	Ultrasound coupled continuous oscillatory baffled crystallizer reduced cycle time of 13–20 h in batch process to 4 h and reduced mean particle size of less than 1500 μm was obtained.	Siddique et al., 2015#
30–50 % w/w	Glycerin (20 % w/w)	–	Heating (°C) = 90 Cooling (°C) = 25 Agitation (rpm) = 500 US frequency (kHz) = 20	Ultrasound assisted *In-situ* seeding and cooling crystallization resulted complete crystallization in 5 min with rod shaped crystals (15–30 μm) having narrow crystal size distribution (CSD). Addition of glycerin showed narrow CSD, smoother surface and high elongation ratio.	Dhumal et al., 2008#
30–50 % w/w	–	–	Heating (°C) = 80 Cooling (°C) = 10–20 Agitation (rpm) = 500 US amplitude (%) = 20–40 Crystallization time (min) = 2–6	Ultrasound enhanced lactose recovery by 39.17 % compared with only cooling crystallization. The maximum lactose recovery of 85.85 % was obtained at optimum sonication conditions. Initial lactose concentration and US time were significant parameters for the lactose recovery.	Patel and Kayastha, 2018#
0.34–0.55 g/g water	Seed crystals (1 g lactose in 40 mL 2-propanol)	–	Jacketed crystallizer Heating (°C) = 80–85 Cooling with circulating water bath Agitation (rpm) = 942–2512	Formation of first nuclei was found independent of agitation speed while secondary nucleation increases with increase in agitation speed. Minimum agitation in the upper metastable limit should be provided to avoid secondary nucleation and promote crystal growth.	Wong et al., 2011#

Table 1.4 (continued….)

Initial lactose concentration	Additives	Antisolvent	Experimental conditions	Results	Reference
31–67 g/g water	–	–	US frequency (kHz) = 20 Temperature (°C) = 22 US power (W/g) = 0.08–0.30 Sonication time (min) = 1–5	Sonicated samples gave 10.6× higher nucleation and 5.6 × higher yield compared to non sonicated samples. Also slurry density was achieved in 1 min of sonication compared to 60 min of stirring.	Zamanipoor et al., 2013
32 % w/w	Protein whey	–	US frequency (kHz) = 20 Heating (°C) = 30 Cooling (°C) = 15 Agitation (rpm) = 650	Smaller crystal size and narrow crystal size distribution was observed with the application of sonication. Application of sonication at the metastable limit helps in further nuclei generation.	Zisu et al., 2014#
0.3 g/g water*	Lactose phosphate, riboflavin, Glucose 6-phosphate, KCl	–	Continuous stirred glass vessel (2 L volume) Heating (°C) = 80 Cooling (°C) = 30	Increased lactose phosphate (LP) concentration gave decreased growth rate constant, particle median size and yield. Riboflavin gave similar growth rate as LP with unchanged crystal shape. No negative effects for growth rate was observed with addition of glucose 6-phosphate and KCl.	Lifran et al., 2007#
5.0 % w/w	Lactic acid (0.2–1.0 % w/w) Calcium (0.12 % w/w)	–	Heating (°C) = 90 Cooling (°C) = 30 Agitation (rpm) = 500 ± 100	Presence of low content (0.2 % w/w) of lactic acid improved lactose yield (77 %) while higher content (1 % w/w) reduced the yield (59 %). Calcium concentration of 0.072 % w/w along with 0.2 % w/w lactic acid improved crystal size.	Chandrapala et al., 2016#

NM – Not mentioned, * – Calculated lactose concentration, # – cooling crystallization, LM – lactose monohydrate

1.3.3.4 Analysis from literature review on lactose crystallization and scope for research

Table 1.4 shows literature review on lactose antisolvent crystallization and cooling crystallization. It also shows the effect of additives, initial lactose concentration, antisolvent, process conditions on overall lactose recovery or yield and crystal size, shape and morphology. Some authors also showed the effect of seeding on primary and secondary nucleation (Mimouni et al., 2009; Wong et al., 2011). Lactose cooling crystallization was studied with (Dhumal et al., 2008; Zisu et al., 2014; Siddique et al., 2015; Patel and Kayastha, 2018; Sánchez-García et al., 2018) and without (Lifran et al., 2007; Mimouni et al., 2009; Wong et al., 2011; Gernigon et al., 2013; Chandrapala et al., 2016) the assistance of ultrasound. Seeded cooling crystallization showed an impact on mutarotation, nucleation and crystal growth (Mimouni et al., 2009). Increase in agitation during seeding boosted secondary nucleation, hence minimum agitation in the upper metastable limit should be provided to avoid secondary nucleation and promote crystal growth (Wong et al., 2011). Supplementation of additives during crystallization may boost or retard nucleation and crystal growth.

Supplementation of organic acids (lactate, citrate) during cooling crystallization boosted crystallization whereas presence of whey proteins slowed down the crystal growth (Gernigon et al., 2013). Lifran (Lifran et al., 2007) showed the effect of presence of lactose phosphate, riboflavin, glucose 6-phosphate and potassium chloride (KCl) on crystal shape, size, growth rate and yield. Crystal growth rate constant, particle size and yield were decreased with an increase in lactose phosphate concentration. Addition of riboflavin also gave similar results as that of lactose phosphate but the addition of glucose phosphate and KCl gave positive effects

for crystal growth rate. Presence of lower content (0.2% w/w) of lactic acid improved lactose yield while its combination with calcium (0.072% w/w) improved crystal size (Chandrapala et al., 2016).

Application of ultrasound during cooling crystallization showed positive impact on crystal size, shape and morphology. Application of ultrasound in the presence of additives κ-carrageenan and whey proteins gave smallest crystal size, narrowed crystal size distribution and reduction in the amorphous lactose generation (Sánchez-García et al., 2018). Crystallization cycle time and mean particle size was reduced by coupling ultrasound with continuous oscillatory baffled crystallizer (Siddique et al., 2015). Ultrasound assisted *In-situ* seeding (glycerin) and cooling crystallization resulted in narrow crystal size distribution, smaller particles with smoother surface and high elongation ratio (Dhumal et al., 2008). Patel and Kayastha (Patel and Kayastha, 2018) showed an enhancement in lactose recovery by 39 % with the application of ultrasound compared to only cooling crystallization. Application of sonication at the metastable limit helps to generate further nuclei (Zisu et al., 2014).

Antisolvent crystallization with or without the presence of additives showed better results in terms of particle engineering of lactose compared to cooling crystallization. Various antisolvents (acetone, ethanol, butanol, DMSO, n-propanol, isopropanol) solely or in combination were added to find its impact on crystallization. When acetone (Brito and Giulietti, 2007; Patel and Murthy, 2009; Patel and Murthy, 2011a; Simone et al., 2019) was used as an antisolvent, it gave lactose yield of around 90%. Combination of acetone and isopropanol improved lactose yield but better morphology was observed when acetone was used solely (McFhionnghaile et al., 2017). Addition of n-propanol and protein improved lactose yield and purity with ultrasonic irradiation. Increase in irradiation time improved yield to around 98% with

reduced particle size and span of crystal size distribution (Gajendragadkar and Gogate, 2017). Also provision of agitation along with ultrasound helped to increase crystal growth rate and yield.

Ethanol, being a GRAS (generally recognized as safe) solvent, greatly used in the food industries. Effective ethanol concentration in the lactose solution affects mutarotation to form either α-lactose, β-lactose or a combination of both. Vinodhini and Srinivasan (Vinodhini and Srinivasan, 2018) reported that ethanol concentration of upto 45% v/v form α-lactose monohydrate while that in between 65–85% v/v forms β-lactose monohydrate. Combination of ethanol and butanol (20 and 80 mL respectively) gave 100% lactose yield for 30% w/v of initial lactose concentration and gave reduced mean diameter and span of CSD (Kaialy and Nokhodchi, 2012). Ethanol as an antisolvent increased lactose recovery or yield more than 90% (Bund and Pandit, 2007a; Bund and Pandit, 2007b) with the application of sonication. All above studies, whether it is cooling crystallization or antisolvent crystallization generates scope for further research as: (1) antisolvent (solely or in combination) addition rate must be optimized to get better results on crystallization, (2) use of modern techniques such as ultrasound at optimum conditions to get better insight on lactose particle engineering and (3) supply of inert gas (at elevated pressure) such as nitrogen over the reaction volume to observe the changes in crystal size, shape and morphology.

1.4 PRINCIPLES OF ULTRASOUND AND CAVITATION

Ultrasound refers to the sound waves with the frequency beyond the human hearing range (16 Hz – 16 kHz), or typically in the range of 20 kHz to approximately 500 MHz. Sound waves are produced inside the liquid medium with the help of transducer i.e. electric energy is converted to mechanical energy. These sound waves pass in series of alternative compression and rarefaction cycles due to oscillatory motion of fluid elements in the direction of propagation of the wave. The sound wave is characterized based on its frequency (f) and acoustic pressure (P_A) generated inside the liquid medium. The bulk pressure generated inside the liquid medium undergoes periodic variation during propagation of wave. The relation between pressure amplitude (P_A) and bulk pressure inside the liquid medium (P_t) at time t for frequency f can be obtained as (Shah et al., 1999):

$$P_A = P_{A,\max} \sin\left(2\pi ft\right)$$

$$P_t = P_o - P_{A,\max} \sin\left(2\pi ft\right)$$

where, $P_{A,max}$ is the maximum pressure amplitude of the ultrasound wave and P_o is the static pressure in the bulk liquid medium.

Cavitation is a secondary effect of ultrasound. Cavitation can be defined as formation of nuclei, their growth and implosive transient collapse of gas or vapour bubbles inside the liquid medium (see Figure 1.3).

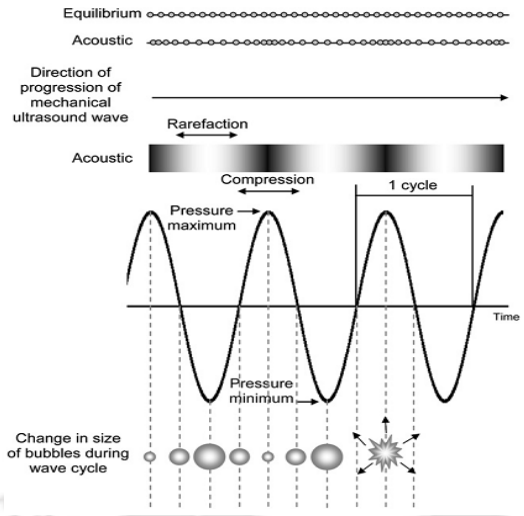

Figure 1.3: Ultrasonic cavitation (Soria and Villamiel, 2010)

Cavitation phenomenon can be explained as follows: During oscillatory motion of the sonic waves, the fluid elements get pulled away from each other. The bond between these fluid elements thus get broken when the amplitude of the sonic waves get strong enough to overcome the Laplace pressure $(2\sigma/r)$ of the liquid medium. This breakage of bond creates void or cavity between the fluid elements. During subsequent compression, this cavity acquires excess energy which leads to the implosion. Theoretically, a cavity is created when the acoustic pressure overcomes the van der Waal's distance between the two molecules which requires enormous pressure of the sonic waves. Typically, this pressure must be greater than 10000 bar. Practically, cavitation occurs at very low pressure of 1.2 bar due to the availability of the nuclei, weak spots or trapped air or gas inside the liquid medium which assists in occurrence of cavitation. The gas pockets or bubbles inside the liquid medium expand due to pressure variation caused by ultrasound which gives rise to the cavitation effect.

1.4.1 Cavitation Bubble Dynamics

As discussed earlier, cavitation is a phenomenon which occurs due to the variations in bulk pressure of liquid medium with the passage of sonic waves through it. Cavitation can be categorized based on this criterion as follows:

Acoustic Cavitation: Acoustic cavitation is generated due to the pressure variations inside the liquid medium with the passage of acoustic wave. It occurs in a frequency range of 20 kHz – 1 MHz.

Hydrodynamic Cavitation: Hydrodynamic cavitation occurs when fluid is passed through different flow geometries which create pressure variations in liquid flow velocity. It occurs at low frequencies ranging from 100 Hz to 10 kHz.

Optical Cavitation: Optical cavitation is a result of local evaporation of liquid due to intense local energy dissipation caused due to sources such as high–intensity laser.

Particle Cavitation: Particle cavitation is produced by any elementary particle (such as proton) rupturing the liquid.

The cavitation phenomenon is influenced by the physical properties of the liquid medium and also many physical factors related to ultrasound. Brief descriptions of the physical properties which affect the cavitation in terms of radial motion of the cavitation bubbles are listed below.

Ultrasound Frequency: An implosive collapse of the bubble in compression half cycle depends on the formation and expansion of the bubble in the rarefaction half cycle. With an increase in ultrasonic frequency, the period of compression and rarefaction half cycle decreases, as a result of which expansion of the bubble reduces and in turn intensity of subsequent transient collapse also reduces. This indicates that the cavitation effect gets lower at higher frequencies. For sonochemical reactions, power ultrasound is generally used in the range of 20-30 kHz. However, higher

frequencies are preferred in oxidation reactions due to the formation of hydroxyl radicals at these frequencies. The acoustic pressure amplitude and net power input required to cause transient cavitation at higher frequencies (in the range of 100-500 kHz) is significantly higher than that for 20 kHz.

Ambient or Static Pressure in the Medium: These factors are of great importance in governing the expansion of the cavitation bubble in the rarefaction half cycle of ultrasound. An ambient pressure inside the liquid medium must be lower so as to form the bubbles of bigger size in the rarefaction half cycle. If the static pressure is at higher side, higher acoustic pressure is needed otherwise the transient cavitation effect gets eliminated and only micro-mixing effect remains.

Acoustic Intensity: Acoustic intensity or acoustic pressure amplitude also plays a major role in cavitation. A minimum pressure amplitude (transient cavitation threshold) is required to create high temperature and pressure peaks in the bubble during the collapse which ultimately requires the expansion of the bubble to at least twice of the initial size. Below this pressure, smaller size bubbles with small amplitude, stable, oscillatory motion will be formed which is not energy intensive. Here, the transient cavitation equals to the static pressure in the liquid medium. The transient cavitation threshold for atmospheric static pressure is about 1.2 to 1.5 bar and the corresponding size range of initial bubble radii that undergo transient motion are 2 – 20 microns.

Physical Properties: Viscosity, Surface Tension and Vapor Pressure: Viscosity of a liquid is a function of solute concentration and temperature. Increase in liquid viscosity retards the radial motions of the bubbles. Also it is responsible for the loss in energy of acoustic waves into thermal. Increase in viscosity limits maximum size of bubbles during radial motion. Also increase in viscosity decreases cavitation intensity

which is a function of temperature and pressure during bubble collapse.

Surface tension is also a phenomenon of cohesive forces between liquid molecules as that of viscosity. Increase in surface tension creates difficulty for cavitation phenomenon to occur by increasing cavitation threshold (minimum pressure amplitude required for cavitation). Increase in surface tension of liquid medium increases intensity of cavitation bubble collapse.

Vapor pressure is a function of the temperature of liquid medium. Ultrasonic irradiation increases the temperature due to thermal and viscous dissipation of the momentum of ultrasonic waves. Increase in vapour pressure causes evaporation of solvent vapor in the bubble which cushions the bubble collapse in compression half cycle of the wave and hence reduces the intensity of collapse. But also some of the vapor gets entrapped in the bubble which generates radical species during the collapse.

1.4.2 Chemical Effects of Cavitation

The chemical effect generated due to ultrasound is popularly known as sonochemical effect. It is the generation of highly reactive radicals such as $^{\bullet}O$, $^{\bullet}OH$ and $HO_2^{\bullet}$ during transient collapse of bubbles. Thermal dissociation of the vapor molecules which are entrapped in cavitation bubbles produces radicals during transient collapse. The temperature at this stage reaches to maximum. Radical generation is due to two major factors viz. composition inside the bubble (number of gas or vapor molecules) and temperature attained inside the bubble at the time of collapse. The composition inside the bubble varies during radial motion due to the phenomenon of gas diffusion, chemical reactions, rectification or water vapor condensation/evaporation. The chemical effects of cavitation during microbial

fermentation, extraction and crystallization can be obtained in details in coming chapters of this thesis.

1.5 AIM, APPROACH AND SCOPE OF THE PRESENT THESIS

As noted in previous sections, development of modern food processing techniques is an urgent need of the hour to overcome the disadvantages of conventional food processing. Modern techniques such as ultrasound has gained good attention in the recent past due to the generation of physical and chemical effects which helps to enhance mass transfer and in turn product yield. Sonication can be applied in extraction of bioactive compounds from plants and microbial/microalgal cells. Sonication can also be applied during fermentation at mild intensity to unfold intracellular enzymes to enhance product yield. Application of ultrasound during crystallization can help to improve product recovery with reduction in agglomeration and amorphous product formation.

The present thesis is aimed at development, optimization and intensification of three food processes with three model systems viz. extraction (astaxanthin), fermentation (riboflavin) and crystallization (lactose). The micro-organisms used for astaxanthin and riboflavin synthesis are *Phaffia rhodozyma* and *Debaryomyces hansenii var. hansenii* respectively. Glucose was used solely as a carbon source in these two food processes. Lactose crystallization is studied with the use of antisolvent at different flow conditions. Process conditions of all these food processes are optimized for maximum product yield. Further, all these food processes are intensified with the application of ultrasound. This thesis comprises of total 6 chapters (including this) and brief content of each chapter is as follows:

- Chapter 1 presents the general introduction to the conventional food processes

and about the three food processes of the study. Various techniques of extraction, fermentation and crystallization for the chosen model systems have been discussed. A brief review of literature on each model system has been presented followed by description of aim and approach of the thesis.

- Chapter 2 presents investigations in ultrasound induced enhancement of astaxanthin from *Phaffia rhodozyma*. The methodology used in this study was statistical optimization of medium components and process parameters, followed by application of sonication at optimum conditions. An attempt was made in the enhancement of intracellular astaxanthin content (comparable to some of the mutant strains) with the application of ultrasound (intermittently) during fermentation. Conventional DMSO (dimethyl sulphoxide) method was used for extraction of astaxanthin from dried cells of *Phaffia rhodozyma.*
- Chapter 3 presents mechanistic investigations in ultrasound assisted astaxanthin extraction from *Phaffia rhodozyma* cells. A preliminary study was performed for screening of effective solvent for maximum astaxanthin extraction yield in different protocols. Screened solvent along with DMSO was used as an extracting solvent. Cell disruption and extraction was done with ultrasonic probe for varying solvent composition. Results on extraction yield were analyzed base on UNIFAC (Universal Quasi-Chemical Functional-Group Activity Coefficients) method and bubble dynamics simulation to get an insight on the factors responsible for maximum astaxanthin extraction.
- Chapter 4 presents investigations in ultrasound induced enhancement of riboflavin from *Debaryomyces hansenii var. hansenii*. The methodology adopted for this study is as follows: (1) Statistical optimization of medium components and process parameters, (2) supplementation of additives such as glycin, $FeCl_3$, $ZnCl_2$ and

$CoCl_2$, and (3) Application of ultrasound during fermentation at optimized conditions. Kinetic study was done using Monod growth model to see the effects of ultrasound on maximum specific growth rate and Monod constant. This chapter also involves the results on flow cytometry and SDS-PAGE analysis to observe changes in cell morphology and expressions of intracellular enzymes respectively with the application of sonication.

- Chapter 5 presents investigations in ultrasound assisted antisolvent crystallization of lactose monohydrate. Antisolvent at different flow rates was added to lactose solutions with mechanical shaking and ultrasound. Ultrasound was applied intermittently after a specific amount of antisolvent addition to observe its effect on lactose recovery and morphology. In addition, some experiments were performed at elevated pressure conditions with application of ultrasound. Recovered lactose crystals were analyzed using FESEM to observe the effects of ultrasound on number of crystals, crystal shape and size, and crystal size distribution (or mean crystal size).
- Chapter 6 represents the summary of the results obtained for all three food processes and overall conclusion of the thesis. Some suggestions have been made based on the results for further study at advanced level.

REFERENCES

Abbas, C.A., Sibirny, A.A., 2011. Genetic control of biosynthesis and transport of riboflavin and flavin nucleotides and construction of robust biotechnological producers. Microbiol. Mol. Biol. Rev. 75 (2), 321–360.

Aguiar, T.Q., Silva, R., Domingues, L., 2015. *Ashbya gossypii* beyond industrial riboflavin production: A historical perspective and emerging biotechnological applications. Biotechnol. Adv. 33 (8), 1774–1786.

Aguiar, T.Q., Silva, R., Domingues, L., 2017. New biotechnological applications for *Ashbya gossypii*: Challenges and perspectives. Bioengineered 8 (4), 309–315.

Amit, S.K., Uddin, M.M., Rahman, R., Islam, S.M.R., Khan, M.S., 2017. A review on mechanisms and commercial aspects of food preservation and processing. Agric & Food Secur 6:51.

An, G.H., Cho, M.H., Johnson, E.A., 1999. Monocyclic Carotenoid Biosynthetic Pathway in the Yeast *Phaffia rhodozyma* (*Xanthophyllomyces dendrorhous*). J. Biosci. Bioeng. 88 (2), 189–193.

Barredo, J.L., García-Estrada, C., Kosalkova, K., Barreiro, C., 2017. Biosynthesis of Astaxanthin as a Main Carotenoid in the Heterobasidiomycetous Yeast *Xanthophyllomyces dendrorhous*. J. Fungi 3, 44.

BASF. 1996. http://www.basf.com/corporate/index.html

Bhatt, P.C., Ahmad, M., Panda, B.P., 2013. Enhanced bioaccumulation of astaxanthin in *Phaffia rhodozyma* by utilising low–cost agro products as fermentation substrate. Biocatal. Agric. Biotechnol. 2, 58–63.

Bhosale, P., Bernstein, P.S., 2005. Microbial xanthophylls. Appl. Microbiol. Biot. 68, 445–455.

Bjerkeng, B., Peisker, M., Schwartzenberg, K.V., Ytrestoyl, T., Asgard, T., 2007. Digestibility and muscle retention of astaxanthin in Atlantic salmon, *Salmo salar*, fed diets with the red yeast *Phaffia rhodozyma* in comparison with synthetic formulated astaxanthin. Aquac. 269, 476–489.

Boretsky, Y.R., Pynyaha, Y.V., Boretsky, V.Y., Fedorovych, D.V., Fayura, L.R., Protchenko, O., Philpott, C.C., Sibirny, A.A., 2011. Identification of the genes affecting the regulation of riboflavin synthesis in the flavinogenic yeast *Pichia guilliermondii* using insertion mutagenesis. FEMS Yeast Res. 11 (3), 307–314.

Brito, A.B.N., Giulietti, M., 2007. Study of lactose crystallization in water-acetone solutions. Cryst. Res. Tech. 42 (6), 583–588.

Bruer, U., Harms, H., 2006. *Debaryomyces hansenii* — an extremophilic yeast with

biotechnological potential. Yeast 23, 415–437.

Bund, R.K., Pandit, A.B., 2007a. Sonocrystallization: Effect on lactose recovery and crystal habit. Ultrason. Sonochem. 14, 143–152.

Bund, R.K., Pandit, A.B., 2007b. Rapid lactose recovery from buffalo whey by use of 'anti-solvent, ethanol'. J. Food Eng. 82 (3), 333–341.

Cannizzaro, C., Rhiel, M., Marison, I., Stockar, U. V., 2003. On–line monitoring of *Phaffia rhodozyma* fed–batch process with in situ dispersive Raman spectroscopy. Biotechnol. Bioeng. 83 (6), 668–680.

Carlos Augusto Monteiro R.B.L., Rafael Moreira Claro, Inês Rugani Ribeiro de Castro, Geofrey Cannon, 2010. A new classifcation of foods based on the extent and purpose of their processing. Cad Saúde Pública 6 (11), 2039–2049.

Chandrapala, J., Wijayasinghe, R., Vasiljevic, T., 2016. Lactose crystallization as affected by presence of lactic acid and calcium in model lactose systems. J. Food Eng. 178, 181–189.

Chaudhuri, S., Batabyal, S., Polley, N., Pal., S.K., 2014. Vitamin B_2 in Nanoscopic Environments under Visible Light: Photosensitized Antioxidant or Phototoxic Drug? J. Phys. Chem. A. 118, 3934–3943.

Chemat, F., Zill-e-Huma, Khan, M.K., 2011. Applications of ultrasound in food technology: Processing, preservation and extraction. Ultrason. Sonochem. 18 (4), 813–835.

Choi, Seok-Keun, Kim, Jeong-Hwan., Park, Young-Sam., Kim, Young-Jin., Chang, Hyo-Ihl., 2007. An Efficient Method for the Extraction of Astaxanthin from the Red Yeast *Xanthophyllomyces dendrorhous*. J. Microbiol. Biotechnol. 17 (5), 847–852.

Crisp, J.L., Dann, S.E., Blatchford, C.G., 2011. Antisolvent crystallization of pharmaceutical excipients from aqueous solutions and the use of preferred orientation in phase identification by powder X-ray diffraction. Eur. J. Pharm. Sci. 42 (5), 568–577.

Cruz, J.M., Parajo, J.C., 1998. Improved astaxanthin production by

Xanthophyllomyces dendrorhous growing on enzymatic wood hydrolysates containing glucose and cellobiose. Food Chem. 63, 479–484.

da Fonseca, R.A. dos Santos., Rafael, R. da Silva., Kalil, S.J., Burkert, C.A.V., Burkert, J.F. de Medeiros., 2011. Different cell disruption methods for astaxanthin recovery by *Phaffia rhodozyma*. Afric. J. Biotechnol. 10 (7), 1165–1171.

Dhumal, R.S., Biradar, S.V., Paradkar, A.R., York, P., 2008. Ultrasound assisted engineering of lactose crystals. Pharm. Res. 25, 2835–2844.

Dmytruk, K.V., Yatsyshyn, V.Y., Sybirna, N.O., Fedorovych, D.V., Sibirny, A., 2011. Metabolic engineering and classic selection of the yeast *Candida famata* (*Candida flareri*) for construction of strains with enhanced riboflavin production. Metab. Eng. 13, 82–88.

Dmytruk, K., Lyzak, O., Yatsyshyn, V., Kluz, M., Sibirny, V., Puchalski, C., Sibirny, A., 2014. Construction and fed-batch cultivation of *Candida famata* with enhanced riboflavin production. J. Biotechnol. 172, 11–17.

Dmytruk, K.V., Abbas, C.A., Voronovsky, A.Y., Kshanovska, B.V., Sybirna, K.A., Sybirny, A.A., 2004. Cloning of structural genes involved in riboflavin synthesis of the yeast *Candida famata*. Ukr. Biokhim. Zh. (1999) 76 (1), 78–87.

Dmytruk, K.V., Sibirny, A.A., 2012. *Candida famata* (*Candida flareri*). Yeast 29, 453–458.

Doyle, M.P. Compendium of the microbiological spoilage of foods and beverages. Food microbiology and food safety. New York: Springer, 2009.

Drake, M.A., Drake, S., Bodyfelt, F.W., Clark, S., Costello, M. The sensory evaluation of dairy products. 2nd ed. New York: Springer; 2008.

Figura, L.O., 1993. The physical modification of lactose and its thermoanalytical identification. Thermochim. Acta. 222 (2), 187–194.

Gajendragadkar, C.N., Gogate, P.R., 2017. Ultrasound assisted intensified recovery of lactose from whey based on antisolvent crystallization. Ultrason. Sonochem.

38, 754–765.

Gänzle, M.G., Haase, G., Jelen, P., 2008. Lactose: Crystallization, hydrolysis and value-added derivatives. Int. Dairy J. 18 (7), 685–694.

Gernigon, G., Baillon, F., Espitalier, F., Floch-Fouéré, C.L., Schuck, P., Jeantet, R., 2013. Effects of the addition of various minerals, proteins and salts of organic acids on the principal steps of a-lactose monohydrate crystallization. Int. Dairy J. 30, 88–95.

Gogate, P.R., Nadar, S.G., 2015. Ultrasound-assisted Intensification of Extraction of Astaxanthin from *Phaffia rhodozyma*. Indian Chem. Eng. 57, 240–255.

Haase, G., Nickerson, T.A., 1966. Kinetic reactions of alpha and beta lactose. I. Mutarotation. J. Dairy Sci. 49 (2), 127–132.

Hara, K.Y., Morita, T., Mochizuki, M., Yamamoto, K., Ogino, C., Araki, M., Kondo, A., 2014. Development of a multi-gene expression system in *Xanthophyllomyces dendrorhous*. Microb. Cell Fact. 13:175.

Hartel, R.W. Crystallization in foods. New York: Springer 2001.

Hu, J., Lei, P., Mohsin, A., Liu, X., Huang, M., Li, L., Hu, J., Hang, H., Zhuang, Y., Guo, M., 2017. Mixomics analysis of *Bacillus subtilis*: effect of oxygen availability on riboflavin production. Microb. Cell Fact. 16:150.

Hu, Z–C., Zheng, Y–G., Wang, Z., Shen, Y–C., 2006. pH control strategy in astaxanthin fermentation bioprocess by *Xanthophyllomyces dendrorhous*. Enzyme. Microb. Technol. 39 (4), 586–590.

Jasim, A., Hosahalli, S.R., Stefan, K., Joyce, I.B. From odors to behaviors in caenorhabditis elegans. In: Novel Food Processing, pp. 1–6. Boca Raton, Florida: CRC Press, 2009.

Jawad, R., Elleman, C., Vermeer, L., Drake, A.F., Woodhead, B., Martin, G.P., Royall, P.G., 2012. The measurement of the β/α anomer composition within amorphous lactose prepared by spray and freeze drying using a simple (1)H-NMR method. Pharm. Res. 29 (2), 511–524.

Jiménez, A., Santos, M.A., Pompejus, M., Revuelta, J.L., 2005. Metabolic engineering of the purine pathway for riboflavin production in *Ashbya gossypii*. Appl. Environ. Microbiol. 71 (10), 5743–5751.

Kaialy, W., Nokhodchi, A., 2012. Antisolvent crystallisation is a potential technique to prepare engineered lactose with promising aerosolisation properties: Effect of saturation degree. Int. J. Pharm. 437, 57–69.

Karel, M., Lund, D.B. Physical principles of food preservation. 2nd ed. New York: CRC Press; 2003.

Kato, T., Park, E.Y., 2012. Riboflavin production by *Ashbya gossypii*. Biotechnol. Lett. 34 (4), 611–618.

Kothari, D., Lee, J.H., Chon, J.W., Seo, K.H., Kim, S.K., 2019. Improved astaxanthin production by *Xanthophyllomyces dendrorhous* SK984 with oak leaf extract and inorganic phosphate supplementation. Food Sci. Biotechnol. 28 (4), 1171–1176.

Kougoulos, E., Marziano, I., Miller, P.R., 2010. Lactose particle engineering: Influence of ultrasound and anti-solvent on crystal habit and particle size. J. Cryst. Growth 312 (23), 3509–3520.

Kurtzman, C.P., Robnett, C.J., 2013. Relationships among genera of the *Saccharomycotina* (*Ascomycota*) from multigene phylogenetic analysis of type species. FEMS Yeast Res. 13, 23–33.

Ledesma Amaro, R., Serrano Amatriain, C., Jiménez, A., Revuelta, J.L., 2015. Metabolic engineering of riboflavin production in *Ashbya gossypii* through pathway optimization. Microb. Cell Fact. 14:163.

Lewin, A. Real food fermentation: preserving whole fresh food with live cultures in your home kitchen, 4th ed. Quarry Books; 2012.

Lifran, E.V., Vu, T.T.L., Durham, R.J., Hourigan, J.A., Sleigh, R.W., 2007. Crystallisation kinetics of lactose in presence of lactose phosphate. Powder Technol. 179, 43–54.

Lim, Gio-Bin., Lee, Sang-Yun., Lee, Eun-Kyu., Haam, Seung-Joo., Kim, Woo-Sik.,

2002. Separation of astaxanthin from red yeast *Phaffia rhodozyma* by supercritical carbon dioxide extraction. Biochem. Eng. J. 11, 181–187.

Lim, S.H., Choi, J.S., Park, E.Y., 2001. Microbial Production of Riboflavin Using Riboflavin Overproducers, *Ashbya gossypii*, *Bacillus subtilis*, and *Candida famate*: An Overview. Biotechnol. Bioprocess Eng. 6, 75–88.

Linehan, V., Thorpe, S., Andrews, N., Kim, Y., Beaini, F., 2012. Food demand to 2050: Opportunities for Australian agriculture: Assessment of risks and opportunities—summary is available at: daff.gov.au/abares/publications.

Liu, Y.S., Wu, J.Y., 2008. Modeling of *Xanthophyllomyces dendrorhous* growth on glucose and overflow metabolism on batch and fed–batch cultures for astaxanthin production. Biotechnol. Bioeng. 101, 996–1004.

Liu, Z.Q., Zhang, J.F., Zheng, Y.G., Shen, Y.C., 2008. Improvement of astaxanthin production by a newly isolated *Phaffia rhodozyma* mutant with low–energy ion beam implantation. J. Appl. Microbiol. 104 (3), 861–872.

MacFhionnghaile, P., Svoboda, V., McGinty, J., Nordon, A., Sefcik, J., 2017. Crystallization Diagram for Antisolvent Crystallization of Lactose: Using Design of Experiments To Investigate Continuous Mixing Induced Supersaturation. Cryst. Growth Des. 17, 2611–2621.

Mateos, L., Jimenez, A., Revuelta, J., Santos, M.A., 2006. Purine biosynthesis, riboflavin production, and trophic-phase span are controlled by a myb-related transcription factor in the fungus *Ashbya gossypii*. Appl. Environ. Microbiol. 72 (7), 5052–5060.

Mayne, S.T., 1996. Beta–carotene, carotenoids, and disease prevention in humans. FASEB. J. 10, 690–701.

McLeod, J.S., Paterson, A.H.J., Bronlund, J.E., Jones, J.R., 2016. The effect of agitation on the nucleation of α-lactose monohydrate. Int. Dairy J. 61, 114–119.

Medeiros, F.O., Alves, F.G., Lisboa, C.R., Martins, D.S., Kalil, S.J., 2008. Ultrasonic waves and glass pearls: a new method of extraction of β-galactosidase for use

in laboratory. Quim. Nova. 31 (2), 336−339.

Michael Davidson, P., Sofos, J.N., Larry Branen, A. Antimicrobials in Food, 3rd ed. Food Science and Technology. CRC Press; 2005.

Michelon, M., de Borba, T. de Matos., Rafael, R. da Silva., Burkert, C.A.V., Burkert, J.F. de Medeiros., 2012. Extraction of Carotenoids from *Phaffia rhodozyma*: A Comparison between Different Techniques of Cell Disruption. Food. Sci. Biotechnol. 21 (1), 1−8.

Mimouni, A., Schuck, P., Bouhallab, S., 2009. Isothermal batch crystallization of alpha lactose: A kinetic model combining mutarotation, nucleation and growth steps. Int. Dairy J. 19, 129−136.

Moriel, D.G., Chociai, M.B., Machado, I.M.P., Fontana, J.D., Bonfim, T.M.B., 2005. Effect of Feeding Methods on the Astaxanthin Production by *Phaffia rhodozyma* in fed-batch Process. Braz. Arch. Biol. Technol. 48 (3), 397−401.

Moriel, D.G., Machado, I.M.P., Fontana, J.D., Bonfim, T.M.B., 2004. Optimization of biomass and astaxanthin production by the yeast *Phaffia rhodozyma*. Braz. J. Pharma. Sci. 40 (3), 421−424.

Nakano, T., Tosa, M., Takeuchi, M., 1995. Improvement of biochemical features in fish health by red yeast and synthetic astaxanthin. J. Agric. Food. Chem. 43, 1570−1573.

National Collection of Yeast Cultures, 2017. Available from: http://www.ncyc.co.uk/

Ni, H., Chen, Q.H., Ruan, H., Yang, Y.F., Li, L.J., Wu, G.B., Hu, Y., He, G.Q., 2007. Studies on optimization of nitrogen sources for astaxanthin production by *Phaffia rhodozyma*. J. Zhejiang. Univ. Sci. B. 8 (5), 365−370.

Ni, H., Chen, Q., He, G., Wu, G., Yang, Y., 2008. Optimization of acidic extraction of astaxanthin from *Phaffia rhodozyma*. J. Zhejiang. Univ. Sci. B. 9 (1), 51−59.

Ohlsson, T., Bengtsson, N. Minimal processing technologies in the food industry. 1st ed. Florida: CRC Press; 2002.

Omar, C.S., Dhenge, R.M., Osborne, J.D., Althaus, T.O., Palzer, S., Hounslow, M.J.,

Salman, A.D., 2015. Roller compaction: Effect of morphology and amorphous content of lactose powder on product quality. Int. J. Pharm. 496 (1), 63–74.

Oraei, M., Razavi, S.H., Khodaiyan, F., 2018. Optimization of effective minerals on riboflavin production by *Bacillus subtilis subsp. subtilis* ATCC 6051 using statistical designs. Avicenna J. Med. Biotech. 10 (1), 49–55.

Palmer, T., Bonner, P. Enzymes, 2nd ed.; Horwood Publishing Limited, 2008.

Pan, X., Wang, B., Gerken, H.G., Lu, Y., Ling, X., 2017. Proteomic analysis of astaxanthin biosynthesis in *Xanthophyllomyces dendrorhous* in response to low carbon levels. Bioprocess Biosyst. Eng. 40 (7), 1091–1100.

Pandalaneni, K., Amamcharla, J.K., Marella, C., Metzger, L.E., 2018. Influence of milk protein concentrates with modified calcium content on enteral dairy beverage formulations: Physicochemical properties. J. Dairy Sci. 101 (11), 9714–9724.

Pandalaneni, K., Amamcharla, K., 2016. Focused beam reflectance measurement as a tool for in situ monitoring of the lactose crystallization process. J. Dairy Sci. 99, 5244–5253.

Parajo, J.C., Santos, V.V., Vazquez, M., 1998. Production of carotenoids by *Phaffia rhodozyma* growing on media made from hemicellulosic hydrolysates of eucalyptus globulus wood. Biotechnol. Bioeng. 59 (4), 501–506.

Parimaladevi, P., Srinivasan, K., 2014. Influence of supersaturation level on the morphology of α-lactose monohydrate crystals. Int. Dairy J. 39 (2), 301–311.

Patel, S.R., Kayastha, P.R., 2018. Ultrasound Assisted Cooling Crystallization of Lactose Monohydrate. Int. J. Chem. Mol. Eng. 12 (2), 58–61.

Patel, S.R., Murthy, Z.V.P., 2009. Ultrasound assisted crystallization for the recovery of lactose in an anti-solvent acetone. Cryst. Res. Technol. 44 (8), 889–896.

Patel, S.R., Murthy, Z.V.P., 2011a. Effect of process parameters on crystal size and morphology of lactose in ultrasound-assisted crystallization. Cryst. Res. Technol. 46 (3), 243–248.

Patel, S.R., Murthy, Z.V.P., 2011b. Waste valorization: Recovery of lactose from partially deproteinated whey by using acetone as anti-solvent. Dairy Sci. & Technol. 91, 53–63.

Pawar, N., Agrawal, S., Methekar, R., 2018. Modeling, Simulation, and Influence of Operational Parameters on Crystal Size and Morphology in Semibatch Antisolvent Crystallization of α Lactose Monohydrate. Cryst. Growth Des. 18, 4511–4521.

Persike, D.S., Bonfim, T.M.B., Santos, M.H.R., Lyng, S.M.O., Chiarello, M.D., Fontana, J.D., 2002. Invertase and urease acivities in the carotenogenic yeast *Xanthophyllomyces dendrorhous*. Bioresour. Technol. 82, 79–85.

Pisponen, A., Pajumägi, S., Mootse, H., Karus, A., Poikalainen, V., 2013. The lactose from Ricotta cheese whey: the effect of pH and concentration on size and morphology of lactose crystals. Dairy Sci. & Technol. 93, 477–486.

Plaut G.W., 1954. Biosynthesis of riboflavin. I. Incorporation of C14-labeled compounds into rings B and C. J. Biol. Chem. 208, 513–520.

Raghavan, S.L., Ristic, R.I., Sheen, D.B., Sherwood, J.N., 2001. The bulk crystallization of α-lactose monohydrate from aqueous solution. J. Pharm. Sci. 90 (7), 823–832.

Ramirez, J., Gutierrez, H., Gschaedler, A., 2001. Optimization of astaxanthin production by *Phaffia rhodozyma* through factorial design and response surface methodology. J. Biotechnol. 88, 259–268.

Ribeiro, A.C.F., Ortona, O., Simões, S.M.N., Santos, C.I.A.V., Prazeres, P.M.R.A., Valente, A.J.M., Lobo, V.M.M., Burrows, H.D., 2006. Binary Mutual Diffusion Coefficients of Aqueous Solutions of Sucrose, Lactose, Glucose, and Fructose in the Temperature Range from (298.15 to 328.15) K. J. Chem. Eng. Data 51 (5), 1836–1840.

Sabaj, J.A.L., 1979. Caderno de Práticas de Bioquímica Fundamental. Edgrafurg, Rio Grande, Rio Grande do Sul, Brasil.

Sánchez-García, Y.I., García-Vega, K.S., Leal-Ramos, M.Y., Salmeron, I., Gutiérrez-

Méndez, N., 2018. Ultrasound-assisted crystallization of lactose in the presence of whey proteins and κ-carrageenan. Ultrason. Sonochem. 42, 714–722.

Sauer, U., Hatzimanikatis, V., Hohmann, H., Manneberg, M., van Loon, A.P.G.M., Bailey, J.E., 1996. Physiology and metabolic fluxes of wild-type and riboflavin-producing *Bacillus subtilis*. Appl. Environ. Microbiol. 62 (10), 3687–3696.

Schewe, H., Kreutzer, A., Schmidt, I., Schubert, C., Schrader, J., 2017. High concentrations of biotechnologically produced astaxanthin by lowering pH in a *Phaffia rhodozyma* bioprocess. Biotechnol. Bioproc. E. 22 (3), 319–326.

Seda-Miró, J.M., Arroyo-González, N., Pérez-Matos, A., Govind, N.S., 2007. Impairment of cobalt-induced riboflavin biosynthesis in a *Debaryomyces hansenii* mutant. Can. J. Microbiol. 53 (11), 1272–1277.

Sedmak, J., Weerasinghe, D., Jolly, S., 1990. Extraction and quantification of Astaxanthin from *Phaffia rhodozyma*. Biotechnol. Techniq. 4 (2) 107–112.

Shah, Y.T., Pandit, A.B., Moholkar, V.S., 1999. Cavitation reaction engineering. Plenum Press, New York.

Siddique, H., Brown, C.J., Houson, I., Florence, A.J., 2015. Establishment of a continuous sonocrystallization process for lactose in an oscillatory baffled crystallizer. Org. Process Res. Dev. 19 (12), 1871–1881.

Silva, E., Aguiar, T.Q., Oliveira, R., Domingues, L., 2019. Light exposure during growth increases riboflavin production, reactive oxygen species accumulation and DNA damage in *Ashbya gossypii* riboflavin-overproducing strains. FEMS Yeast Res. 19 (1), foy114.

Simone, E., Tyler, A.I.I., Kuah, D., Bao, X., Ries, M.E., Baker, D., 2019. Optimal Design of Crystallization Processes for the Recovery of a Slow-Nucleating Sugar with a Complex Chemical Equilibrium in Aqueous Solution: The Case of Lactose. Org. Process Res. Dev. 23 (2), 220–233.

Soria, A.C., Willamiel, M., 2010. Effect of ultrasound on the technological properties

and bioactivity of food. Trends Food Sci. Tech. 21, 323–331.

Stahmann, K.P., Revuelta, J.L., Seulberger, H., 2000. Three biotechnical processes using *Ashbya gossypii*, *Candida famata*, or *Bacillus subtilis* compete with chemical riboflavin production. Appl. Microbiol. Biotechnol. 53 (5), 509–516.

Survase, S.A., Bajaj, I.B., Singhal, R.S., 2006. Biotechnological Production of Vitamins. Food Technol. Biotechnol. 44 (3) 381–396.

Suzuki, G.T., Gabriela, L.F., Macedo, A., 2012. Influence of Nitrogen and Carbon Sources on Riboflavin Production by Wild Strain of *Candida sp*. Food Bioprocess Tech. 5 (2), 466–473.

Suzuki, G.T., Macedo, J.A., Macedo, G.A., 2011. Medium composition influence on biotin and riboflavin production by newly isolated *candida sp*. Braz. J. Microbiol. 42, 1093–1100.

Tao, Y., Sun, D.W., 2015. Enhancement of food processes by ultrasound: a review. Crit. Rev. Food Sci. Nutr. 55 (4), 570–594.

Thomsen, M.K., Lauridsen, L., Skibsted, L.H., Risbo, J., 2005. Two Types of Radicals in Whole Milk Powder. Effect of Lactose Crystallization, Lipid Oxidation, and Browning Reactions. J. Agric. Food Chem. 53 (5), 1805–1811.

Ulrich, J., Strege, C., 2002. Some aspects of the importance of metastable zone width and nucleation in industrial crystallizers. J. Cryst. Growth 237–239 (3), 2130–2135.

United Nations 2011, *World population prospects, the 2010 revision,* United Nations, New York, available at http://esa.un.org/unpd/wpp/index.htm

van der Mensbrugghe, D., Osorio Rodarte, I., Burns, A., Baffes, J., 2009. 'How to feed the World in 2050: Macroeconomic environment, commodity markets – A longer term outlook', paper prepared for How to feed the World in 2050: High-level expert forum, 12–13 October 2009, Rome, available at ftp://ftp.fao.org/docrep/fao/012/ak967e/ak967e00.pdf.

Vanga, S.K., Singh, A., Raghavan, V., 2017. Review of conventional and novel food processing methods on food allergens. Crit. Rev. Food Sci. Nutr. 57 (10),

2077–2094.

Vinodhini, K., Srinivasan, K., 2018. Crystallization of Alpha- Lactose Monohydrate (α-LM) from Aqueous Solution through Gas-Phase Diffusion and Anti-Solvent Crystallization Methods. Mech. Mat. Sci. Eng. DOI: 10.2412/mmse.20.93.441.

Voronovsky, A.Y., Abbas, C.A., Dmytruk, K.V., Ishchuk, O.P., Kshanovska B.V., Sybirna, K.A., Gaillardin, C., Sibirny, A.A., 2004. *Candida famata* (*Debaryomyces hansenii*) DNA sequences containing genes involved in riboflavin synthesis. Yeast 21, 1307–1316.

Vu, L.T.T., Huynh, L., Hourigan, J.A., 2009. Effects of solvents on characteristics of crystalline lactose extracted in ternary and quaternary systems. Adv. Powder Technol. 20, 251–256.

Wang, G., Chen, T., Ma, X., Shen, Z., Zhao, X., 2011. Enhancement of riboflavin production with *Bacillus subtilis* by expression and site-directed mutagenesis of *zwf* and *gnd* gene from *Corynebacterium glutamicum*. Bioresour. Technol. 102 (4), 3934–3940.

Wang, W., Yu, L., 2009. Effects of oxygen supply on growth and carotenoids accumulation by *Xanthophyllomyces dendrorhous*. Z. Naturforsch. C. J. Biosci. 64, 853–858.

Wei, S., Hurley, J., Jiang, Z., Wang, S., Wang, Y., 2012. Isolation and characterization of an *Ashbya gossypii* mutant for improved riboflavin production. Braz. J. Microbiol. 43 (2), 441–448.

Wong, S.Y., Bund, R.K., Connell, R.K., Hartel, R.W., 2011. Determination of the dynamic metastable limit for α-lactose monohydrate crystallization. Int. Dairy J. 21 (11), 839–847.

Wong, S.Y., Bund, R.K., Connell, R.K., Hartel, R.W., 2012. Designing a lactose crystallization process based on dynamic metastable limit. J. Food Eng. 111 (4), 642–654.

Wong, S.Y., Hartel, R.W., 2014. Crystallization in Lactose Refining–A Review. J.

Food Sci. 79 (3), 257–272.

Wu, Q.L., Chen, T., Gan, Y., Chen, X., Zhao, X.M., 2007. Optimization of riboflavin production by recombinant *Bacillus subtilis* RH44 using statistical designs. Appl. Microbiol. Biotechnol. 76 (4), 783–794.

Xiao, A., Jianga, X., Ni, H., Yang, Q., Cai, H., 2015. Study on the relationship between intracellular metabolites and astaxanthin accumulation during *Phaffia rhodozyma* fermentation. Electron. J. Biotechnol. 18 (3), 148–153.

Xie, H., Zhou, Y., Hu, J., Chen, Y., Liang, J., 2014. Production of astaxanthin by a mutant strain of *Phaffia rhodozyma* and optimization of culture conditions using response surface methodology. Ann. Microbiol. 64 (4), 1473–1481.

Xin, Z., Pu, L., Gao, W., Wang, Y., Wei, J., Shi, T., Yao, Z., Guo, C., 2017. Riboflavin deficiency induces a significant change in proteomic profiles in HepG2 cells. Sci. Rep. 7:45861.

Yaguchi, A., Rives, D., Blenner, M., 2017. New kids on the block: emerging oleaginous yeast of biotechnological importance. AIMS Microbiol. 3 (2), 227–247.

Zamanipoor, M.H., Dincer, T.D., Zisu, B., Jayasena, V., 2013. Nucleation and growth rates of lactose as affected by ultrasound in aqueous solutions. Dairy Sci. & Technol. 93, 595–604.

Zeng, X.M., Martin, G.P., Marriott, C., Pritchard, J., 2000. The Influence of Crystallization Conditions on the Morphology of Lactose Intended for Use as a Carrier for Dry Powder Aerosols. J. Pharm. Pharmacol. 52 (6), 633–643.

Zheng, Y.G., Hu, Z.C., Wang, Z., Shen, Y.C., 2006. Large–scale production of astaxanthin by *Xanthophyllomyces dendrorhous*. Food Bioprod. Process. 84 (2), 164–166.

Zhu, Y., Chen, X., Chen, T., Zhao, X., 2007. Enhancement of riboflavin production by overexpression of acetolactate synthase in a pta mutant of *Bacillus subtilis*. FEMS Microbiol. Lett. 266 (2), 224–230.

Zisu, B., Sciberras, M., Jayasena, V., Weeks, M., Palmer, M., Dincer, T.D., 2014.

Sonocrystallisation of lactose in concentrated whey. Ultrason. Sonochem. 21, 2117–2121.

Ultrasound-Induced Enhancement of Intracellular Astaxanthin in *Phaffia rhodozyma*

2.1 INTRODUCTION

Astaxanthin production from wild and mutant strains of *Phaffia rhodozyma* is studied which revealed significance of medium composition and process parameters on intracellular accumulation of astaxanthin. Also astaxanthin yield depends on proper cell disruption method to break the cell completely and extract astaxanthin using effective solvent with high solubility of astaxanthin in it. Astaxanthin efficiency can be enhanced by optimization of medium composition and process parameters. The approach of optimization was found successful in enhancing astaxanthin production with simultaneous reduction in operating cost as demonstrated by several previous authors (An et al., 1999; Ramirez et al., 2001; Moriel et al., 2004; Ni et al., 2007; Ni et al., 2008; Bhatt et al., 2013; Xie et al., 2014; Schewe et al., 2017).

One of the recent techniques of enhancing kinetics and yields of the biochemical processes is sonication. Exposure of the fermentation mixture to sonication (or ultrasound irradiation) of low to moderate intensity results in significant enhancement of both enzymatic and microbial processes. The efficacy of sonication in enhancement of numerous biochemical processes has been well demonstrated in previous works (Borah et al., 2016; Agarwal et al., 2016; Bhasarkar et al., 2015a; Bhasarkar et al., 2015b; Singh et al., 2015a; Singh et al., 2015b). This enhancement is attributed to several physical phenomena associated with physical and chemical effects of ultrasound and cavitation. The principal physical effect of sonication is generation of intense microturbulence in the medium, while the chemical effect is generation of radical and other reactive species from dissociation of solvent vapor inside the transient cavitation bubble. The microturbulence generated by cavitation bubble not only intensifies the mass transfer in the system, but also induces conformational changes in the secondary structure of intracellular enzymes, which augments their activity. These effects are manifested in terms of enhancement of cell metabolism with faster kinetics and higher yields of the fermentation products.

This chapter reports influence of sonication on enhancement of astaxanthin synthesis by wild strain *P. rhodozyma* MTCC 7536. The approach in this study is 3–fold, viz. (1) optimization of the fermentation medium, (2) optimization of fermentation conditions (or parameters), and (3) application of sonication at different stages of fermentation carried out at optimum conditions using optimized media. With the methodology of statistical optimization of *P. rhodozyma* fermentation coupled with sonication, astaxanthin yield from wild strain of *P. rhodozyma* has been enhanced several fold – comparable to the yield from mutant strains – as explained in subsequent sections.

2.2 MATERIALS AND METHODS

2.2.1 Microbial strain and preparation of seed culture

Culture of *Phaffia rhodozyma* MTCC 7536 was obtained from Institute of Microbial Technology (IMTECH), Chandigarh, India, and was maintained on slants of Yeast–Malt Agar (YMA) medium at 4°C and sub–cultured for further use. The cells of *P. rhodozyma* from the slant were incubated at 22°C for 48 h at 150 rpm in an Erlenmeyer flask (250 mL) containing 100 mL sterilized growth medium (10 g glucose, 5 g peptone, 3 g malt extract, 3 g yeast extract, 1000 ml Millipore water).

2.2.2 *P. rhodozyma* fermentation in shake flask

Fermentation of *P. rhodozyma* was carried out in a 250 mL Erlenmeyer flask containing 100 mL of fermentation medium prepared using Millipore water with following composition: 20 g/L glucose, 2 g/L $(NH_4)_2SO_4$, 1 g/L KH_2PO_4, 0.5 g/L $MgSO_4 \cdot 7H_2O$, 0.1 g/L $CaCl_2$, 2 g/L yeast extract. The pH of medium was adjusted to 6.0 as per results of previous literature (Ni et al., 2008). Prior to fermentation, the medium was sterilized by autoclaving at 121°C for 20 min. The sterilized fermentation medium was inoculated with 5% v/v of the seed culture and incubated at 20°C for 84 h with shaking at 150 rpm. Fermentation period was decided on the basis of several preliminary experiments in which the final astaxanthin concentration was monitored. Although the optical density (indicating cell concentration in the medium) in the growth curve of *P. rhodozyma* remained nearly constant from 48 h till 120 h, the actual astaxanthin yield reduced after 84 h. This essentially is a result of degradation or in–situ consumption of astaxanthin by the microbial cells. On the basis of this result, the total time of fermentation in all experiments was fixed at 84 h.

After completion of fermentation, the broth was transferred to centrifuge tubes, and

was centrifuged at 10000 rpm for 10 min to separate the cells. The supernatant was discarded and dry cell weight was determined after drying the cell pellets in hot air oven at 50°C.

2.2.3 Extraction and quantification of astaxanthin

The procedure described by Sedmak (Sedmak et al., 1990) was followed for extraction and analysis of carotenoids accumulated in the yeast cells. The dried yeast was disrupted by addition of hot dimethyl sulphoxide (DMSO) at 55°C followed by vortexing for 5 min. The solution was held stagnant for one hour, and acetone was added to extract the product. In a typical experiment, 0.5 g of dried cells were taken in centrifuge tube, and mixture of DMSO:Acetone in ratio 2:6 mL was added to it. The mixture was vortex agitated for 20–30 s prior to centrifugation at 10000 rpm for 10 min to get the product in the organic phase. Supernatant was filtered prior to analysis with 0.2 µm syringe filter. High performance liquid chromatography (HPLC) was performed for astaxanthin analysis in Shimadzu C18 reverse phase column with UV detector using methanol:water in the ratio of 90:10 (Ni et al., 2008). UV detection was made at 480 nm. The flow rate was maintained at 1.2 mL/min with injection volume of 20 µL.

2.2.4 Statistical Design of Experiments (DoE) for medium optimization

The two step procedure was followed for the optimization of fermentation medium, viz. Plackett–Burman design followed by central composite design (CCD).

2.2.4.1 Plackett–Burman design

Published literature on astaxanthin production from *P. rhodozyma* has reported

use of many medium components (Yamane et al., 1997; Hu et al., 2007; Ni et al., 2008; Lu et al., 2010, Xie et al., 2014, Ye et al., 2015). On the basis of published literature, 5 potential media components, viz. $(NH_4)_2SO_4$, KH_2PO_4, $MgSO_4 \cdot 7H_2O$, $CaCl_2$ and yeast extract, were selected for optimization of fermentation medium. The concentration limits of these medium components were decided on the basis of published literature. Plackett–Burman experimental design with five medium components comprised of 12 experimental runs. Two concentration levels were selected for each medium component, coded as (–1) for lower level and (+1) for higher level, as depicted in Table 2.1. MINITAB (Release 15.1, PA, USA, Trial Version) was used for devising the Plackett–Burman design, and also for the analysis and processing of the data. Plackett–Burman design is a 2–level factorial design that follows 1st order polynomial equation:

$$Y = \beta_o + \sum_{i=1}^{n} \beta_i X_i \qquad (2.1)$$

Notations: Y – response variable (Astaxanthin), β_0 – model intercept, β_i – linear coefficient and X_i – optimization variable (or medium component) (Plackett and Burman, 1946). The significant variables (or media components) from this analysis were used for devising central composite design (CCD) of experiments.

Table 2.1. Factors and levels of Plackett–Burman experimental design

Factors	Levels	
	Low (–1)	High (+1)
(X_1) – $(NH_4)_2SO_4$ (g/L)	1	10
(X_2) – KH_2PO_4 (g/L)	0.5	5
(X_3) – $MgSO_4 \cdot 7H_2O$ (g/L)	0.1	5
(X_4) – $CaCl_2$ (g/L)	0.05	0.3
(X_5) – yeast extract (g/L)	1	10

2.2.4.2 Central composite design (CCD) for medium optimization

Central composite design is used to study individual influence and significant interaction effect between optimization parameters on the response variable. Three significant medium components, viz. $(NH_4)_2SO_4$, $CaCl_2$ and yeast extract, obtained from the Plackett–Burman analysis was used for devising the central composite design. For the experimental design, five levels of the variables mentioned above, coded as $-\alpha$, -1, 0, $+1$, $+\alpha$ were used. The experimental design constituted 20 individual runs ($= 2^k + 2k + n_o$), where 'k' is the number of independent variables, and n_o is the number of replicate runs at the center point of the variable. The statistical analysis was performed according to the response surface methodology using MINITAB software (Release 15.1, PA, USA, Trial Version).

2.2.4.3 Statistical analysis and model fitting

The experimental data of Plackett-Burman and CCD for medium composition was fitted to the following quadratic model containing coefficients corresponding to individual and interactive effects of parameters:

$$Y = \beta_0 + \sum_{i=1}^{k} \beta_i X_i + \sum_{i=1}^{k} \beta_{ii} X_i^2 + \sum_{i \neq j} \sum_{i} \beta_{ij} X_i X_j \qquad (2.2)$$

$$x = (x_i - x_o) / \Delta x \qquad (2.3)$$

where, i = 1, 2, 3…, x_i is the dimensionless value of the variables; x_o is the value of x_i at center point; and Δx is the step change. The analysis of variance (ANOVA) was also done to determine the significance of each factor in fitted model also to determine the goodness of fit. ANOVA of the linear, quadratic and interaction regression coefficients are represented by $F-$ value and $p-$ value. The $F-$ and $p-$ values essentially exhibit the individual and interactive effects of the independent

variables.

2.2.5 Experimental design for fermentation parameters optimization

In addition to composition of the fermentation medium, the operational parameters of fermentations were also optimized using statistical central composite experimental design (CCD). Four parameters were considered for this optimization study, viz. medium pH, temperature, % inoculum and shaking speed. Two concentration levels were selected for each fermentation parameter, coded as (–1) for lower level and (+1) for higher level, as depicted in Table 2.2.

Table 2.2. Factors and levels of central composite design for process parameters

Factors	Levels	
	Low (–1)	High (+1)
(X_1) – Medium pH	4	7
(X_2) – Temperature (°C)	18	24
(X_3) – Shaking speed (rpm)	130	180
(X_4) – Inoculum size (% v/v)	3	8

For the experimental design, five levels of the variables mentioned above, coded as $-\alpha$, -1, 0, $+1$, $+\alpha$ were used. The experimental design constituted 31 individual runs for fermentation/process parameters. The experimental design with permutation/combination of all parameters was devised using MINITAB (Release 15.1, PA, USA, Trial Version) software similar to medium composition and the statistical analysis was performed using response surface methodology. The experimental data was fitted to the quadratic model (stated earlier in eq. 2.2). The analysis of variance (ANOVA) was also done to exhibit the individual and interactive effects of the independent variables on the response variable, i.e. astaxanthin concentration.

2.2.6 Validation experiments

The accuracy of the statistical analysis for optimizations of both media composition and fermentation parameters was assessed with validation experiments. These experiments were carried out in two phases as follows: (1) fermentation using optimized composition of the medium, but unoptimized fermentation parameters viz. pH 6.0, temperature 20°C, mechanical shaking at 150 rpm and inoculum addition of 5% v/v, and (2) fermentation with optimized parameters and optimized medium composition. The substrate concentration, i.e. glucose, was kept same (20 g/L) in all experiments, and total fermentation period was 84 h, as noted earlier. Reproducibility of results of *P. rhodozyma* fermentation was ascertained by performing all validation experiments in triplicate.

2.2.7 *P. rhodozyma* fermentation with sonication

P. rhodozyma fermentation with sonication was carried out using the optimized media composition and fermentation parameters of pH, temperature, inoculum size and mechanical shaking (as per results of statistical central composite experimental design mentioned earlier). For sonication of the *P. rhodozyma* fermentation mixture, an ultrasound bath (PCi Analytics, India, 3.5 L) with the dimensions 30 cm × 15 cm ×10 cm, operating frequency of 33 kHz and power rating of 100W was used. Prior to fermentation experiments, the ultrasound bath was characterized using calorimetric technique for actual power input to the liquid medium in the bath (i.e. water) and the pressure amplitude of the acoustic waves generated in the medium. Pressure amplitude of the ultrasound waves generated in the medium was determined as 1.4 bar (or 140 kPa). Sonication of the fermentation mixture was carried out using pre–optimized duty cycle of 10% (i.e. 1 min of

sonication and 9 min of mechanical shaking in every 10 min of reaction).The reaction flask containing *P. rhodozyma* fermentation mixture was placed at the center of the bath. The position of the flask was carefully maintained same in all experiments in view of spatial variation of the acoustic intensity in the bath (Moholkar et al., 2000; 2002). The temperature of the water in the bath was maintained at 20 ± 2°C using a pump attached to a circulator. In each experiment, sonication of the fermentation mixture was carried out in stationary phase of the *P. rhodozyma* cells (i.e. after 48h of fermentation). In between 48^{th} h till end of fermentation (84^{th} h), the broth was subjected to sonication in three phases (or time divisions), viz. 48 to 60 h, 60 to 72 h and 72 to 84 h. It should be noted that total duration of fermentation (in concurrence with validation experiments) was 84h in each case. The fermentation was subjected to mechanical shaking at 205 rpm for the period other than sonication time division. The experimental setup and protocol is represented by Figs. 2.1 and 2.2 respectively.

Figure 2.1. Experimental setup for ultrasound-assisted *P. rhodozyma* fermentation

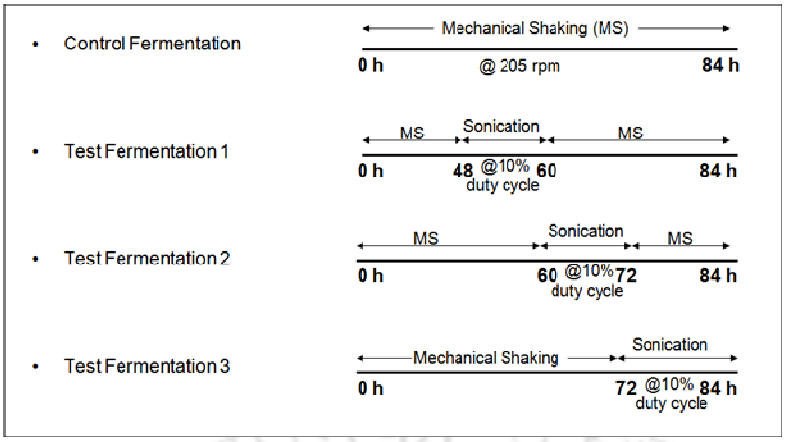

Figure 2.2. Protocol for ultrasound-assisted *P. rhodozyma* fermentation (application of sonication after the cells have reached stationary phase at 48 h)

2.2.8 Determination of change in morphology and viability of yeast cells under ultrasound

Sonication-induced morphological changes in *P. rhodozyma* MTCC 7536 cells were investigated using Flow cytometry (BD CaliburTM Flow Cytometer, BD Biosciences, USA). Samples from both control and test experiments were analyzed using 488 nm laser and 530 nm emission filter. Morphological changes in the cells were evaluated on the basis of FSC (Forward Scatter) and SSC (Side Scatter). Forward-scattered light (FSC) is proportional to cell-surface area or size and side-scattered light (SSC) is proportional to cell granularity or internal complexity.

Viability of *P. rhodozyma* MTCC 7536 cells treated with mechanical shaking and mechanical shaking with sonication (10% duty cycle) was assessed by methylene blue staining method (Painting and Kirsop, 1990). Yeast broth and methylene blue solution (0.1% w/v) were mixed in a ratio of 1:1 and incubated for 5 min. Cells were counted on haemocytometer at 40× magnification. The cell viability was calculated using the following formula:

$$Viability\ (\%) = \frac{No.\ of\ live\ (unstained) cells}{No.\ of\ live\ (unstained) cells + No.\ of\ dead\ (stained) cells} \times 100$$

2.3 RESULTS AND DISCUSSION

2.3.1 Optimization of fermentation medium

2.3.1.1 Plackett-Burman experimental design

The results of initial screening of five medium components using Plackett–Burman experimental design are given in Table 2.3. In the 12 experiments of Plackett–Burman design, the astaxanthin concentration varied from 0.1 to 3.8 mg/L. The statistical analysis of Plackett–Burman design is given in Table 2.4A and B. The 1st–order model coefficients for all five variables along with *t*– and *p*–values are depicted in Table 2.4A, while the ANOVA of the model is given in Table 2.4B. The Pareto plot of the Plackett–Burman analysis is shown in Fig. 2.3, which shows that *t*–value limit for this analysis is 2.447. The *t*–values for $(NH_4)_2SO_4$ (X_1), $CaCl_2$ (X_4) and yeast extract (X_5) are higher than this limit, which indicates their significant influence on the response variable. The overall regression coefficient for the model (R^2 = 0.956) along with adjusted (R^2 = 0.919) represent best fit of the model to experimental data.

Table 2.3. Plackett–Burman design in coded units and astaxanthin titer (mg/L)

Run order	X_1	X_2	X_3	X_4	X_5	Astaxanthin (mg/L)	
						Experimental	Predicted
1	−1	+1	+1	−1	+1	1.3 ± 0.006	1.3
2	−1	−1	+1	+1	+1	0.4 ± 0.002	0.5
3	+1	−1	+1	−1	−1	2.9 ± 0.004	2.7
4	+1	−1	−1	−1	+1	0.3 ± 0.001	0.4
5	−1	+1	+1	+1	−1	2.3 ± 0.007	2.0
6	−1	−1	−1	−1	−1	3.8 ± 0.009	3.4
7	+1	+1	−1	+1	+1	0.9 ± 0.004	1.3
8	+1	+1	+1	−1	+1	0.1 ± 0.001	0.2
9	+1	−1	+1	+1	−1	1.1 ± 0.005	1.4
10	−1	+1	−1	−1	−1	2.4 ± 0.003	2.9
11	+1	+1	−1	+1	−1	0.4 ± 0.002	0.6
12	−1	−1	−1	+1	+1	0.1 ± 0.001	0.2

Table 2.4. Results of Plackett–Burman experimental design for media optimization

(A) Coefficient values, *t*– and *p*– values for each variable

Model term	Coefficient estimate	Computed *t*–value	*p*–value
Intercept	1.188	10.42	0.000*
X_1	0.528	4.63	0.004*
X_2	0.251	2.20	0.070
X_3	–0.161	–1.41	0.208
X_4	0.618	5.42	0.002*
X_5	0.967	8.48	0.000*

*Significant *p* values, $p \leq 0.05$; $R^2 = 0.956$; Predicted $R^2 = 0.823$; Adjusted $R^2 = 0.919$

(B) Analysis of variance (ANOVA) of model

Term	SS	DF	MS	*F*– value	*p*–value
Constant	20.212	5	4.043	25.93	0.000
X_1	3.345	1	3.345	21.45	0.004
X_2	0.756	1	0.756	4.85	0.070
X_3	0.310	1	0.311	1.99	0.210
X_4	4.583	1	4.583	29.39	0.002
X_5	11.218	1	11.218	71.95	0.000
Residual Error	0.936	6	0.156		
Total	21.148	11			

SS – sum of squares; DF – degree of freedom; MS – mean square

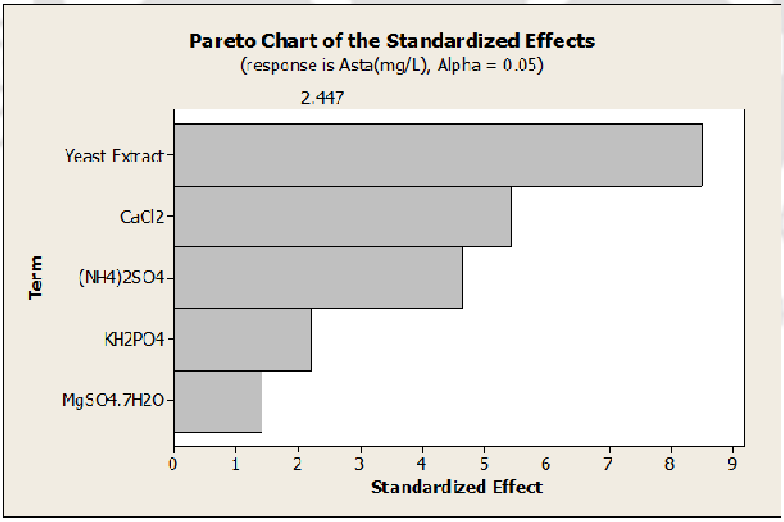

Figure 2.3. Pareto plot for Plackett-Burman analysis

It should be noted that although ANOVA analysis of Plackett–Burman design has indicated that KH_2PO_4 is an insignificant component (due to *p*–value = 0.07), the

t–value of KH_2PO_4 is 2.35, which is slightly lower than the Pareto plot limit of 2.447. Neglecting the insignificant components, the model equation for astaxanthin production could be written as:

$$Y_{yield} = 1.188 + 0.528\ X_1 + 0.618\ X_4 + 0.967\ X_5 \quad (2.4)$$

These results indicate that KH_2PO_4 is not a completely insignificant component of the fermentation medium. The role of KH_2PO_4 in the medium is 3–fold, viz. potassium and phosphate are important growth enhancing nutrients for yeasts. Potassium ion is required for activation of some enzymes catalyzing phosphoryl transfer or elimination reactions, which are part of carotenoid metabolic pathway. Moreover, KH_2PO_4 acts as buffering agent and helps maintaining pH of the fermentation broth at desired value (Yalcin and Ozbas, 2008). Preliminary fermentation experiments with only $(NH_4)_2SO_4$, $CaCl_2$ and yeast extract as medium components resulted in very low astaxanthin yield, which was lesser than the yield in any of the 12 experiments of Placket–Burman design. Therefore, as per the results of Plackett–Burman design KH_2PO_4 was also included in the fermentation medium. In view of the important role of KH_2PO_4 in *P. rhodozyma* fermentation as stated above, it has been added to the fermentation medium in the CCD experiments; albeit in concentration equal to the lower limit of Plackett–Burman design, i.e. 0.5 g/L.

2.3.1.2 Central composite design for medium optimization

The central composite design (CCD) was used to optimize the actual values (or concentrations) of the significant variables (or medium components) from Plackett–Burman design. The full factorial CCD matrix of these variables is given in Table 2.5 along with the response variable of actual and predicted astaxanthin concentration. The coefficients of the quadratic response model (given in eq. 2.2)

along with the *p*– and *t*–values of linear, quadratic and interaction coefficients are given in Table 2.6A. The second–order regression equation for the fitted data is as follows:

$$Y_{yield} = 3.296 + 0.094\,X_1 - 0.794\,X_4 - 0.496\,X_5 - 0.583\,X_1^2 + 0.222\,X_4^2 + 0.387\,X_5^2 - 0.146\,X_1\,X_4 - 0.651\,X_1\,X_5 - 0.447\,X_4\,X_5 \quad (2.5)$$

Table 2.5. Central composite design matrix of significant medium components in coded and actual (in parentheses) values

Run order	$(NH_4)_2SO_4$ (X_1)	$CaCl_2$ (X_4)	Yeast extract (X_5)	Astaxanthin (mg/L)	
				Experimental	Predicted
1	0 (3.5)	0 (0.2)	+α (6.02)	3.6 ± 0.07	3.6
2	0 (3.5)	0 (0.2)	0 (3.5)	3.3 ± 0.05	3.3
3	0 (3.5)	0 (0.2)	−α (0.97)	5.2 ± 0.07	5.2
4	0 (3.5)	0 (0.2)	0 (3.5)	3.3 ± 0.06	3.3
5	0 (3.5)	+α (0.37)	0 (3.5)	2.6 ± 0.03	2.6
6	+α (6.02)	0 (0.2)	0 (3.5)	1.8 ± 0.09	1.8
7	0 (3.5)	0 (0.2)	0 (3.5)	3.3 ± 0.02	3.3
8	+1 (5.0)	+1 (0.3)	−1 (2.0)	4.1 ± 0.01	4.1
9	+1 (5.0)	−1 (0.1)	−1 (2.0)	5.0 ± 0.04	5.1
10	−1 (2.0)	−1 (0.1)	−1 (2.0)	3.3 ± 0.03	3.3
11	0 (3.5)	0 (0.2)	0 (3.5)	3.3 ± 0.04	3.3
12	−1 (2.0)	+1 (0.3)	+1 (5.0)	2.3 ± 0.01	2.3
13	−α (0.97)	0 (0.2)	0 (3.5)	1.5 ± 0.07	1.5
14	−1 (2.0)	−1 (0.1)	+1 (5.0)	4.5 ± 0.02	4.5
15	+1 (5.0)	+1 (0.3)	+1 (5.0)	0.9 ± 0.04	0.9
16	0 (3.5)	0 (0.2)	0 (3.5)	3.3 ± 0.05	3.3
17	0 (3.5)	0 (0.2)	0 (3.5)	3.3 ± 0.02	3.3
18	−1 (2.0)	+1 (0.3)	−1 (2.0)	2.9 ± 0.04	2.9
19	+1 (5.0)	−1 (0.1)	+1 (5.0)	3.6 ± 0.08	3.7
20	0 (3.5)	−α (0.03)	0 (3.5)	5.3 ± 0.06	5.3

The values of the regression coefficients, viz. R^2 = 0.999, predicted R^2 = 0.999, adjusted R^2 = 0.999, not only indicates that the model fits well to the experimental data, but also that 99.9% of the effect on astaxanthin concentration was explained by variation of the optimization parameters (or medium components). The ANOVA for the fitted model is described in Table 2.6B. The desirability function plot for optimum levels of the medium components is shown in Fig. 2.4.

Table 2.6. Results of central composite design for medium optimization

(A) Coefficient values, *t* and *p* values for each variable

Model term	Coefficient	*t*–value	*p*–value
Intercept	3.296	517.69	0.000*
$(NH_4)_2SO_4$ (X_1)	0.094	22.25	0.000*
$CaCl_2$ (X_4)	–0.794	–187.97	0.000*
Yeast Extract (X_5)	–0.496	–117.39	0.000*
$(NH_4)_2SO_4$ (X_1) × $(NH_4)_2SO_4$ (X_1)	–0.583	–141.79	0.000*
$CaCl_2$ (X_4) × $CaCl_2$ (X_4)	0.222	53.90	0.000*
Yeast Extract (X_5) × Yeast Extract (X_5)	0.387	94.01	0.000*
$(NH_4)_2SO_4$ (X_1) × $CaCl_2$ (X_4)	–0.146	–26.43	0.000*
$(NH_4)_2SO_4$ (X_1) × Yeast Extract (X_5)	–0.651	–117.88	0.000*
$CaCl_2$ (X_4) × Yeast Extract (X_5)	–0.447	–81.02	0.000*

*Significant *p* values, $p \leq 0.05$; $R^2 = 0.999$; Predicted $R^2 = 0.999$; Adjusted $R^2 = 0.999$

(B) ANOVA of quadratic model

Source	SS	DF	MS	*F*– value	*p*–value
Regression	25.858	9	2.873	11790.97	0.000
Linear	12.088	3	4.029	16535.73	0.000
Square	8.615	3	2.872	11784.68	0.000
Interaction	5.156	3	1.719	7052.49	0.000
Residual (error)	0.002	10	0.000		
Lack of fit	0.002	5	0.000	1.82	0.260
Pure Error	0.001	5	0.000		
Total	25.861	19			

SS – sum of squares; DF – degree of freedom; MS – mean square

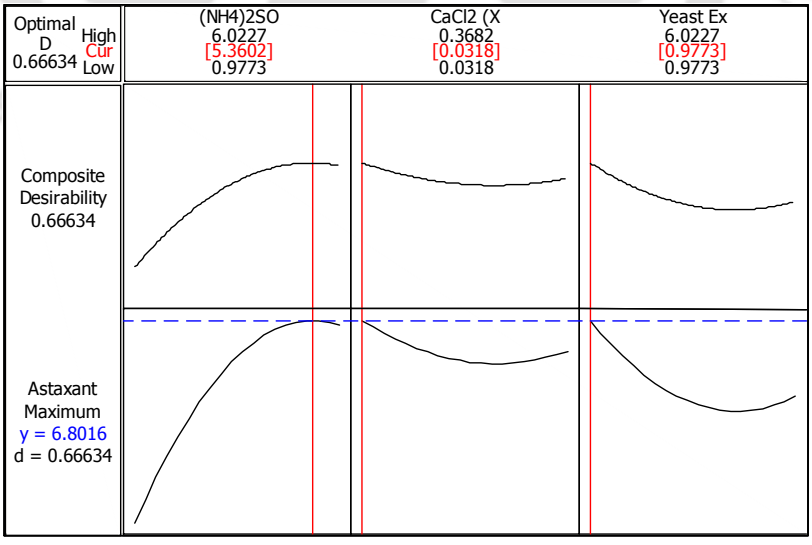

Figure 2.4. Desirability function plot for optimum levels of medium components

The *t*–test, *F*–values and *p*–values of these coefficients are indicative of the significance of these variables. A large *t*–stat value and *p*–value < 0.05 indicates significance of the coefficient and the optimization variable (or medium component) to which the coefficient belongs. Relative *F*–values of linear interaction and quadratic coefficient indicate the significance of the individual effect of the optimization variable and the magnitude of interaction between them. As per ANOVA results given in Table 2.6B, *F*–value of overall regression is 11790.97, while *F*–value of linear coefficient is 16535.73. *p*–values of all linear, quadratic and interaction coefficients are < 0.05, which indicates their significance. The Lack of Fit *F*–value of 1.82 and *p*–value of 0.26 implies that Lack of Fit is not significant as compared to the pure error or in other words the model was significant. It should however be noted that the quadratic regression model is valid only within the limits of optimization variables used in the experimental design. The optimum values of medium components concentrations corresponding to maximum astaxanthin are: a. $(NH_4)_2SO_4$ = 5.36 g/L, b. $CaCl_2$ = 0.032 g/L, c. yeast extract =0.98 g/L. For these optimum values of concentrations of media components, maximum astaxanthin predicted by the quadratic model was 6.8 mg/L.

2.3.2 Optimization of fermentation conditions (or parameters)

Full factorial CCD matrix for optimization of fermentation parameters is given in Table 2.7 along with the response variable of actual and predicted astaxanthin. The coefficients of the quadratic response model (eq. 2.2) fitted to this data, along with the *p*– and *t*–values of linear, quadratic and interaction coefficients, are given in Table 2.8A. The second–order regression equation for the fitted data is as follows:

$$Y_{yield} = 5.472 - 0.091 \cdot X_1 - 0.284 \cdot X_2 + 0.353 \cdot X_3 - 0.449 \cdot X_4 - 0.631 \cdot X_1^2 - 0.517 \cdot X_2^2 - 0.0111 \cdot X_3^2 - 0.455 \cdot X_4^2 - 0.0575\ X_1 \cdot X_2 - 0.551\ X_1 \cdot X_3 - 0.480\ X_1 \cdot X_4 + 0.149\ X_2 \cdot X_3 + 0.0539\ X_2 \cdot X_4 - 0.218\ X_3 \cdot X_4 \quad (2.6)$$

The values of the regression coefficients, viz. R^2 = 0.999, predicted R^2 = 0.998, adjusted R^2 = 0.999 indicate best fit of the model to the experimental data. The ANOVA for the fitted model is described in Table 2.8B. As per ANOVA results given in Table 2.8B, *F*–value of overall regression is 2330.60, while *F*–value of linear coefficient is 1983.08. *p*–values of all linear, quadratic and interaction coefficients are < 0.05, which indicates their significance. The Lack of Fit *F*–value of 2.17 and *p*–value of 0.18 implies that Lack of Fit is not significant as compared to the pure error or in other words the model was significant. It should however be noted that the quadratic regression model is valid only within the limits of optimization variables used in the experimental design. The optimum values of fermentation parameters corresponding to maximum astaxanthin are: a. pH = 4.4, b. temperature = 21.1°C; c. mechanical shaking = 205 rpm, d. % inoculum = 4 % v/v. For these optimum values of fermentation parameters, maximum astaxanthin predicted by the quadratic model was 6.82 mg/L. The desirability function plot showing optimum levels of process parameters is shown in Fig. 2.5.

Table 2.7. Full factorial central composite design matrix of 4 fermentation parameters in coded and actual (in parentheses) values

Run order	Medium pH (X_1)	Temperature (°C) (X_2)	Shaking speed (rpm) (X_3)	Inoculum size (% v/v) (X_4)	Astaxanthin (mg/L)	
					Experimental	Predicted
1	+1 (7.0)	−1 (18)	+1 (180)	+1 (8.0)	2.5 ± 0.02	2.6
2	0 (5.5)	0 (21)	0 (155)	0 (5.5)	5.4 ± 0.06	5.5
3	0 (5.5)	0 (21)	−α (105)	0 (5.5)	4.7 ± 0.03	4.7
4	−1 (4.0)	+1 (24)	+1 (180)	+1 (8.0)	4.7 ± 0.02	4.6
5	0 (5.5)	0 (21)	0 (155)	0 (5.5)	5.5 ± 0.05	5.5
6	+1 (7.0)	+1 (24)	−1 (130)	+1 (8.0)	2.8 ± 0.04	2.8
7	−1 (4.0)	−1 (18)	+1 (180)	−1 (3.0)	5.2 ± 0.04	5.2
8	+1 (7.0)	+1 (24)	+1 (180)	−1 (3.0)	4.5 ± 0.01	4.5
9	−1 (4.0)	−1 (18)	−1 (130)	+1 (8.0)	3.6 ± 0.07	3.6
10	0 (5.5)	0 (21)	0 (155)	−α (0.5)	4.5 ± 0.02	4.5
11	+1 (7.0)	−1 (18)	−1 (130)	+1 (8.0)	3.7 ± 0.08	3.7
12	0 (5.5)	−α (15)	0 (155)	0 (5.5)	3.9 ± 0.03	3.9
13	−α (2.5)	0 (21)	0 (155)	0 (5.5)	3.1 ± 0.05	3.1
14	+1 (7.0)	+1 (24)	−1 (130)	−1 (3.0)	4.1 ± 0.09	4.1
15	+1 (7.0)	−1 (18)	+1 (180)	−1 (3.0)	5.0 ± 0.01	4.9
16	−1 (4.0)	+1 (24)	−1 (130)	−1 (3.0)	2.4 ± 0.01	2.4
17	+α (8.5)	0 (21)	0 (155)	0 (5.5)	2.8 ± 0.09	2.8
18	0 (5.5)	+α (27)	0 (155)	0 (5.5)	2.8 ± 0.07	2.8
19	−1 (4.0)	−1 (18)	−1 (130)	−1 (3.0)	3.2 ± 0.02	3.2
20	0 (5.5)	0 (21)	+α (205)	0 (5.5)	6.1 ± 0.08	6.1
21	0 (5.5)	0 (21)	0 (155)	0 (5.5)	5.5 ± 0.03	5.5
22	−1 (4.0)	+1 (24)	−1 (130)	+1 (8.0)	2.9 ± 0.03	2.9
23	0 (5.5)	0 (21)	0 (155)	0 (5.5)	5.5 ± 0.01	5.5
24	−1 (4.0)	−1 (18)	+1 (180)	+1 (8.0)	4.7 ± 0.07	4.6
25	−1 (4.0)	+1 (24)	+1 (180)	−1 (3.0)	4.9 ± 0.02	4.9
26	0 (5.5)	0 (21)	0 (155)	0 (5.5)	5.5 ± 0.06	5.4
27	0 (5.5)	0 (21)	0 (155)	0 (5.5)	5.5 ± 0.01	5.4
28	0 (5.5)	0 (21)	0 (155)	+α (10.5)	2.8 ± 0.09	2.7
29	+1 (7.0)	+1 (24)	+1 (180)	+1 (8.0)	2.3 ± 0.07	2.2
30	0 (5.5)	0 (21)	0 (155)	0 (5.5)	5.5 ± 0.05	5.4
31	+1 (7.0)	−1 (18)	−1 (130)	−1 (3.0)	5.2 ± 0.03	5.2

Table 2.8. Statistical analysis of central composite experimental design for process parameters

(A) Coefficient values, *t*– and *p*– values for each variable

Model term	Coefficient	t–value	*p*–value
Intercept	5.472	409.01	0.000*
Medium pH (X_1)	–0.091	–12.48	0.000*
Temperature (X_2)	–0.284	–39.24	0.000*
Mechanical shaking (X_3)	0.353	48.81	0.000*
% Inoculum (X_4)	–0.449	–62.09	0.000*
Medium pH (X_1) × Medium pH (X_1)	–0.631	–95.26	0.000*
Temperature (X_2) × Temperature (X_2)	–0.517	–78.11	0.000*
Mechanical shaking (X_3) ×Mechanical shaking (X_3)	–0.011	–1.68	0.110
% Inoculum (X_4) × % Inoculum (X_4)	–0.455	–68.74	0.000*
Medium pH (X_1) × Temperature (X_2)	–0.057	–6.50	0.000*
Medium pH (X_1) ×Mechanical shaking (X_3)	–0.551	–62.25	0.000*
Medium pH (X_1) × % Inoculum (X_4)	–0.480	–54.24	0.000*
Temperature (X_2) ×Mechanical shaking (X_3)	0.149	16.78	0.000*
Temperature (X_2) × % Inoculum (X_4)	0.054	6.09	0.000*
Mechanical shaking (X_3) × % Inoculum (X_4)	–0.218	–24.67	0.000*

*Significant *p* values, $p \leq 0.05$; $R^2 = 0.999$; Predicted $R^2 = 0.998$; Adjusted $R^2 = 0.999$

(B) ANOVA for quadratic model

Source	SS	DF	MS	*F*– value	*p*–value
Regression	40.888	14	2.920	2330.60	0.000
Linear	9.940	4	2.485	1983.08	0.000
Square	21.189	4	5.297	4227.18	0.000
Interaction	9.759	6	1.626	1297.89	0.000
Residual (error)	0.0201	16	0.0013		
Lack of fit	0.0157	10	0.0016	2.17	0.18
Pure Error	0.0043	6	0.0007		
Total	40.908	30			

SS – sum of squares; DF – degree of freedom; MS – mean square

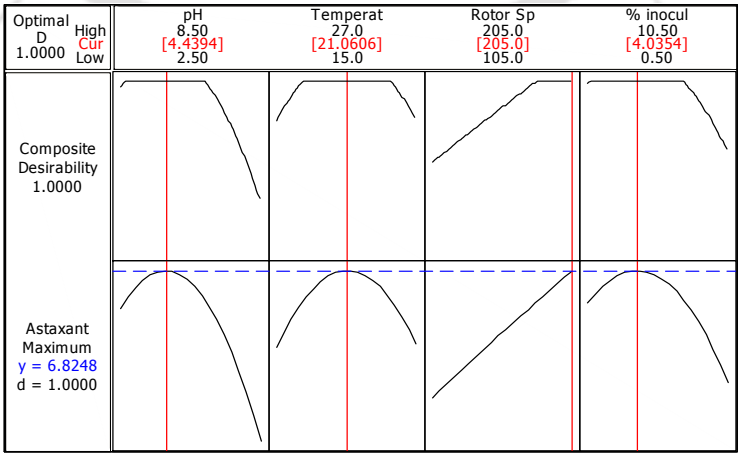

Figure 2.5. Desirability function plot for optimum levels of process parameters

2.3.3 Validation experiment of *P. rhodozyma* fermentation with optimized media and fermentation parameters

Validation of the statistical analyses for optimization of media components and fermentation parameters for astaxanthin production was done by conducting *P. rhodozyma* fermentation using results of the CCD analyses described in preceding sections. The astaxanthin concentrations achieved in this fermentation was 6.8 ± 0.04 mg/L (yield = 1360 µg/g DCW), which was in close agreement with the predictions of the quadratic model of CCD, i.e. 6.82 mg/L. This result essentially corroborates that optimizations of media components and fermentation parameters enhance astaxanthin production by wild strain of *P. rhodozyma*.

2.3.4 Sonication–induced enhancement of Astaxanthin synthesis

As noted in section 2.2.7, the fermentation mixture was subjected to sonication in three phases after the microbial cultures reached stable phase at 48th hour of fermentation. As compared to the astaxanthin concentration (6.8 ± 0.04 mg/L) obtained in fermentation with mechanical shaking, the sonication assisted fermentation shows significant enhancement in astaxanthin synthesis. For the three fermentation experiments, in which sonication was employed in different phases (or stages), the astaxanthin concentrations (represented in Fig. 2.6) were as follows: 48 to 60 h = 7.9 ± 0.07 mg/L (yield = 1521 µg/g DCW), 60 to 72 h = 7.6 ± 0.09 mg/L (yield = 1490 µg/g DCW) and 72 to 84 h = 8.6 ± 0.05 mg/L (yield = 1728 µg/g DCW). This essentially means that sonication of fermentation mixture in the final phase is more effective in enhancing astaxanthin yield. This is an interesting result, and some possible explanations and plausible conjectures for the same can be given as follows: Microbial cultures of *P. rhodozyma* are known to exhibit mixed growth associated

product formation in which the concentration of carotenoids did not coincide with increase in biomass. This feature has been reported by several previous authors (e.g. Park et al., 2007; Kim et al., 2006; Acheampong and Martin, 1995). Yeasts divide by budding on own growth and the growing population of yeast cells has changing cell–age distribution. The intracellular carotenoids content in *P. rhodozyma* depended on the physical maturation towards adulthood. Park et al. (2007) have analyzed the influence of oxygen and glucose on primary metabolism and astaxanthin production. Astaxanthin production rate was found to reduce remarkably under limited oxygen or high concentration of glucose. However, astaxanthin production enhanced with increasing oxygen uptake under aerobic conditions. Liu and Wu (2008) have suggested two–stage strategy for astaxanthin production as follows: (1) during lag phase and early exponential phase, glucose concentration in the fermentation mixture need to be maintained at nearly 25 g/L so that biomass could reach maximum value and (2) low glucose concentration (nearly 5g/L) be used in the exponential/ stationary phase. This strategy resulted in higher biomass production with greater astaxanthin content.

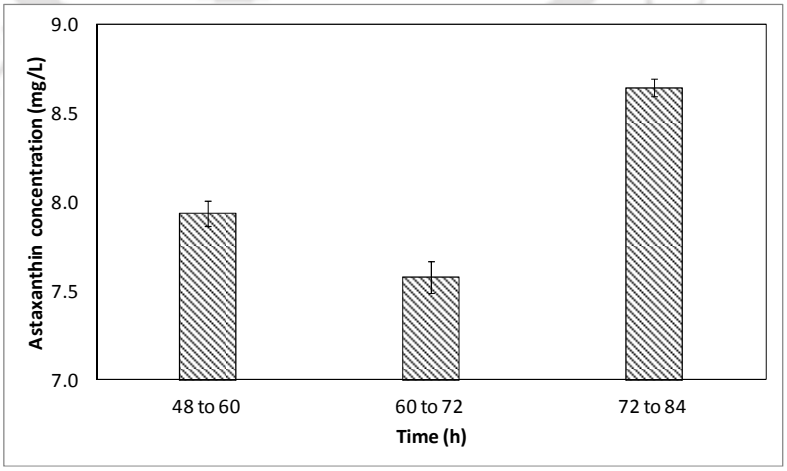

Figure 2.6. Trends in astaxanthin concentration from *P. rhodozyma* fermentation with application of sonication at different stages of fermentation

In present study, sonication of the fermentation mixture in different phases resulted in achieving fermentation conditions similar to those reported by Park et al. (2007) and Liu and Wu (2008). Sonication of the fermentation mixture helped in increasing the degree of physical maturation towards adulthood. Intense mixing induced by ultrasound and cavitation eliminated concentration gradients in the fermentation mixture, and lowered the net concentration of glucose in the fermentation mixture, as the stationary phase of *P rhodozyma* cells was reached after 48 h. Moreover, the micro–mixing induced by sonication is also known to enhance gas–liquid mass transfer, and enhances oxygen uptake in fermentation mixture from atmosphere above the liquid surface (Kumar et al., 2004). All of these phenomena contribute to enhancement of astaxanthin production by *P. rhodozyma* cells. Moreover, these effects are more pronounced when sonication is applied in final 12 h of fermentation (72 to 84 h). Intense microturbulence generated by sonication induces conformational changes in secondary enzyme structure that enhances kinetics of metabolism. As demonstrated in previous work (Borah et al., 2016; Bhasarkar et al., 2015a; Agarwal et al., 2016; Dikshit et al., 2016), sonication of the microbial cells results in unfolding of enzyme with reduction in α–helix content and rise in β–sheets and random coil content. This phenomenon can augment the activity and kinetics of the intracellular enzymes involved in metabolism. For deeper physical insight into biophysical mechanism of ultrasound–induced enhancement in astaxanthin synthesis, further studies are needed along the conjectures presented above.

A comparative analysis of results of present study with published literature on mutant and wild strains of *P rhodozyma* is presented in chapter 1 and it could be inferred that astaxanthin yield in present study (1728 μg/g DCW) is comparable to most of the mutant strains. It should also be noted that experiments in present study have been

performed in shake–flask level, while most of the previous studies have been performed on bioreactor scale, with precise control over fermentation parameters. It is expected that the methodology of ultrasound–assisted astaxanthin synthesis described in present study would yield even better results when applied on bioreactor scale.

2.3.5 Investigations on morphological changes and viability of yeast cells

Flow cytometry analysis was performed to ascertain about morphological changes in the cells obtained after ultrasound-assisted fermentation. The results of which are shown in Fig. 2.7. SSC (side scatter) is a measure roughness of cell surface induced by stress conditions, while FSC (forward scatter) is a measure of the size of the cells, i.e. the higher the FSC greater will be the cell size. Figs. 2.7A and B show acquisition dot plots for control and test samples respectively. As per results shown in Fig. 2.7, no significant change in FSC and SSC is observed for the cells from control and test fermentations, which indicated that internal complexity and morphology of yeast cells remains unaltered during ultrasound exposure. This is represented by the presence of majority of cells in the lower left quadrant in control fermentation (99.8 %), and test fermentation (99.6 %).

Figure 2.8 A and B represents methylene blue staining of cells obtained from control and ultrasound induced fermentation respectively. Methylene blue staining (presented in supplementary material) and calculation of viability of cell count method revealed that no cell death occurred during sonication. Yeast cell viability in control and test samples was ~85% and ~87% respectively. These results on morphology and viability of yeast cells represent no morphological change in *P. rhodozyma* cells due to exposure to sonication.

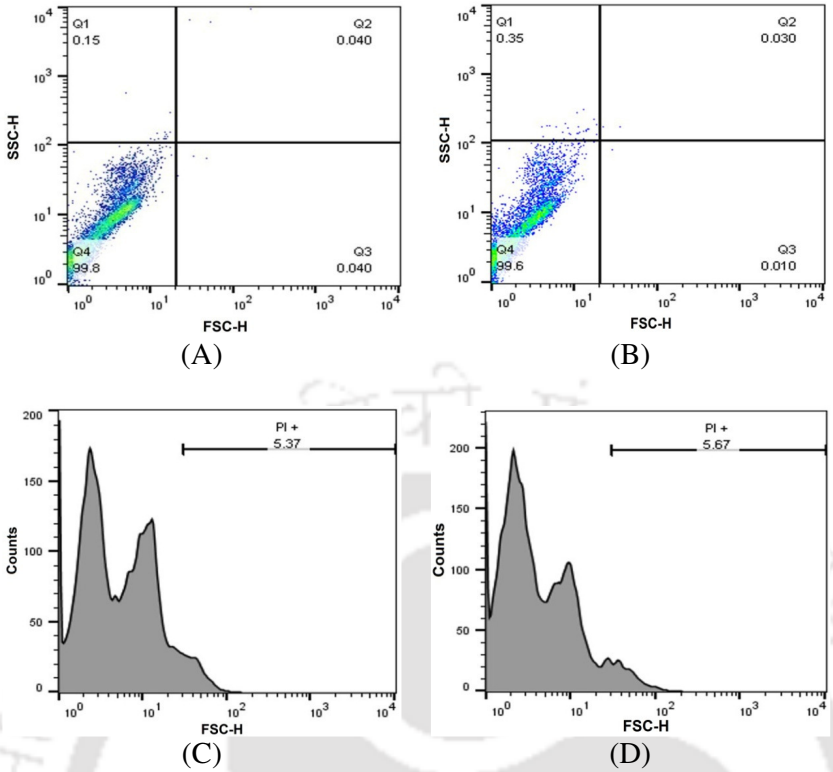

Figure 2.7. Flow cytometric analysis for detecting morphological changes in *P. rhodozyma* cells under the influence of ultrasound. (A) and (B) Acquisition dot plots of *P. rhodozyma* in control and test samples, respectively, (C) and (D) Histogram plots of *P. rhodozyma* in control and test samples, respectively.

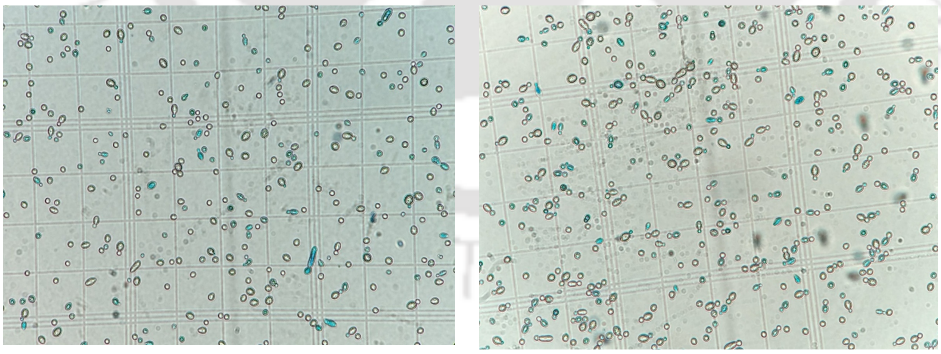

(A) (B)

Figure 2.8. Micrographs of methylene blue stained yeast cells after completion of fermentation in (A) control experiments and (B) test experiments.

2.4 CONCLUSION

Statistical optimization of medium composition and fermentation parameters for astaxanthin production from wild strain of *P. rhodozyma* has been done, followed by intensification using sonication. Under optimum conditions of media composition and fermentation parameters, wild strain of *P. rhodozyma* yielded 6.8 mg/L or 1360 µg/g DCW astaxanthin, which enhanced to 8.6 mg/L or 1728 µg/g DCW with application of 33 kHz sonication. This enhancement is attributed to intense micromixing induced by sonication, which has several possible implications such as physical maturation of cells, reduction in substrate inhibition and conformational changes in secondary structure of intracellular enzymes.

REFERENCES

Acheampong, E.A., Martin, A.M., 1995. Kinetic studies on the yeast *Phaffia rhodozyma*. J. Basic. Microbiol. 35, 147–155.

Agarwal, M., Dikshit, P.K., Bhasarkar, J.B., Borah, A.J., Moholkar, V.S., 2016. Physical Insight into Ultrasound–Assisted Biodesulfurization using Free and Immobilized Cells of *Rhodococcus rhodochrous* MTCC 3552. Chem. Eng. J. 295, 254–267.

An, G.H., Cho, M.H., Johnson, E.A., 1999. Monocyclic Carotenoid Biosynthetic Pathway in the Yeast *Phaffia rhodozyma (Xanthophyllomyces dendrorhous)*. J. Biosci. Bioeng. 88 (2), 189–193.

Barredo, J.L., García-Estrada, C., Kosalkova, K., Barreiro, C., 2017. Biosynthesis of Astaxanthin as a Main Carotenoid in the Heterobasidiomycetous Yeast *Xanthophyllomyces dendrorhous*. J. Fungi. 3, 44.

Bhasarkar, J.B., Borah, A.J., Goswami, P., Moholkar, V.S., 2015a. Mechanistic analysis of ultrasound assisted enzymatic desulfurization of liquid fuels using *horseradish peroxidase*. Bioresour. Technol. 196, 88–98.

Bhasarkar, J.B., Dikshit, P., Moholkar, V.S., 2015b. Ultrasound Assisted Biodesulfurization of Liquid Fuel using Free and Immobilized Cells of *Rhodococcus rhodochrous* MTCC 3552: A Mechanistic Investigation. Bioresour. Technol. 187, 369–378.

Bhatt, P.C., Ahmad, M., Panda, B.P., 2013. Enhanced bioaccumulation of astaxanthin in *Phaffia rhodozyma* by utilising low–cost agro products as fermentation substrate. Biocatal. Agric. Biotechnol. 2, 58–63.

Bhosale, P., Bernstein, P.S., 2005. Microbial xanthophylls. Appl. Microbiol. Biot. 68, 445–455.

Borah, A.J., Agarwal, M., Poudyal, M., Goyal, A., Moholkar, V.S., 2016. Mechanistic investigation in ultrasound induced enhancement of enzymatic hydrolysis of invasive biomass species. Bioresour. Technol. 213, 342–349.

Cannizzaro, C., Rhiel, M., Marison, I., Stockar, U.V., 2003. On–line monitoring of *Phaffia rhodozyma* fed–batch process with in situ dispersive Raman spectroscopy. Biotechnol. Bioeng. 83 (6), 668–680.

Dikshit, P.K., Moholkar, V.S., 2016. Optimization of 1,3–dihydroxyacetone production from crude glycerol by immobilized *Gluconobacter oxydans* MTCC 904. Bioresour. Technol. 216, 1058–1065.

Hu, Z., Zheng, Y., Wang, Z., Shen, Y., 2007. Production of Astaxanthin by *Xanthophyllomyces dendrorhous* ZJUT46 with Fed–Batch fermentation in 2.0 m^3 fermentor. Food. Technol. Biotechnol. 45 (2), 209–212.

Hu, Z–C., Zheng, Y–G., Wang, Z., Shen, Y–C., 2005. Effect of sugar–feeding strategies on astaxanthin production by *Xanthophyllomyces dendrorhous*. World. J. Microbiol. Biotechnol. 21 (5), 771−775.

Hu, Z–C., Zheng, Y–G., Wang, Z., Shen, Y–C., 2006. pH control strategy in astaxanthin fermentation bioprocess by *Xanthophyllomyces dendrorhous*. Enzyme. Microb. Technol. 39 (4), 586−590.

Kim, J.H., Choi, S.K., Park, Y.S., Yun, C.W., Cho, W.D., Chee, K.M., Chang, H.I., 2006. Effects of culture conditions on astaxanthin formation in red yeast *Xanthophyllomyces dendrorhous* mutant JH1. J. Microbiol. Biotechnol. 16, 438−442.

Kumar, A., Gogate, P.R., Pandit, A.B., Delmas, H., Wilhelm, A.M., 2004. Gas–liquid mass transfer studies in sonochemical reactors. Ind. Eng. Chem. Res. 43, 1812−1819.

Kusdiyantini, E., Gaudin, P., Goma, G., Blanc, P.J., 1998. Growth kinetics and astaxanthin production of *Phaffia rhodozyma* on glycerol as a carbon source during batch fermentation. Biotechnol. Lett. 20 (10), 929−934.

Liu, Y.S., Wu, J.Y., 2008. Modeling of *Xanthophyllomyces dendrorhous* growth on glucose and overflow metabolism on batch and fed–batch cultures for astaxanthin production. Biotechnol. Bioeng. 101, 996−1004.

Liu, Z.Q., Zhang, J.F., Zheng, Y.G., Shen, Y.C., 2008. Improvement of astaxanthin production by a newly isolated *Phaffia rhodozyma* mutant with low–energy ion beam implantation. J. Appl. Microbiol. 104 (3), 861−872.

Lu, M., Zhang, Y., Zhao, C., Zhou, P., Yu, L., 2010. Analysis and Identification of Astaxanthin and its Carotenoid Precursors from *Xanthophyllomyces*

dendrorhous by High–Performance Liquid Chromatography. J. Phy. Sci. 65 c 489–494.

Mayne, S.T., 1996. Beta–carotene, carotenoids, and disease prevention in humans. FASEB. J. 10, 690–701.

Meyer, P.S., du Preez, J.C., 1993. Effect of acetic acid on astaxanthin production by *Phaffia rhodozyma*. Biotechnol. Lett. 15 (9), 919–924.

Meyer, P.S., du Preez, J.C., 1994. Astaxanthin production by a *Phaffia rhodozyma* mutant on grape juice. World. J. Microbiol. Biotechnol. 10 (2), 178–183.

Moholkar, V.S., Huitema, M., Rekveld, S., Warmoeskerken, M.M.C.G., 2002. Characterization of an ultrasonic system using wavelet transforms. Chem. Eng. Sci. 57, 617–629.

Moholkar, V.S., Sable, S.P., Pandit, A.B., 2000. Mapping the cavitation intensity in an ultrasonic bath using the acoustic emission. AIChE. J. 46, 684–694.

Moriel, D.G., Machado, I.M.P., Fontana, J.D., Bonfim, T.M.B., 2004. Optimization of biomass and astaxanthin production by the yeast *Phaffia rhodozyma*. Braz. J. Pharma. Sci. 40 (3), 421–424.

Nakano, T., Tosa, M., Takeuchi, M., 1995. Improvement of biochemical features in fish health by red yeast and synthetic astaxanthin. J. Agric. Food. Chem. 43, 1570–1573.

Ni, H., Chen Q.H., Ruan, H., Yang, Y.F., Li, L.J., Wu, G.B., Hu, Y., He, G.Q., 2007. Studies on optimization of nitrogen sources for astaxanthin production by *Phaffia rhodozyma*. J. Zhejiang. Univ. Sci. B. 8 (5), 365–370.

Ni, H., Chen, Q., He, G., Wu, G., Yang, Y., 2008. Optimization of acidic extraction of astaxanthin from *Phaffia rhodozyma*. J. Zhejiang. Univ. Sci. B. 9 (1), 51–59.

Painting, K., Kirsop, B., 1990. A quick method for estimating the percentage of viable cells in a yeast population using methylene blue staining. World J. Microbiol. Biotechnol. 6, 346–347.

Plackett, R.L., Burman, J.P., 1946. The design of optimum multifactorial experiments. Biometrika. 33, 305–325.

Ramirez, J., Gutierrez, H., Gschaedler, A., 2001. Optimization of astaxanthin production by *Phaffia rhodozyma* through factorial design and response surface methodology. J. Biotechnol. 88, 259–268.

Schewe, H., Kreutzer, A., Schmidt, I., Schubert, C., Schrader, J., 2017. High Concentrations of Biotechnologically Produced Astaxanthin by lowering pH in a *Phaffia rhodozyma* Bioprocess. Biotechnol. Bioproc. Eng. 22, 319–326.

Sedmak, J., Weerasinghe, D., Jolly, S., 1990. Extraction and quantification of Astaxanthin from *Phaffia rhodozyma*. Biotechnol. Techniq. 4 (2), 107–112.

Singh, S., Sarma, S., Agrawal, M., Goyal, A., Moholkar, V.S., 2015a. Mechanistic insight into ultrasound induced enhancement of simultaneous saccharification and fermentation of *Parthenium hysterophorus* for ethanol production. Ultrason. Sonochem. 26, 245–256.

Singh, S., Sarma, S., Agrawal, M., Goyal, A., Moholkar, V.S., 2015b. Ultrasound enhanced ethanol production from *Parthenium hysterophorus*: A mechanistic investigation. Bioresour. Technol. 188, 287–294.

Xiao, A., Jiang, X., Ni, H., Yang, Q., Cai, H., 2015. Study on the relationship between intracellular metabolites and astaxanthin accumulation during *Phaffia rhodozyma* fermentation. Electron. J. Biotechn. 18, 148–153.

Xie, H., Zhou, Y., Hu, J., Chen, Y., Liang, J., 2014. Production of astaxanthin by a mutant strain of *Phaffia rhodozyma* and optimization of culture conditions using response surface methodology. Ann. Microbiol. 64, 1473–1481.

Yalcin, S.K., Ozbas, Z.Y., 2008. Effects of ammonium sulfate concentration on growth and glycerol production kinetics of two endogenic wine yeast strains. Indian. J. Biotechnol. 7, 89–93.

Yamane, Y., Higashida, K., Nakashimada, Y., Kakizono, T., Nishio, N., 1997. Astaxanthin production by *Phaffia rhodozyma* enhanced in fed–batch culture with glucose and ethanol feeding. Biotechnol. Lett. 19 (11), 1109–1111.

Ye, L., Xie, W., Zhou, P., Yu, H., 2015. Biotechnological Production of Astaxanthin through Metabolic Engineering of Yeasts. Chem. Bio. Eng. Rev. 2, 1–12.

Zheng, Y.G., Hu, Z.C., Wang, Z., Shen, Y.C., 2006. Large–scale production of astaxanthin by *Xanthophyllomyces dendrorhous*. Food. Bioprod. Process. 84 (2), 164–166.

Ultrasound-Assisted Extraction of Astaxanthin from *Phaffia rhodozyma* cells

3.1 INTRODUCTION

Astaxanthin production from microbial/microalgal strains depends on two major techniques viz. optimized conditions of medium components and process parameters and effective cell disruption (using disrupting agents/mechanical means) and astaxanthin extraction using effective solvent with high solubility of astaxanthin in it. The technique of optimum conditions have assured in accumulation of more astaxanthin inside the cells as seen in previous chapter. Proper cell disruption and complete extraction of intracellular astaxanthin can be assured by observing color change of cells from reddish brown to complete white. The microbial cells of *Phaffia rhodozyma* have rigid cell wall which is difficult to disrupt. Conventional mechanical techniques of cell wall disruption include bead milling, abrasion with celite (Valduga

et al., 2007), abrasion with glass pearls (Medeiros et al., 2008; da Fonseca et al., 2011), or ultrasound treatment (da Fonseca et al., 2011; Michelon et al., 2012; Gogate and Nadar, 2015). The chemical methods for cell disruption and astaxanthin extraction include treatment with DMSO (Dimethyl sulfoxide) or acid pretreatment (Sedmak et al., 1990; Persike et al., 2002; Ni et al., 2008; Bhatt et al., 2013; Batghare et al., 2018). Some authors have also applied combination of two or more techniques such as sonication with DMSO treatment or acid treatment with sonication or lactic acid treatment with sonication (Bhatt et al., 2013; Gogate and Nadar, 2015; Batghare et al., 2018). Summary of previous literature on different techniques of *P. rhodozyma* cell disruption and extraction of astaxanthin is provided in chapter 1. In previous chapter, application of ultrasound during fermentation found to increase intracellular astaxanthin content although cell disruption and extraction was done by conventional DMSO method with the use of acetone as a solvent which resulted in maximum astaxanthin yield of 1.728 mg/g DCW (dry cell weight).

In this chapter, an attempt was made to address the issue of application of sonication in the downstream process of astaxanthin recovery from dry cells of *P. rhodozyma* after completion of fermentation. In this study, astaxanthin fermentation has been conducted using conventional technique of mechanical shaking in an incubator-shaker. The extent of astaxanthin extraction depends on two factors, viz. the solubility of astaxanthin in the extractant (or solvent) and intensity of convection in the extraction mixture. In the present study, an attempt was made to gain a mechanistic insight into the process of extraction of astaxanthin from dry cells of *P. rhodozyma*. The solvent employed in present study is mixture of acetone and DMSO with varying composition. Moreover, sonication has been applied during the extraction. The experimental results on astaxanthin extraction have been analyzed vis-

à-vis two models: (1) the thermodynamic model for prediction of astaxanthin solubility in mixtures of acetone and DMSO (based on UNIFAC (Universal Quasi-Chemical Functional-Group Activity Coefficients) method for estimation of activity coefficients), and (2) bubble dynamics model for estimation of intensity of convection generated in the extraction mixture during sonication. The convection generated during sonication is attributed to three physical mechanisms, viz. microstreaming, microturbulence and acoustic waves. The intense convection generated by sonication on extremely small spatial scale is highly effective in enhancing the mass transfer characteristics of the system, as illustrated in previous studies (Bhasarkar et al., 2015a; Bhasarkar et al., 2015b; Singh et al., 2015a; Singh et al., 2015b; Agarwal et al., 2016; Borah et al., 2016). On the basis of this analysis, we have tried to optimize the composition of DMSO and acetone for maximum astaxanthin extraction.

3.2 MATERIALS AND METHODS

3.2.1 Analytical Reagents

The astaxanthin standard for calibration was obtained from Sigma Aldrich Co. Ltd. Other reagents such as DMSO, acetone, petroleum ether, methanol and ethanol of analytical grade were obtained from Himedia Ltd. All the media components required for fermentation were obtained from Himedia Ltd. Deionized water was used for the preparation of growth and fermentation media solution from the Mili Q Plus (Elix 3, Millipore SA) water treatment system.

3.2.2 *P. rhodozyma* growth and maintenance

The details of microbial strain and preparation of seed culture is as per the information provided in chapter 2. An un-optimized fermentation media was used for

fermentation with following composition: 20 g/L glucose, 2 g/L $(NH_4)_2SO_4$, 1 g/L KH_2PO_4, 0.5 g/L $MgSO_4 \cdot 7H_2O$, 0.1 g/L $CaCl_2$, 2 g/L yeast extract. The fermentation media was sterilized by autoclaving at 121°C for 20 min prior to fermentation with an adjusted pH of 6.0. The sterilized fermentation medium was inoculated with 5% v/v of the seed culture (growth media) and incubated at 20°C for 84 h (fermentation period) with mechanical shaking at 150 rpm. After completion of fermentation, the cells were harvested by centrifugation and vacuum filtration. The dry cell weight (DCW) was determined after drying the cell pellets in hot air oven at 50°C. The dried cell mass was used for extraction experiments.

3.2.3 Preliminary experiments: Screening of extraction solvents

Preliminary experiments were performed to decide the solvent system in which extraction efficiency of different solvents was screened. In these experiments, following solvents were tested for extraction of astaxanthin: petroleum ether, methanol, acetone and ethanol. The total volume of extraction mixture was maintained constant at 15 mL. For every solvent, extraction experiments were carried out using three protocols (– with three experimental runs or replicates in each protocol to assess reproducibility) as shown in Table 3.1.

Table 3.1. Preliminary experiments for screening of extraction solvents

Experimental protocols	Dry cell mass (g)	DMSO (mL)	Solvent[@] (mL)
Protocol 1[*]	0.4	–	15
Protocol 2[#]		5	10
Protocol 3[*]		5	10

* – application of sonication, # – mechanical shaking, @ – acetone, ethanol, methanol or petroleum ether

Extraction mixture was sonicated using an ultrasonic probe (13 mm dia.), operated at a frequency of 20 kHz (Model VCX 500, 20 kHz, 500 W) with the help of

a microprocessor controlled unit. The sonicator system was operated at 20% amplitude corresponding to theoretical power dissipation of 100 W. An important feature of ultrasound-assisted extraction is the duty cycle of sonication. In order to optimize this parameter, preliminary experiments were carried out with 20, 40, 60 and 80% duty cycles and also with continuous sonication (100% duty cycle). Extent of cell disruption was negligible for 20 and 40% duty cycles. Some cell disruption occurred for 60% duty cycle (as seen from moderate change of color of pellets brown to white). Almost total change of color of pellets was seen for 80% duty cycle indicating complete disruption of the cells. However, for continuous sonication, the temperature of the solution increased rapidly which could possibly lead to denaturing/ degradation of the astaxanthin. On the basis of these results, optimum duty cycle was maintained at 80% (i.e. 48 s sonication and 12 s silent period per min of treatment) in all experiments. Total time of treatment in all three protocols was 30 min. After completion of extraction treatment, the mixture was centrifuged and organic phase was collected for analysis. The astaxanthin yields per unit mass of dry cell weight in the three protocols employing four solvents are depicted in Figure 3.1. It could be inferred from Figure 3.1 that the highest astaxanthin yield of 1.510 mg/g DCW was obtained for the third protocol with acetone as the solvent for extraction.

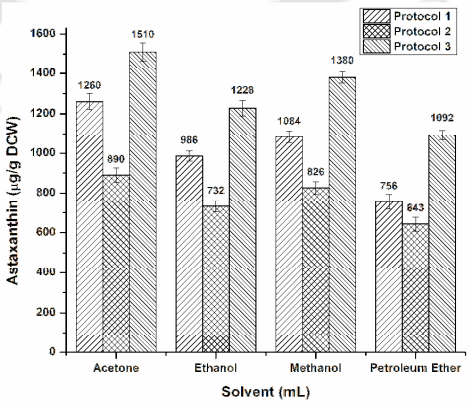

Figure 3.1. Preliminary experiments on extraction of astaxanthin using different solvents

Comparing the results shown in Figure 3.1 for acetone as extraction solvent for three protocols outlined in this section, we can determine the efficiency of sonication on the basis of incremental yields of astaxanthin with addition of cell disrupting agent (DMSO) and sonication.

(1) Extraction with mixture of acetone (67% v/v) and DMSO (33% v/v) with mechanical stirring yielded 890 µg/g DCW astaxanthin – the least among all protocols.

(2) Extraction with pure acetone as solvent with sonication yielded 1260 µg/g DCW astaxanthin – which was an enhancement of ~ 42%.

(3) Extraction with mixture of acetone (67% v/v) and DMSO (33% v/v) with sonication yielded 1510 µg/g DCW astaxanthin – which was further enhancement of 22%.

Simultaneous application of cell disrupting agent DMSO and sonication is expected to give almost complete recovery of astaxanthin from dry cell weight. Use of sonication thus obviates repetitive use of DMSO for complete disruption of microbial cells and full extraction/recovery of astaxanthin.

On the basis of these results, further experiments were carried out using acetone as the solvent for extraction, with varying quantities of DMSO in the extraction mixture, in presence of sonication.

3.2.4 Main experiments on astaxanthin extraction

In concurrence with preliminary experiments, the total volume of the extraction mixture was fixed as 15 mL with 0.4 g of dried and finely powdered cells of *P. rhodozyma*. Moreover, the experiments were carried out in presence of sonication (80% duty cycle) using mixture of acetone and DMSO as the solvent. In

order to assess individual roles of acetone and DMSO in the extraction process, the volume ratio (% v/v) of these two solvents in mixture was varied in 4 proportions, viz. 20:80, 33:67, 40:60, 50:50, as shown in Table 3.2. For every solvent mixture, three experimental runs or replicates were conducted to assess reproducibility of astaxanthin yield. Temperature of the extraction mixture was maintained to 20°C using an ice bath containing flaked ice to avoid the degradation of product. Once the sonication was completed, the mixture then transferred to a 50 mL centrifuge tube and centrifuged at 10000 rpm for 10 min. The supernatant was carefully taken out for filtration and analysis.

Astaxanthin concentration was determined using high performance liquid chromatography (HPLC). The HPLC instrument (Model: Prominence HPLC system, Make: M/s Shimadzu, Singapore) was used with C18 reverse phase column (5 µm particle size, 4.6 × 250 mm dimension) and a UV detector. The eluent was methanol:water mixture in the ratio of 90:10 (Ni et al., 2008). Wavelength for UV detection was decided using spectrophotometric analysis of astaxanthin standard and fixed it to 480 nm. The flow rate and sample injection volume was fixed to 1.2 mL/min and 20 µL respectively. All samples of the extract were filtered with 0.2 µm syringe filter previous to injection in HPLC. Astaxanthin content of the total carotenoids was measured in accordance with the standard quantification curve.

3.3 Physical models

As noted earlier, we have correlated the experimental results on ultrasound-assisted extraction of astaxanthin in solvent with different composition of acetone and DMSO to two physical models: (1) the thermodynamic model for solid-liquid equilibria using UNIFAC (Universal Quasi-Chemical Functional-Group Activity

Coefficients), and (2) cavitation bubble dynamics model. The first model essentially predicts solubility of astaxanthin in solvent with different composition of acetone and DMSO, while the second model predicts the intensity of convection generated in the medium. These models are described below:

3.3.1 Astaxanthin solubility using UNIFAC (Universal Quasi-Chemical Functional-Group Activity Coefficients) method

For estimation of solubility of astaxanthin in mixtures of acetone and DMSO, we have used the theoretical framework described by Gracin et al. (2002), Jakob et al. (1995) and Gmehling et al. (1978). The solid solute is represented by subscript 2 and the liquid solvent is designated by superscript 1. The phase equilibrium for the solute is given by equality of the fugacities (*f*) in solid (*s*) and liquid (*L*) phase:

$$f_2^{\,s} = f_2^{\,L} \tag{3.1.1}$$

The fugacity of solute in the liquid phase is written as:

$$f_2^{\,L} = \gamma_2 x_2 f_{pure2}^{L} \tag{3.1.2}$$

If the solvent (component 1) has no solubility in solid phase, we can write:

$$f_2^{\,s} = f_{pure2}^{s} \tag{3.1.3}$$

As per the analysis of fugacities of species in non-simple mixtures presented by Prausnitz (Prausnitz, 1969), the fugacity ratio $\left(f^s / f^L\right)_{pure2}$ is given as:

$$\ln\left(\frac{f^s}{f^L}\right)_{pure2} = \frac{\Delta h_f}{RT}\left[\frac{T}{T_m} - 1\right] \tag{3.1.4}$$

Equation 3.1.4 neglects correction terms proportional to ΔC_p as these corrections are

likely to be small in comparison with uncertainties in the activity coefficient.

For the solid (astaxanthin) in the present context, enthalpy of fusion and melting temperature are obtained from the DSC analysis shown in Figure 3.2. Substitution of equation 3.1.4 in equation 3.1.2 gives desired solubility x_2, provided the activity coefficient γ_2 of solute is known as a function of composition.

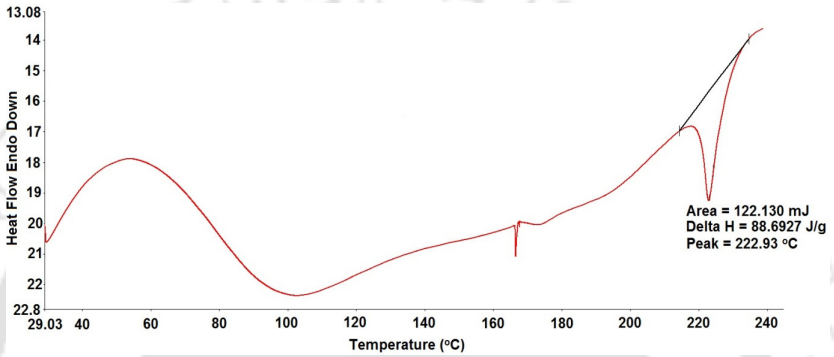

Figure 3.2. DSC analysis of pure astaxanthin showing melting temperature and heat of fusion

In the present study, we have determined the activity coefficient using UNIFAC method, as provided below:

***Determination of activity coefficient using UNIFAC method*:** UNIFAC method (Fredenslund et al., 1975, Fredenslund et al., 1977, Gmehling and Onken, 1977) is widely used for calculating the activity coefficient γ_2 in equation 3.1.2. As per UNIFAC method, activity coefficient comprises of two parts: the combinatorial contribution, due mostly to differences in molecular size and shape, and the residual contribution, arising mostly from differences in intermolecular forces of attraction. For a component i in a multi-component solution, the above contributions are represented as:

$$\ln \gamma_i = \ln \gamma_i^c + \ln \gamma_i^R \qquad (3.1.5)$$

$$\ln \gamma_i^c = \ln \frac{\phi_i}{x_i} + \frac{z}{2} q_i \ln \frac{\theta_i}{\phi_i} + l_i - \frac{\phi_i}{x_i} \sum_j x_j l_j \tag{3.1.6}$$

where: $l_i = \frac{z}{2}(r_i - q_i) - (r_i - 1)$ (3.1.7)

The numerical value of coordination number z is 10 (Gmehling et al., 1978). The relation between the mole fraction *x*, area fraction θ and the segment fraction ϕ is given as:

$$\theta_i = \frac{q_i x_i}{\sum_j q_i x_i} \text{ and } \phi_i = \frac{r_i x_i}{\sum_j r_j x_j} \tag{3.1.8}$$

The parameters r_i and q_i (for pure components) are measures of molecular (van der Waals) volumes and molecular surface areas, respectively. r_i and q_i are given by group contributions R_k and Q_k as:

$$r_i = \sum_k \nu_k^{(i)} R_k \text{ and } q_i \sum_k \nu_k^{(i)} Q_k \tag{3.1.9}$$

where $\nu_k^{(i)}$ always an integer, is the number of groups of type k in molecule i. Group contributions R_k and Q_k are given by Fredenslund et al. (1977). The residual contribution to activity coefficient γ_i is given by:

$$\ln \gamma_i^R = \sum_{\substack{k \\ \text{all groups in the solution}}} \nu_k^{(i)} \left[\ln \Gamma_k - \ln \Gamma_k^{(i)} \right] \tag{3.1.10}$$

where Γ_k is the group residual activity coefficient and $\Gamma_k^{(i)}$ is the residual activity coefficient of group k in a reference solution containing only molecules of type i. It may be noted that the term $\ln \Gamma_k^{(i)}$ is necessary to attain the normalization that activity

coefficient $\gamma_i \to 1$ as $x_i \to 1$. Γ_k is essentially a function of composition of the mixture and temperature as:

$$\ln \Gamma_k = Q_k \left[1 - \ln \sum_m \theta_m \psi_{mk} - \sum_m \left(\theta_m \psi_{km} / \sum_n \theta_n \psi_{nm} \right) \right] \tag{3.1.11}$$

θ_m is the area fraction of group m and the sums are over all groups:

$$\theta_m = \frac{Q_m X_m}{\sum_n Q_n X_n} \tag{3.1.12}$$

where, X_m is the mole fraction of group m in the mixture. The group interaction parameter ψ_{mn} is a function of temperature and is written as:

$$\psi_{mn} = \exp\left[-\left(\frac{U_{mn} - U_{nm}}{RT} \right) \right] = \exp\left(-a_{mn} / T \right) \tag{3.1.13}$$

where, U_{mn} is a measure of the energy of interaction between groups m and n. The group-interaction parameters a_{mn} and a_{nm} $\left(a_{mn} \neq a_{nm} \right)$ are evaluated from vapor-liquid and liquid-liquid equilibrium data (Fredenslund et al., 1977).

3.3.2 Model for cavitation bubble dynamics

Simulations of cavitation bubble dynamics were performed using following equation (Lofstedt et al., 1995, Hilgenfeldt et al., 1996, Barber et al., 1997):

$$R\frac{d^2R}{dt^2} + \frac{3}{2}\left(\frac{dR}{dt} \right)^2 = \frac{1}{\rho}\left(p\left(R,t\right) - P_0 - P\left(t\right) \right) + \frac{R}{\rho c}\frac{d}{dt}\left[p\left(R,t\right) - P\left(t\right) \right] - \frac{4\mu}{\rho R}\frac{dR}{dt} - \frac{2\sigma}{\rho R} \tag{3.2.1}$$

$p\left(R,t\right)$ and $P\left(t\right)$ are written as:

$$p(R,t)=\left(P_0+\frac{2\sigma}{R_0}-P_v\right)\left(\frac{R_0^3-h^3}{R^3-h^3}\right)^{\nu}+P_v \tag{3.2.2}$$

$$P(t)=P_A\cos(2\pi ft)=P_A\cos(\omega t) \tag{3.2.3}$$

Equation 3.2.1 gets transformed into two simultaneous ordinary differential equations as:

$$dR/dt=s \tag{3.2.4}$$

$$\frac{ds}{dt}=\frac{1}{R\rho}\left[p(R,t)-P(t)-P_0\right]+\frac{1}{\rho c}\left[\frac{-3\gamma R^3 p(R,t)}{(R^3-h^3)}\frac{dR}{dt}\right]+\frac{1}{\rho c}\omega P_A sin(\omega t)-\frac{4\mu}{\rho R^2}\frac{dR}{dt}-\frac{2\sigma}{\rho R^2}-\frac{3}{2}\frac{s^2}{R} \tag{3.2.5}$$

Equations 3.2.4 and 3.2.5 were solved using RK (Runge-Kutta) adaptive step size method (Press et al., 1992). The magnitude of the convective effects, viz. $u(r,t)$ and $P_s(r,t)$ can be calculated as follows:

$$u(r,t)=\frac{R^2}{r^2}\left(\frac{dR}{dt}\right) \tag{3.2.6}$$

$$P_s(r,t)=\rho\frac{R}{r}\left[2\left(\frac{dR}{dt}\right)^2+R\frac{d^2R}{dt^2}\right] \tag{3.2.7}$$

***Simulation parameters*:** The physical properties of the mixture of DMSO and acetone have been approximated by using the linear mixing rule based on mole fractions of the components in the mixture. Bubble dynamics models employing either linear or geometric mixing rule have successfully explained behavior of sonoluminescing bubble as well as trends in sonochemistry experiments. Values of other physical parameters required for numerical solution of equations 3.2.4 and 3.2.5 are estimated as follows: Frequency (f) = 20 kHz; P_A = 1.5 bar (Sivasankar et al., 2007); R_0 = 5 µm (representative value, Mettin et al., 1997); $\gamma=1/3$ (polytropic constant);

$h = (R_0 / 8.86)$ (van der Waal's hard core radius); r = 1 mm (representative value); c = 1162 m/s (for *acetone*) and 1502.6 m/s (for DMSO) (Palaiologou et al., 2006). The sonic velocity in the solvent mixture was determined using the empirical formula given by Nomoto (1958) and Gonsalez et al. (2002). Other physical properties of the acetone + DMSO mixtures required for bubble dynamics simulations (viz., vapor pressure, surface tension, viscosity and density) are given in Table 3.3. Vapor pressures of acetone and DMSO were determined using Antoine correlations, and the vapor pressure of the mixture was calculated using Raoult's law. Other physical properties of surface tension, viscosity and density were measured experimentally (see the footnote of Table 3.3).

3.4 RESULTS AND DISCUSSION

3.4.1 Experimental results on astaxanthin extraction

The extent of astaxanthin extraction from the dry cells of *P. rhodozyma* for different compositions of acetone and DMSO is shown in Table 3.2. Maximum astaxanthin yield of 1536 ± 3 µg/g DCW (with extract concentration 7.60 ± 0.3 mg/L) is obtained for the solvent composition 33% v/v DMSO + 67% v/v acetone. The least yield of 970 ± 4 µg/g DCW is obtained for composition 20% v/v DMSO + 80% v/v acetone, while for an equal-volume (50% v/v each) mixture of acetone and DMSO, a moderate yield of 1383 ± 4 µg/g DCW (with extract concentration of 6.05 ± 0.2 mg/L) was obtained. Literature review on astaxanthin yields from several wild and mutant strains of *P. rhodozyma* using different extraction techniques is provided in chapter 1. Although a direct comparison between yields from strains originating from different sources is not possible, the astaxanthin yield in present study is higher than two other studies employing MTCC cultures, viz. Gogate and Nadar (2015) and Bhatt

et al. (2013).

Table 3.2 Experimental results of ultrasound assisted astaxanthin extraction from *P. rhodozyma*

Sr. No.	DMSO		Acetone		Astaxanthin yield*	Astaxanthin titer in extract*
	%	mL	%	mL	(µg/g DCW)	(mg/L)
1	20	3.0	80	12	970 ± 4	5.58 ± 0.1
2	33	4.95	67	10.05	1536 ± 3	7.60 ± 0.3
3	40	6.0	60	9.0	1240 ± 2	5.90 ± 0.1
4	50	7.5	50	7.5	1383 ± 4	6.05 ± 0.2

* – ± values indicate standard deviations in astaxanthin titer and yield

In previous chapter, we have reported yield of 1728 µg/g DCW, which is higher than present study. The protocol followed in the previous study was: optimization of medium components and process parameters and application of sonication during fermentation in the stationary phase, although extraction of astaxanthin was carried out with conventional technique. Application of sonication during fermentation of *P. rhodozyma* cells significantly boosted the astaxanthin synthesis by the cells. In this chapter, an un-optimized fermentation media (at un-optimized process conditions) was chosen for fermentation, cells were harvested and probe sonication was applied to the extraction mixture (cells + disrupting agent/solvent) to check the influence of sonication and extracting solvent on extraction yield of astaxanthin.

3.4.2 UNIFAC prediction of astaxanthin solubility

UNIFAC calculations were performed using the MATLAB® program provided with the book Chemical, Biochemical and Engineering Thermodynamics (4th edition) by Sandler (2006). This program has in-built database of group volume (R) and surface area (Q) for more than 100 different functional groups that occur in

organic molecules. Other input data required for this program includes temperature of the system, mole fractions of the components and their vapor pressures. The program provides a plot and series of activity coefficients vs. mole fraction of solute. This data is used to determine the solubility as per the equation 3.1.4 using the heat of fusion (determined separately) (Sandler, 2006):

$$\ln\left(\frac{f^s}{f^L}\right)_{pure2} = \ln\left(x_2\gamma_2\right) = \frac{\Delta h_f}{RT}\left[\frac{T}{T_m} - 1\right] \tag{3.1.4}$$

$$x_2\gamma_2 = \exp\left\{\frac{\Delta h_f}{RT}\left[\frac{T}{T_m} - 1\right]\right\} \tag{3.1.14}$$

The DSC analysis of pure astaxanthin is shown in Figure 3.2. The melting temperature (T_m) and heat of fusion (Δh_f) were obtained from DSC analysis as: 222.9°C and 88.69 J/g. With these values, the RHS of equation 3.1.14 at T = 293 K (20°C) is determined as: 1.375 × 10^{-4}. The data series of x vs γ obtained from UNIFAC method can be interpolated to simultaneously obtain numerical values of x and γ that satisfy the RHS.

UNIFAC calculations: The molecular structures of astaxanthin, DMSO and acetone are shown in scheme 3.1. For the UNIFAC calculations, different functional groups in astaxanthin, acetone and DMSO were identified as follows:

Astaxanthin: CH = 14, C = 4, CH_3 = 4, Ac CH_3 = 6, Ac CH_2 = 2, AC = 6,

HO–CH–C=O = 2

DMSO: DMSO = 1

Acetone: CH_3 = 1, CH_3CO = 1

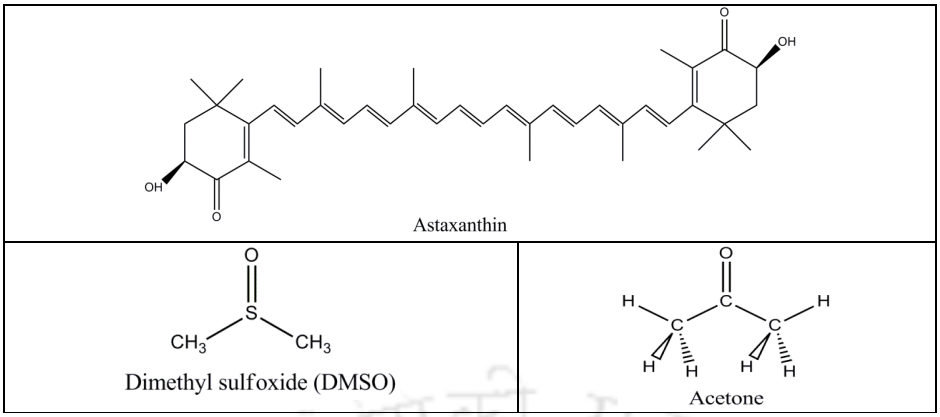

Scheme 3.1: Molecular structures of solute (astaxanthin) and solvents (DMSO and acetone)

Mole fraction of solute (astaxanthin) was always taken as 1, while the mole fractions of acetone and DMSO for different volumetric compositions are given in Table 3.3. The molar volume of acetone + DMSO mixture was calculated using ideal relation: $V_{mix} = \sum x_i V_i$, while the average molecular weight of the mixture was determined as: $M_{mix} = \sum x_i M_i$. The results of UNIFAC calculations are shown in Figure 3.3, which show profiles of activity coefficients (γ_2) with solute composition (x_2) in DMSO:acetone mixtures of different compositions. The values of x_2 and γ_2 obtained after interpolation of the UNIFAC profiles (as per equation 3.1.14) are listed in Table 3.3. It could be seen from Table 3.3 that activity coefficient of astaxanthin in DMSO:acetone mixture (% v/v) 33:67 is 0.99 with the highest saturation mole fraction of 1.4×10^{-4}. The saturation astaxanthin solubility corresponding to this mole fraction is 1.57 g/L. The astaxanthin solubility shows reduction with further increase in volumetric proportion of DMSO to 50 % v/v. For the 20:80 % v/v mixture of DMSO:acetone as well, the astaxanthin solubility is reduced to 1.22 g/L with saturation mole fraction of 1.1×10^{-4}. The reduction in solubility is attributed to rise in the activity coefficient of astaxanthin.

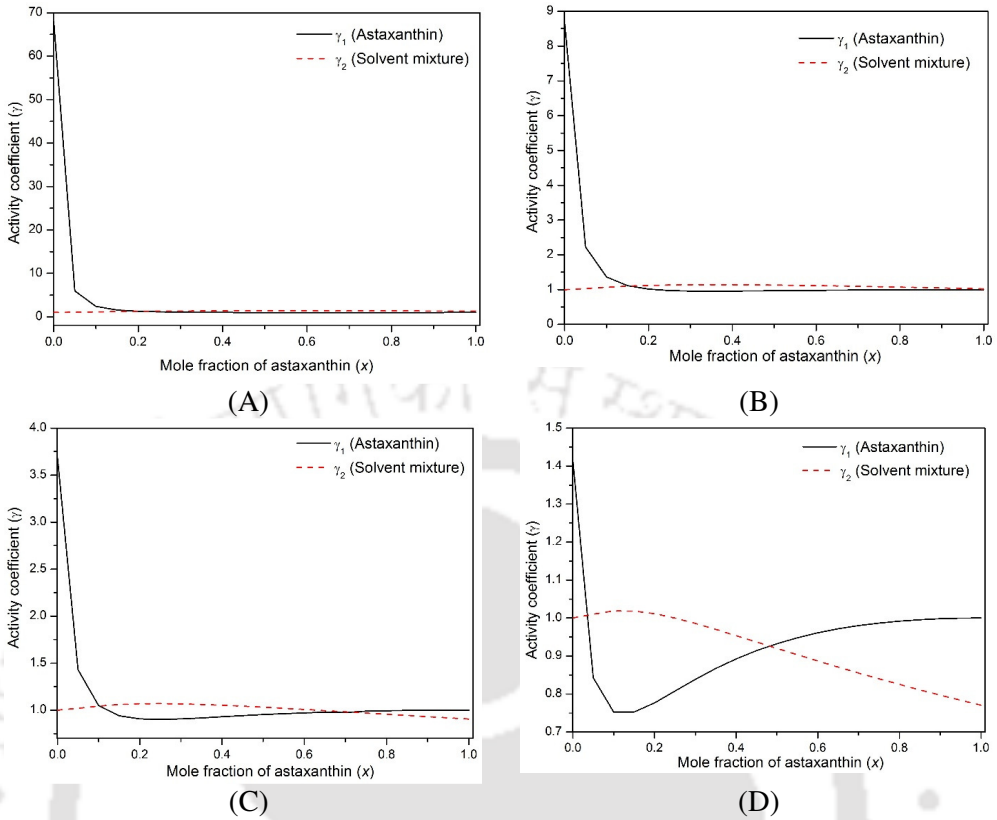

Figure 3.3. UNIFAC predictions for the activity coefficients of the system comprising astaxanthin and solvent (viz. DMSO:acetone) mixtures in different compositions (% v/v). (A) 20:80, (B) 33:67, (C) 40:60, (D) 50:50

Table 3.3. Summary of UNIFAC calculations for prediction of solubility of astaxanthin in acetone+DMSO mixture

Sr. No.	Volumetric composition of DMSO:Acetone mixtures				Molar volume of DMSO + Acetone mixture (mL)	x (saturation mole fraction)	γ (activity coefficient)	Astaxanthin solubility (g/L)
	Volume %	Mole Fraction	Volume %	Mole Fraction				
1	20	0.21	80	0.79	53.76	1.1×10^{-4}	1.28	1.22
2	33	0.34	67	0.66	53.10	1.4×10^{-4}	0.99	1.57
3	40	0.41	60	0.59	52.75	1.1×10^{-4}	1.27	1.20
4	50	0.51	50	0.49	52.26	0.97×10^{-4}	1.41	1.10

Note: Total volume of mixture = 15 mL, Molar volume of acetone + DMSO mixture calculated according to formula: $V_{mix} = \sum x_i V_i$, Molecular weight of acetone + DMSO mixture calculated as: $M_{mix} = \sum x_i M_i$.

Table 3.4. Physical properties of DMSO:acetone mixtures and results of bubble dynamics simulations

Sr. No.	Volumetric composition of DMSO:Acetone mixtures				Physical properties				Bubble dynamics simulations results	
	%	mL	%	mL	Density$^{\$}$ (kg/m^3)	Viscosity$^{\$}$ (Pa·s)	Surface Tension$^{\$}$ (mN/m)	Vapor Pressure$^{\#}$ (kPa)	P_{max} (bar)	V_{turb} (m/s)
1	20	3.0	80	12	939.1	1.1107×10^{-3}	27.31	15.85	105.9	3.95×10^{-3}
2	33	4.95	67	10.05	990.9	8.864×10^{-4}	29.44	12.10	79.45	3.44×10^{-3}
3	40	6.0	60	9.0	1010.7	1.0124×10^{-3}	30.22	10.35	61.67	3.075×10^{-3}
4	50	7.5	50	7.5	1046.5	2.5315×10^{-3}	31.84	81.05	46.62	2.817×10^{-3}

Vapor pressure of the solvent mixture @ 293 K is calculated using Raoult's law ($P_{v,mix} = x_1 \cdot P_{v1} + x_2 \cdot P_{v2}$, where x_1 and x_2 are individual mole fractions of the two solvents and P_{v1}, P_{v2} are the individual vapor pressures at 293K determined using Antoine correlations)

$ The physical properties were measured experimentally. Surface tension – Tensiometer (Model No.: DY300; Make: M/s Kwoya, Japan), Viscosity – Rheometer (Model No.: Rheostress RS 1; Make: M/s Thermo Electron, Germany), Density –Density bottle (10 mL volume), P_{max} – magnitude of acoustic wave generated by bubble, V_{turb} – magnitude of microturbulence velocity generated by bubble.

3.4.3 Results of bubble dynamics simulations

Representative results of simulations of cavitation bubble dynamics, i.e. radial motion of the cavitation bubbles and the convection generated by them (through microturbulence and shock waves), in DMSO:acetone (33:67% v/v) mixture are shown in Figure 3.4. It is evident from Figure 3.4 that acoustic waves emitted by cavitation bubble have discrete or intermittent nature, while the microturbulence velocity is of continuous oscillatory type. The summary of the bubble dynamics simulations in all DMSO:acetone mixtures is given in Table 3.4, where the values of magnitudes of acoustic pressure waves and microturbulence generated by the bubbles are listed.

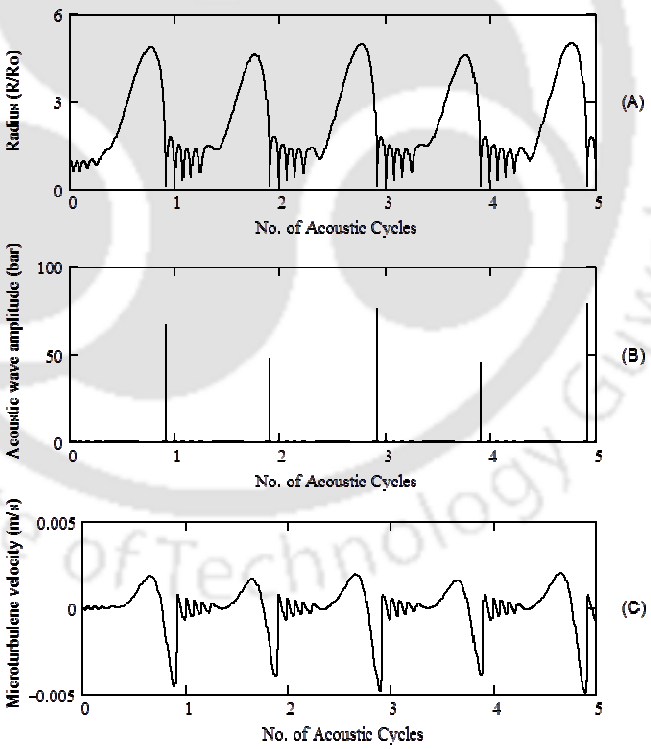

Figure 3.4. Simulations of the radial bubble motion and its physical effects in 33% v/v DMSO + 67% v/v acetone mixture: time history of (A) normalized bubble radius (R/Ro); (B) acoustic waves emitted by the bubble and (C) velocity of microturbulence generated by the bubble.

It could be inferred from simulation results given in Table 3.4 that highest convection intensity by cavitation bubbles is generated in the DMSO:acetone mixture of proportion 20:80 (% v/v); with acoustic wave amplitude of 105.9 bar and microturbulence velocity of 3.95 m/s. With increasing volume fraction of DMSO in the extraction solvent, the intensity of convection drops sharply with significant reduction in magnitudes of both acoustic waves and microturbulence velocity. This result is attributed to increase in surface tension and viscosity of the DMSO:acetone mixture with increasing proportions of DMSO. The acoustic waves emitted by the cavitation bubbles essentially help in disruption of the cells, while the microturbulence generated by cavitation creates intense local mixing in the medium that helps in effective transfer of carotenoids from cell surface into bulk medium.

3.4.4 Analysis

Concurrent analysis of the experimental results on astaxanthin extraction using solvent with varying composition of DMSO and acetone, predictions of astaxanthin solubility using UNIFAC and the results of bubble dynamics simulations reveals interesting mechanistic facets of the process of astaxanthin extraction. The extent of astaxanthin extraction in a solvent is essentially a function of two factors: (1) the solubility of astaxanthin in the solvent, and (2) the intensity of convection in the extraction mixture as extraction is essentially a mass transfer process. The higher the intensity of convection in the extraction mixture, better the mass transfer characteristics of the system.

The principle role of DMSO in the extraction solvent was to achieve disruption of *P rhodozyma* cells. However as the volumetric fraction of DMSO in solvent mixture increases, the extent of extraction is influenced by the physical

properties of DMSO. The highest astaxanthin yield of 1536 ± 3 µg/g DCW was obtained for the solvent mixture of composition DMSO (33% v/v) + acetone (67% v/v). This result was in concurrence with prediction of astaxanthin solubility using UNIFAC. The highest astaxanthin solubility of 1.57 g/L was predicted for solvent mixture with same composition, viz. DMSO (33% v/v) + acetone (67% v/v). However, quite interestingly, the convection intensity for this solvent composition was moderate. Despite relatively lower magnitudes of microturbulence and shock waves, the astaxanthin yield with 33% v/v DMSO + 67% v/v acetone is almost 60 % higher than the solvent mixture with composition 20% v/v DMSO + 80% acetone; for which the predicted solubility was 1.22 g/L. The above analysis clearly indicates that saturation solubility of the solute (or in other words the solvent selectivity of the solute) is the dominant factor influencing the extraction yield, as compared to the intensity of convection in the extraction mixture, which governs the mass transfer characteristics of the system. The higher the solubility of the solute in extraction solvent, the higher is the driving force for astaxanthin transport from cell into the solvent. The microconvection generated by ultrasound and cavitation essentially helps in maintaining constant concentration gradient for diffusive transfer of astaxanthin (or the carotenoids) from cells by efficient transfer of astaxanthin from close vicinity of cell surface into the bulk medium.

3.5 CONCLUSION

The present study has highlighted mechanistic features of ultrasound-assisted astaxanthin extraction from the sustainable biological source of *P. rhodozyma*. Experiments using extraction solvent with varying composition of DMSO and acetone, coupled with solubility predictions using UNIFAC and simulations of

cavitation bubble dynamics have revealed the relative influence of two factors, viz. saturation solubility and convection intensity, on extraction yield of astaxanthin. Our results have established that saturation solubility of astaxanthin, which decides driving force for extraction, is the dominant factor governing extraction process, as compared to intensity of convection in the extraction mixture – which essentially governs the mass transfer characteristics of the system.

REFERENCES

Agarwal, M., Dikshit, P.K., Bhasarkar, J.B., Borah, A.J., Moholkar, V.S., 2016. Physical Insight into Ultrasound−Assisted Biodesulfurization using Free and Immobilized Cells of *Rhodococcus rhodochrous* MTCC 3552. Chem. Eng. J. 295, 254−267.

Barber, B.P., Hiller, R.A., Lofstedt, R., Putterman, S.J., Weninger, K.R., 1997. Defining the Unknowns of Sonoluminescence. Phys. Rep. 281, 65−143.

Batghare, A.H., Singh, N., Moholkar, V.S., 2018. Investigations in ultrasound–induced enhancement of astaxanthin production by wild strain *Phaffia rhodozyma* MTCC 7536. Bioresour. Technol. 254, 166−173.

Bhasarkar, J.B., Borah, A.J., Goswami, P., Moholkar, V.S., 2015a. Mechanistic analysis of ultrasound assisted enzymatic desulfurization of liquid fuels using *horseradish peroxidase*. Bioresour. Technol. 196, 88−98.

Bhasarkar, J.B., Dikshit, P.K., Moholkar, V.S., 2015b. Ultrasound Assisted Biodesulfurization of Liquid Fuel using Free and Immobilized Cells of *Rhodococcus rhodochrous* MTCC 3552: A Mechanistic Investigation. Bioresour. Technol. 187, 369−378.

Bhatt, P.C., Ahmad, M., Panda, B.P., 2013. Enhanced bioaccumulation of astaxanthin in *Phaffia rhodozyma* by utilising low–cost agro products as fermentation substrate. Biocatal. Agric. Biotechnol. 2, 58–63.

Borah, A.J., Agarwal, M., Poudyal, M., Goyal, A., Moholkar, V.S., 2016. Mechanistic investigation in ultrasound induced enhancement of enzymatic hydrolysis of invasive biomass species. Bioresour. Technol. 213, 342–349.

Choi, S.K., Kim, J.H., Park, Y.S., Kim, Y.J., Chang, H.I., 2007. An efficient method for the extraction of astaxanthin from the red yeast *Xanthophyllomyces dendrorhous*. J. Microbiol. Biotechn. 17 (5), 847–852.

da Fonseca, R.A. dos Santos., Rafael, R. da Silva., Kalil, S.J., Burkert, C.A.V., Burkert, J.F. de Medeiros., 2011. Different cell disruption methods for astaxanthin recovery by *Phaffia rhodozyma*. Afric. J. Biotechnol. 10 (7), 1165–1171.

Fredenslund, A., Gmehling, J., Rasmussen, P., 1977. Vapor-liquid equilibria using UNIFAC; Elsevier, Amsterdam.

Fredenslund, A., Jones, R.L., Prausnitz, J.M., 1975. Group contribution estimation of activity coefficients of nonideal liquid mixtures. AIChE J. 21 (6), 1086–1099.

Gmehling, J., Onken, U., 1977. Vapor-Liquid Equilibrium Data Collection, Vol. I. Chemistry Data Series; Dechema, Frankfurt.

Gmehling, J.G., Anderson T.F., Prausnitz, J.M., 1978. Solid–Liquid Equilibria Using UNIFAC. Ind. Eng. Chem. Fundam. 17 (4), 269–273.

Gogate, P.R., Nadar, S.G., 2015. Ultrasound-assisted Intensification of Extraction of Astaxanthin from *Phaffia rhodozyma*. Indian Chem. Eng. 57, 240–255.

Gonzalez, C., Resa, J.M., Lanz, J., Fanega, M.A., 2002. Speed of Sound and Isentropic Compressibility of Organic Solvents + Sunflower Oil Mixtures at 298.15 K. JAOCS. 79 (6), 543–548.

Gracin, S., Brinck, T., Rasmuson, A.C., 2002. Prediction of Solubility of Solid Organic Compounds in Solvents by UNIFAC. Ind. Eng. Chem. Res. 41 (20), 5114–5124.

Hilgenfeldt, S., Lohse, D., Brenner, M.P., 1996. Phase Diagrams for Sonoluminescing Bubbles. Phys. Fluids 8 (11), 2808–2826.

Jakob, A., Joh, R., Rose, C., Gmehling, J., 1995. Solid–liquid equilibria in binary mixtures of organic compounds. Fluid Phase Equilibr. 113, 117–126.

Lofstedt, R., Weninger, K., Puttermann, S.J., Barber, B.P., 1995. Sonoluminescing Bubbles and Mass Diffusion. Phys. Rev. E 51 (5), 4400–4410.

Mayne, S.T., 1996. Beta–carotene, carotenoids, and disease prevention in humans. FASEB. J. 10, 690–701.

Medeiros, F.O., Alves, F.G., Lisboa, C.R., Martins, D.S., Kalil, S.J., 2008. Ultrasonic waves and glass pearls: a new method of extraction of β-galactosidase for use in laboratory. Quim. Nova. 31 (2), 336–339.

Mettin, R., Akhatov, I., Parlitz, U., Ohl, C.D., Lauterborn, W., 1997. Bjerknes Forces between Small Cavitation Bubbles in a Strong Acoustic Field. Phys. Rev. E. 56 (3), 2924–2931.

Michelon, M., de Borba, T. de Matos., Rafael, R. da Silva., Burkert, C.A.V., Burkert, J.F. de Medeiros., 2012. Extraction of Carotenoids from *Phaffia rhodozyma*: A Comparison between Different Techniques of Cell Disruption. Food. Sci. Biotechnol. 21 (1), 1–8.

Nakano, T., Tosa, M., Takeuchi, M., 1995. Improvement of biochemical features in fish health by red yeast and synthetic astaxanthin. J. Agric. Food. Chem. 43, 1570−1573.

Ni, H., Chen, Q., He, G., Wu, G., Yang, Y., 2008. Optimization of acidic extraction of astaxanthin from *Phaffia rhodozyma*. J. Zhejiang. Univ. Sci. B. 9 (1) 51−59.

Nomoto, O., 1958. Empirical Formula for Sound Velocity in Liquid Mixtures. J. Phys. Soc. Jpn. 13 (12), 1528−1532.

Palaiologou, M.M., Arianas, G.K., Tsierkezos, N.G., 2006. Thermodynamic Investigation of Dimethyl Sulfoxide Binary Mixtures at 293.15 and 313.15 K. J. Solution Chem. 35, 1551−1565.

Persike, D.S., Bonfim, T.M.B., Santos, M.H.R., Lyng, S.M.O., Chiarello, M.D., Fontana, J.D., 2002. Invertase and urease acivities in the carotenogenic yeast *Xanthophyllomyces dendrorhous.* Bioresour. Technol. 82, 79−85.

Prausnitz, J.M., 1969. Molecular Thermodynamics of Fluid-Phase Equilibria, Prentice-Hall, Englewood Cliffs, N.J.

Press, W.H., Teukolsky, S.A., Flannery, B.P., Vetterling, W.T., 1992. Numerical Recipes (2nd Ed.); Cambridge University Press: New York.

Sandler, S.I., 2006. Chemical, Biochemical and Engineering Thermodynamics (4th Ed.); John Wiley & Sons, Inc, New York.

Sedmak, J., Weerasinghe, D., Jolly, S., 1990. Extraction and quantification of Astaxanthin from *Phaffia rhodozyma*. Biotechnol. Techniq. 4 (2), 107−112.

Singh, S., Sarma, S., Agrawal, M., Goyal, A., Moholkar, V.S., 2015a. Mechanistic insight into ultrasound induced enhancement of simultaneous saccharification and fermentation of *Parthenium hysterophorus* for ethanol production. Ultrason. Sonochem. 26, 245−256.

Singh, S., Sarma, S., Agrawal, M., Goyal, A., Moholkar, V.S., 2015b. Ultrasound enhanced ethanol production from *Parthenium hysterophorus*: A mechanistic investigation. Bioresour. Technol. 188, 287–294.

Sivasankar, T., Paunikar, A.W., Moholkar, V.S., 2007. Mechanistic Approach to Enhancement of the Yield of a Sonochemical Reaction. AIChE J. 53 (5), 1132–1143.

Valduga, E., Valerio, A., Luccio, H.T.M.D., 2007. Pretreatment of sugarcane molasses and corn steep liquor for the production of carotenoids. Quim. Nova. 30 (8), 1860–1866.

Xiao, A., Ni, H., Cai, H., Li, L., Su, W., Yang, Q., 2009. An improved process for cell disruption and astaxanthin extraction from *Phaffia rhodozyma*. World J. Microb. Biot. 25, 2029–2034.

Ultrasonic Intensification of Fermentative Riboflavin synthesis from *Debaryomyces hansenii var. hansenii*

4.1 INTRODUCTION

Riboflavin is a yellow colored water-soluble vitamin which plays crucial role in metabolic activities within the body. Being a metabolic precursor of flavin nucleotides, viz. mononucleotides (FMN) and flavin adenine dinucleotide (FAD), involved in oxidative metabolism and various enzymatic reactions (Chaudhuri et al., 2014; Xin et al., 2017). The sources and use of riboflavin is already discussed in chapter 1. Riboflavin is commercially synthesized (as dietary supplement) from *Ashbya gossypii* and *Bacillus subtilis*. Although, researchers are working on enhancement of riboflavin synthesis from strains of *Candida famata* or *Candida*

flareri which have relatively low productivity but have simplest metabolic pathway compared to commercial strains. The strain used in this study is *Debaryomyces hansenii*, which is a telemorph of *Candida famata var. famata* and then *Candida famata* renamed as *Debaryomyces hansenii* (Voronovsky et al., 2004; Kurtzman and Robnett, 2013; National Collection of Yeast Cultures, 2017). There are two varieties of *Debaryomyces hansenii* viz. *D. hansenii var. fabryii* and *var. hansenii* but later *D. hansenii var. fabryii* was renamed as *Debaryomyces fabryii* (Yaguchi et al., 2017). Some author's called *Candida famata* as *Candida flareri* (Dmytruk et al., 2012; Dmytruk et al., 2014). In this chapter, *D. hansenii* refers to *D. hansenii var. hansenii.*

This chapter has addressed the issue of enhancement of riboflavin productivity from wild type or natural strain of *D. hansenii var. hansenii* with three techniques, viz. (1) Statistical optimization of media components and physical parameters, (2) use of external additives for boosting riboflavin production, and (3) application of sonication in different fractional periods of log phase. Fermentation profiles have been analyzed using basic Monod growth kinetics to deduce changes in maximum specific growth rate and Monod saturation constant induced by application of sonication. Also, we have also attempted to gain insight into the mechanism of ultrasound-induced enhancement of riboflavin production using SDS-PAGE analysis of enzymes involved in metabolic pathway of riboflavin production.

4.2 MATERIALS AND METHODS

4.2.1 Microorganism and preparation of inoculum

Culture of *D. hansenii var. hansenii* MTCC 3574 was procured from IMTECH, Chandigarh, India. Yeast–Malt Agar medium was used to prepare the slants and stored at 4°C for culture maintenance and its use after every 30 days. A

loop of yeast cells was transferred to 100 mL yeast malt media (sterilized by autoclave) with a composition of 10 g/L glucose, 5 g/L peptone, 3 g/L yeast extract and 3 g/L malt extract. Millipore water was used to prepare all media solutions. Media was cultivated aerobically at 27°C for a period of 48 h at a shaking speed of 150 rpm.

4.2.2 *D. hansenii var. hansenii* fermentation in shake flask

A 100 mL fermentation medium was prepared for *D. hansenii var. hansenii* fermentation study. Based on previous literature (Wang et al., 2008) the composition of media was fixed as: 0.5 g/L $MgSO_4 \cdot 7H_2O$, 1 g/L KH_2PO_4, 5 g/L $(NH_4)_2SO_4$, 0.1 g/L $CaCl_2 \cdot 2H_2O$, 2 g/L yeast extract and 0.1 g/L NaCl. The pH for this medium composition was adjusted to 5.5. An inoculum of 10% v/v was transferred to the sterilized fermentation medium and incubated at 27°C for five days at shaking speed of 150 rpm. The initial substrate (glucose) concentration was kept as 30 g/L (which is the lower limit of substrate concentration in statistical optimization reported by Dmytruk et al., 2014).

Preliminary experiments were performed to decide the fermentation period for riboflavin production from *D. hansenii var. hansenii*. It was found that actual riboflavin yield was reduced after 72 h of fermentation. This may happen due to degradation or utilization of riboflavin by the yeast cells as substrate, as the concentration of glucose drops to very low values. On basis of these preliminary results, the fermentation period was fixed at 72 h for all experiments. The broth was collected at the end of fermentation, centrifuged and filtered before analysis for concentrations of biomass, substrate, and product.

4.2.3 Analytical methods

Analysis of riboflavin was done as per the high performance liquid chromatography (HPLC) method reported by Hassan and Chee (2001). Riboflavin analysis was done by HPLC (Agilent Technologies, 1220 Infinity LC) employing C18 reverse-phase column (3 mm × 150 mm and particle size of 3.5 μm) with methanol: water (in the ratio of 30:70) as an eluent. Eluent flow rate was maintained to 1 mL/min. A wavelength of 254 nm in UV range was fixed after the analysis of riboflavin standard in UV spectrophotometer. Glucose concentration in the samples was also monitored by HPLC (Perkin Elmer) employing Hiplex-H column (4.6 mm × 300 mm and particle size of 5 μm, temperature = 60°C). H_2SO_4 (0.005 M) was used as an eluent and the flow rate was maintained to 0.6 mL/min (Tizazu and Moholkar, 2018).

4.2.4 Medium composition optimization

Fermentation medium components were optimized in two steps, viz. Plackett–Burman design succeeded by central composite design (CCD). Details of Plackett–Burman design and CCD matrix are as follows:

4.2.4.1 Plackett–Burman design

Published literature on riboflavin production from *D. hansenii* and its anamorph *Candida famata/Candida flareri* has reported use of many medium components (Dmytruk and Sibirny, 2012; Wang et al., 2008; Dmytruk et al., 2014; Roya et al., 2013; Aslam et al., 2008; Oraei et al., 2018). On the basis of published literature, 6 potential media components, viz. $(NH_4)_2SO_4$, KH_2PO_4, $MgSO_4{\cdot}7H_2O$, $CaCl_2{\cdot}2H_2O$, yeast extract and NaCl, with lower (−1) and upper (+1) limit of

concentration were selected for optimization of fermentation medium as depicted in Table 4.1. MINITAB (Release 15.1, PA, USA, Trial Version) was used for devising the Plackett–Burman design, and also for the analysis and processing of the data. Plackett–Burman design follows 1st order polynomial equation (provided in chapter 1 as eqn. 2.1) as reported by Plackett and Burman (1946). Pareto plot (Fig. 4.1) of Plackett–Burman analysis showed four significant components viz. $(NH_4)_2SO_4$, $MgSO_4 \cdot 7H_2O$, NaCl, and yeast extract with *t*–value higher than the limit 2.571 for this analysis. This indicate their significant influence on response variable i.e. riboflavin concentration.

Table 4.1. Factors and levels of Plackett–Burman design for medium optimization

Factors	Levels	
	Low (–1)	High (+1)
(X_1) – $(NH_4)_2SO_4$ (g/L)	1	5
(X_2) – KH_2PO_4 (g/L)	0.5	2.0
(X_3) – $MgSO_4 \cdot 7H_2O$ (g/L)	0.1	0.5
(X_4) – $CaCl_2 \cdot 2H_2O$ (g/L)	0.1	0.5
(X_5) – NaCl (g/L)	0.1	0.5
(X_6) – Yeast Extract (g/L)	1	5

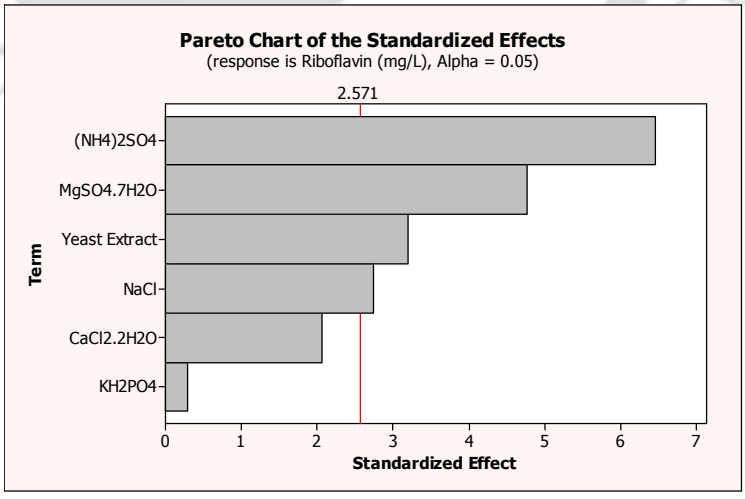

Figure 4.1. Pareto plot showing significant medium components

4.2.4.2 Central composite design (CCD) for medium composition optimization

Plackett–Burman design screened out $(NH_4)_2SO_4$, $MgSO_4 \cdot 7H_2O$, NaCl, and yeast extract as significant medium components. Significant medium components (with lower and upper limits) were used to devise the experiments for CCD. Central composite design (CCD) matrix gave 30 experimental runs (not reported here). Response surface methodology was used for statistical analysis in MINITAB (Release 15.1, PA, USA, Trial version). Individual and interactive effects of medium/physical parameters towards response variable (riboflavin) were obtained by fitting data of Plackett-Burman design and central composite design to the quadratic model (represented as eqn. 2.2 in chapter 2). Significance of each variable and goodness of fit with the model was determined using analysis of variance (ANOVA) method (not reported here). The desirability function plot obtained from central composite experimental design shows optimum levels of the medium components as depicted in Fig. 4.2. The optimum values of medium components for maximum riboflavin are: a. $(NH_4)_2SO_4$ = 3.59 g/L, b. $MgSO_4 \cdot 7H_2O$ = 0.25 g/L, c. NaCl = 0.18 g/L and d. yeast extract = 4.32 g/L.

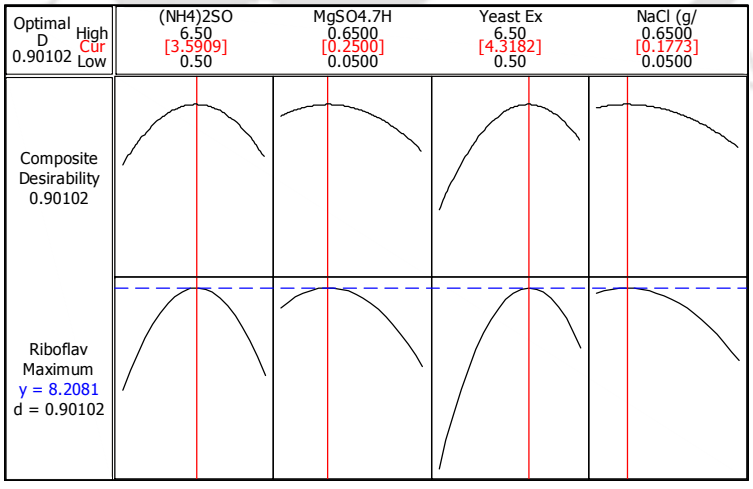

Figure 4.2. Desirability function plot showing optimum values of medium components

4.2.5 Process/physical parameters optimization

Central composite design was used to optimize process/physical parameters (at optimum medium composition) viz. pH, temperature (°C), inoculum (% v/v) and shaking speed (rpm). Lower (–1) and higher (+1) levels of process parameters were selected for optimization as depicted in Table 4.2. For the experimental design, five levels of the variables mentioned above, coded as −α, −1, 0, +1, +α were used and full factorial CCD matrix comprised of 30 individual runs (not reported here). Response surface methodology was used for statistical analysis in MINITAB (Release 15.1, PA, USA, Trial version) to obtain optimum values of variables corresponding to maximum riboflavin concentration. ANOVA of the results of CCD experimental design was done to exhibit the individual and interactive effects of the independent variables on the response variable (not reported here). Initial substrate (glucose) concentration was kept 30 g/L for all experiments and total fermentation time was 72 h. The desirability function plot obtained from CCD of process parameters as depicted in Fig. 4.3 shows optimum values of process parameters for maximum riboflavin as: a. pH = 6.1, b. temperature = 25°C; c. % inoculum = 6.4 % v/v and d. shaking speed = 172 rpm. Final riboflavin concentration at complete optimization (media + process parameters) was 8.83 mg/L which corresponds to the yield of 1.7 mg/g of cells with biomass concentration of 5.2 g/L.

Table 4.2. Factors and levels of central composite design for process parameters

Factors	Levels	
	Low (–1)	High (+1)
(X_1) – Medium pH	4	6
(X_2) – Temperature (°C)	23	27
(X_3) – Inoculum size (% v/v)	4	8
(X_4) – Shaking speed (rpm)	120	170

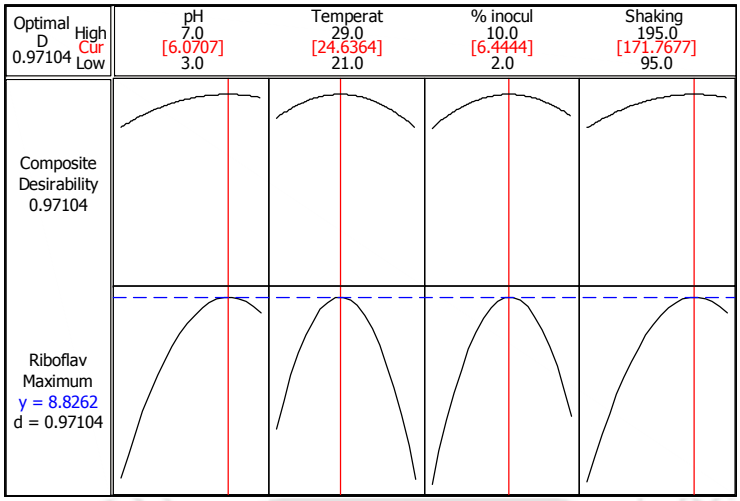

Figure 4.3. Desirability function plot showing optimum values of process parameters

4.2.6 Validation experiments

Validation experiments were performed (in triplicate) at optimum conditions of medium and physical parameters. The results of validation experiments were as follows: Final riboflavin concentration = 9.2 mg/L, biomass concentration = 5.1 g/L, riboflavin yield = 1.8 mg/g of cells. Close match between the predicted and experimental yields essentially validated the results of statistical optimization.

The riboflavin yield after optimization of medium and process parameters was still significantly smaller than the yields from other wild strains reported in literature review of chapter 1 (Sauer et al., 1996; Jiménez et al., 2005; Mateos et al., 2006; Boretsky et al., 2011; Suzuki et al., 2011; Dmytruk et al., 2011; Dmytruk et al., 2014; Ledesma-Amaro et al., 2015; Hu et al., 2017; Oraei et al., 2017). Previous authors (Levine et al., 1949; Heefner et al., 1993) have reported that riboflavin yield can be increased with use of additives such as glycine (0.1 to 0.3 %) and some trace elements of Fe^{3+} (0.04 to 0.06 mg/L), cobalt (0.5 to 2 mg/L) and zinc (5 to 25 mg/L). Glycine (a purine precursor) is an important factor of metabolic pathway of riboflavin production. It gets incorporated into riboflavin molecule – basically distribution of

glycine nitrogen in riboflavin leading to metabolic makeup of purine, as reported by Plaut (1954). This enhances the availability of Guanosine-5′-triphosphate (GTP) as metabolite resulting in improvement of riboflavin production. Transition metal ions (cobalt and zinc) bind to enzymes to form metalloenzymes with higher metabolic activity, while Fe^{3+}, being a part of haemoproteins, assists intracellular oxygen transport (Palmer and Bonner, 2008). In view of this, additional experiments were carried out in triplicate with incorporation of 4 additional components in optimized medium, viz. Glycine (2 g/L or 0.2 %), $FeCl_3$ (0.05 mg/L), $ZnSO_4$ (20 mg/L) and $CoCl_2$ (2 mg/L). Supplementation of the medium with $FeCl_3$, glycine, $ZnSO_4$, and $CoCl_2$ enhanced final riboflavin concentration to 34 ± 4.3 mg/L corresponding to the yield of 4.1 ± 0.5 mg/g of cells. These values were 1.4× the concentration and 1.3× the yield obtained after optimization of medium and physical parameters.

4.2.7 *D. hansenii var.hansenii* fermentation with sonication

Ultrasound-assisted fermentation of *D. hansenii var.hansenii* was conducted at optimum conditions of medium and physical parameters. An ultrasound bath (PCi Analytics, 3.5 L, India) with 33 kHz frequency and 100 W rated power was used. Actual acoustic power intensity (0.78 W/cm^2) in the bath and the pressure amplitude of the ultrasound waves (1.4 bar) were determined using calorimetric techniques (Sivasankar et al., 2007). An important experimental parameter in ultrasound-assisted fermentation is duty cycle of sonication. Continuous sonication of the fermentation mixture leads to disruption and damage of microbial cells. Therefore, sonication is applied intermittently, characterized by the parameter duty cycle; which is fraction of total period of the fermentation during which the broth is exposed to sonication. In the present study, this parameter was optimized in preliminary experiments. A duty cycle

of 10% (1 min sonication and 9 min mechanical agitation @ 172 rpm per 10 min of fermentation) yielded maximum riboflavin with minimum cell damage. Hence, duty cycle of 10% was fixed in all experiments. The conical flask was held at the middle of the sonication bath and its position was maintained the same in all experiments considering spatial variation of acoustic intensity (Moholkar et al., 2000; 2002). The temperature of water in ultrasound bath was maintained at 25° ± 2°C using a circulator. The exact protocol of sonication was decided based on the growth curve of *D. hansenii var.hansenii* cells at optimum medium composition and process parameters. The log or exponential phase of cell life cycle began after 24 h of inoculation and lasted till 72 h. It would rather be impractical to apply sonication in entire 48 h duration of log phase. Because of this, the sonication was applied for only 12 h in different segments of log phase, i.e. 24 to 36 h, 36 to 48 h, 48 to 60 h and 60 to 72 h. This protocol is schematically displayed in Figure 4.4. It may be noted that the total fermentation time was 72 h in all experiments.

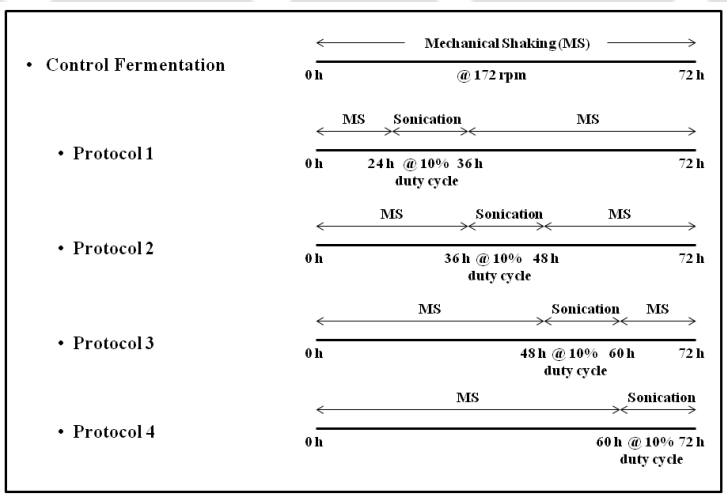

Figure 4.4. Protocols for ultrasound-assisted *Debaryomyces hansenii var. hansenii* fermentation. Sonication was applied in four segments of 12 h (or 720 min) duration each during total log phase of 48 h (between 24–72 h of growth cycle). Total sonication time at 10% duty cycle in each protocol was 72 min.

Dissolved oxygen content: The dissolved oxygen content of the fermentation mixture was assessed before inoculation and after completion of fermentation (A.A. Biotech Pvt. Ltd., Eutech DO−700).

Confirmation of residual intracellular riboflavin: It could be possible that not all riboflavin formed inside the cells was secreted out during fermentation, and some riboflavin was left inside the cells. To confirm this hypothesis, the fermentation broth in the control experiments (conducted with mechanical shaking at 172 rpm) was sonicated for 20 min at the end of 72 h fermentation to release the residual intracellular riboflavin. The riboflavin concentration in the broth was measured before and after the sonication. No detectable change in riboflavin concentration in the broth was seen. In other words, all the riboflavin synthesized inside the microbial cells was secreted out during 72 h fermentation.

Experiments with varying initial substrate concentration: To determine the maximum specific growth rate and Monod saturation constant, fermentation was carried out with varying initial substrate (glucose) concentration from 5 to 30 g/L. Another protocol for the fermentation was exactly the same as stated in previous section.

4.2.8 Kinetic analysis

The Monod kinetic parameters, viz. maximum specific growth rate (μ_{max}) and Monod saturation constant (K_S), for fermentation in control and test experiments were obtained using Lineweaver-Burk plots. The specific growth rate (μ) in the log phase of each fermentation with varying substrate concentration was obtained using basic relation: $dC_X/dt = \mu \cdot C_X$, where C_X is the biomass concentration. The Monod equation is: $\mu = \mu_{max} \cdot C_S/(K_S + C_S)$, where C_S is the substrate concentration. The

maximum specific growth rate (μ_{max}) and Monod constant (K_S) can be obtained according to the Lineweaver–Burk method by rearranging above eqn as:

$1/\mu = K_s/\mu_{max} C_S + 1/\mu_{max}$. The Monod kinetic parameters of μ_{max} and K_S (substrate concentration for which $\mu = \mu_{max}/2$) can be calculated from slope and intercept of the plot of ($1/\mu$) vs. ($1/C_S$).

4.2.9 Analysis of cellular proteins involved in the riboflavin metabolism

SDS-PAGE (Sodium dodecyl sulfate-polyacrylamide gel electrophoresis) was used to separate the cellular proteins based on their molecular size for both control as well as ultrasound-treated cells. After extraction from the cells, the proteins were treated with SDS to get the uniform negative charge. 12.5% (w/v) acrylamide-bisacrylamide gel and buffers were prepared as per the method described by Ahmed (Ahmed et al., 2009). Protein sample for SDS-PAGE was prepared as per following method: 50 mL fermentation broth in both control and test experiments was collected at the end of fermentation (72 h). The cells were harvested by centrifugation at 10000*g* for 10 min at room temperature in a centrifuge (Thermo Fisher Scientific, USA). The cell pellets were collected and re-suspended in 5 mL sodium phosphate buffer (50 mM, pH 7.0). The suspended cells were sonicated (amplitude: 33%, pulse rate: 5s on/10s off).for 20 min in ice bucket using a probe sonicator (Sonics & Materials, Vibra cell). The sonicated broth was centrifuged at 16000*g* for 20 min at 4°C to avoid protein denaturation and to separate the crude supernatant and pellet. Next, 20 µL of cell-free extract and ~5 mg pellet was mixed separately in 5 µL loading dye (Ahmed et al., 2009). The samples were boiled for 4-5 min before loading into the SDS-PAGE. 15 µL of the sample and protein ladder (Hi-Media Prestained

Protein ladder - MBT092) was loaded, and SDS-PAGE was run at 60-80 V. The gel was removed and stained and destained as per protocol of Ahmed et al. (2009). The gel was observed using Gel Doc (Bio-RAD, USA) and Image Lab 5.2.1 software. The protein bands were analyzed according to their respective molecular weights.

4.2.10 Flow cytometry analysis

Flow cytometry analysis was performed to assess morphological changes in *D. hansenii var. hansenii* MTCC 3574 cells induced due to sonication. Wavelengths of laser and emission filters were fixed to 488 nm and 530 nm respectively to analyze control and test samples. SSC (Side Scatter) and FSC (Forward Scatter) were used to distinguish the cells from their mixture based on size and internal complexity. Cell granularity or internal complexity is indicated by the side scattered light while cell size or cell-surface area is indicated by forward scattered light.

4.3 RESULTS AND DISCUSSION

4.3.1 Ultrasound–induced enhancement of riboflavin synthesis

The time profiles of biomass, substrate, and products for the test fermentation with different protocols (as described in Fig. 4.4) are shown in Fig. 4.5. The final riboflavin concentration and yield obtained in four protocols are given in Table 4.3. The results in Table 4.3 clearly show that sonication was most effective in protocol 4, i.e. final 12 hours (60 to 72 h) of exponential (or growth) with riboflavin concentration of 240 mg/L corresponding to yield of 20 mg/g cell.

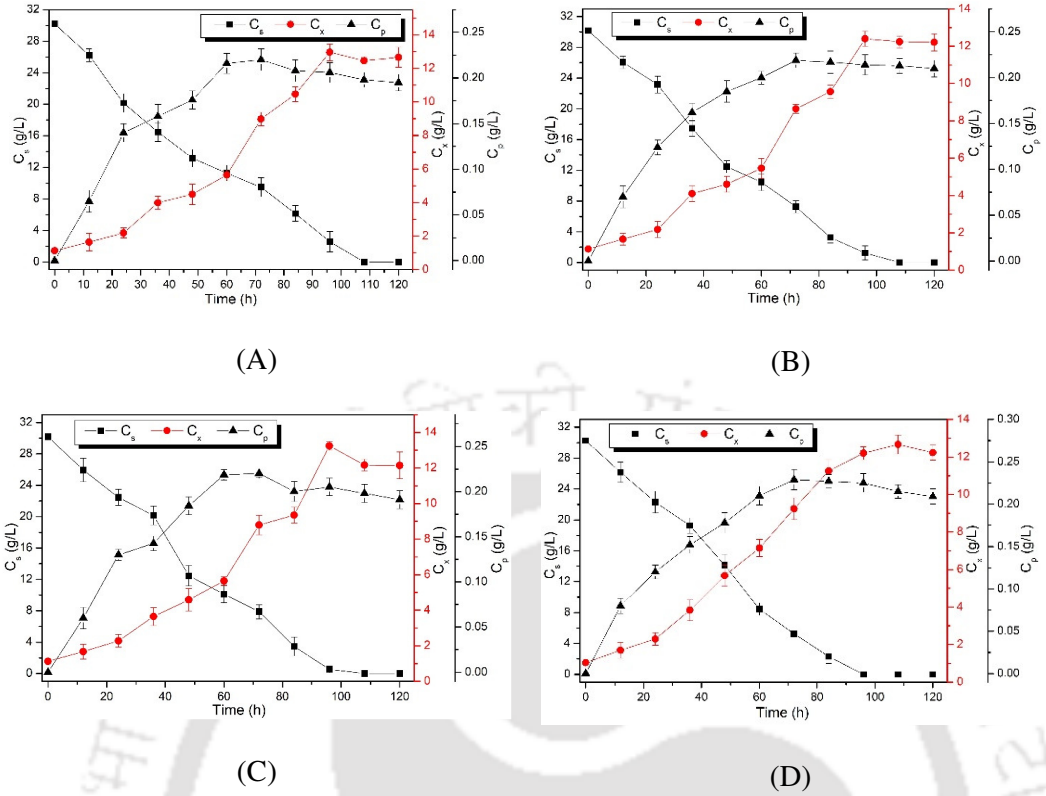

Figure 4.5. Time profiles of biomass (C_X), substrate (C_S) and product (C_P) in test (or ultrasound-assisted) fermentation with different protocols: (A) Protocol 1; (B) Protocol 2; (C) Protocol 3; (D) Protocol 4. Initial substrate concentration in all experiments was 30 g/L.

Table 4.3. Riboflavin concentration and yield for different protocols of ultrasound-assisted fermentation

Test experiment Protocol	Riboflavin production	
	Final concentration mg/L[#]	Yield mg/g of cells
Protocol 1[*]	210 ± 4.6	14 ± 0.7
Protocol 2[*]	215 ± 6.9	16 ± 1.6
Protocol 3[*]	220 ± 8.2	17 ± 2.3
Protocol 4[*]	240 ± 9.1	20 ± 1.8

[*]– Protocols refers to different periods of sonication in log phase
[#]– Concentration at 72 h of fermentation (end of experiment)

4.3.2 Kinetic analysis of test fermentation

The specific growth rate (μ) for control and test experiments was determined from the plots of ln C_X versus t depicted in Figs. 4.6A and B. The complete results of experiments with varying substrate concentration are presented in Table 4.4. For a given initial substrate concentration, the specific growth rate of *D. hansenii var. hansenii* in test fermentation is 3× to 5× higher than control fermentation. This marked rise in the growth rate of *D. hansenii var. hansenii* is clearly an indication of faster metabolism in test fermentation. Lineweaver-Burk plots for the control and test (protocol 4) fermentations are shown in Figs. 4.6C and D, respectively.

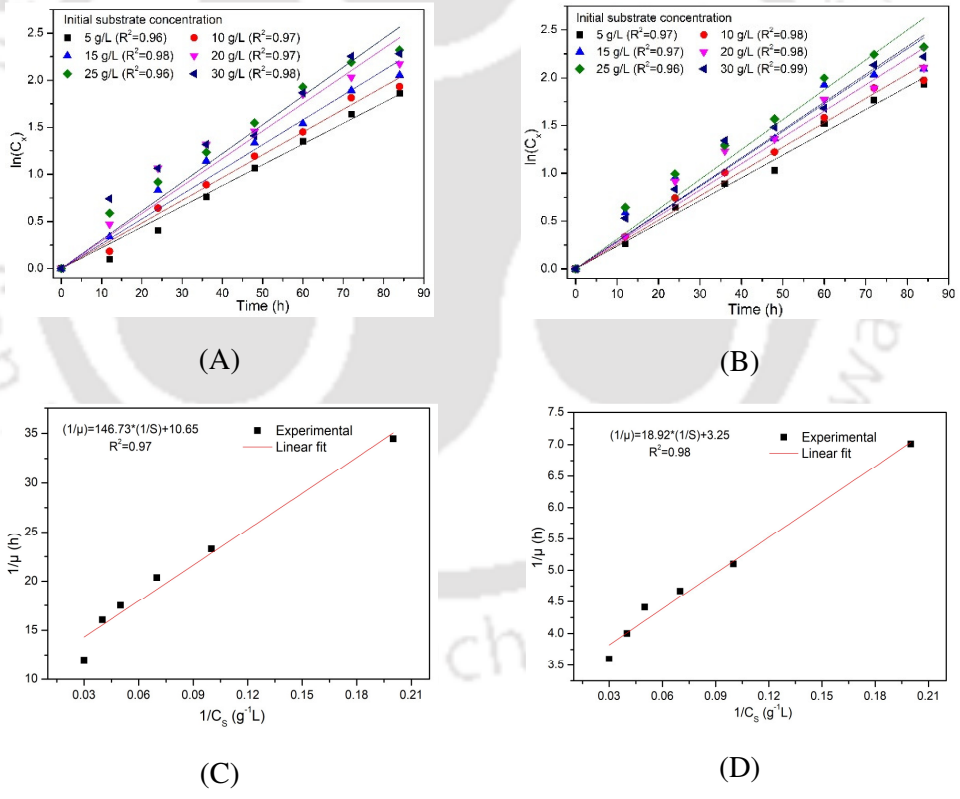

Figure 4.6. (A) and (B) : Evaluation of specific growth rate in the log phase (μ, h^{-1}) for control and test (protocol 4) fermentations, respectively; (C) and (D) : Lineweaver – Burk plots for Monod kinetics for determination of maximum specific growth rate (μ_{max}) and Monod constant (K_S): for control and test (protocol 4) fermentation, respectively.

Table 4.4 Kinetic analysis of control and test (protocol 4) fermentations

Initial substrate (glucose) concentration (g/L)	Kinetic parameters (Control)			Kinetic parameters (Test)		
	μ (h^{-1})	μ_{max} (h^{-1})	K_S (g/L)	μ (h^{-1})	μ_{max} (h^{-1})	K_S (g/L)
5	0.029	0.09	13.20	0.141	0.30	5.67
10	0.043			0.190		
15	0.049			0.212		
20	0.057			0.231		
25	0.063			0.250		
30	0.088			0.298		

The maximum specific growth rate (μ_{max}) for control and test (protocol 4) fermentations was 0.09 and 0.3 h^{-1}, respectively. The Monod saturation constants (K_S) for control and test (protocol 4) fermentations are 13.2 and 5.67 g/L, respectively. Marked rise of 3.33× in the maximum specific growth rate in test fermentation is again a result of faster metabolism or faster substrate utilization under influence of sonication. Concurrent 2.33× reduction in the Monod saturation constant in test fermentation (as compared to control) is also an interesting result. This essentially means that high specific growth rates can be obtained at relatively much smaller substrate concentrations. This result can be attributed to two possible causes, viz. (1) Faster transport of nutrients, substrate, and product across cell membrane – attributed to strong microturbulence generated by ultrasound and cavitation, and (2) rise in enzyme-substrate affinity leading to faster metabolic reactions. A plausible explanation to this result can be given as follows: previous studies (Sulaiman et al., 2011; Nikolic et al., 2010; Choi et al., 2015; Avhad et al., 2015) have shown that microstreaming generated by sonication causes conformational changes in secondary structure of enzymes leading to unfolding of the enzyme proteins. These effects lead to reduction in relative contents of α-helix with concurrent rise in β-sheets and random coils. This leads to exposure of inner hydrophobic groups of enzyme proteins

making access to substrate binding site relatively easy – which is manifested in terms of higher substrate affinity. Indeed, previous studies (Bhasarkar et al., 2015; Dikshit and Moholkar, 2016) have shown similar conformational changes also being induced in intracellular proteins of ultrasound-exposed cells.

4.3.3 Comparative analysis of cellular proteins in control and test fermentation

This study focused on the identification of probable proteins present in *Debaryomyces hansenii var. hansenii* for riboflavin biosynthesis and their relative overexpressions in control and test fermentation. According to Voronovsky et al., 2005, there are five major proteins/genes involved in the riboflavin biosynthesis viz. GTP cyclohydrolase II (*RIB1* gene), HTP reductase (*RIB2* gene), dimethylribityllumazine synthase (*RIB5* gene), dihydroybutanone phosphate synthase (*RIB6* gene) and riboflavin synthase (*RIB7* gene). The molecular weights of *RIB1, RIB2, RIB5, RIB6* and *RIB7* gene producing enzymes are 38.1 kDa, 29.1 kDa, 18.2 kDa, 22.7 kDa, and 26.3 kDa respectively (Voronovsky et al., 2005). The pathway for riboflavin synthesis from *Debaryomyces hansenii var. hansenii* with involved intracellular enzymes is provided in chapter 1 as Fig. 1.2. Figure 4.7 shows the SDS-PAGE image of protein ladder and samples obtained from control and test experiments. It shows the distinct bands of different proteins present in *Debaryomyces hansenii var. hansenii*. The highlighted bands in lane C shows similar molecular weight of enzymes involved in riboflavin biosynthesis pathway viz. GTP cyclohydrolase II (38.1 kDa), HTP reductase (29.1 kDa), dimethylribityllumazine synthase (18.2 kDa), dihydroybutanone phosphate synthase (22.7 kDa) and riboflavin synthase (26.3 kDa). As compared with proteins expressed in control fermentation (pellet free extract, lane B), test fermentation (pellet free extract, lane C) showed

overexpression of above proteins. The pellets of samples from test fermentation (lane E) are also showed the overexpression of the respective proteins. Overexpression of these proteins in the ultrasound-assisted fermentation results in faster metabolism which is manifested as enhanced product yield.

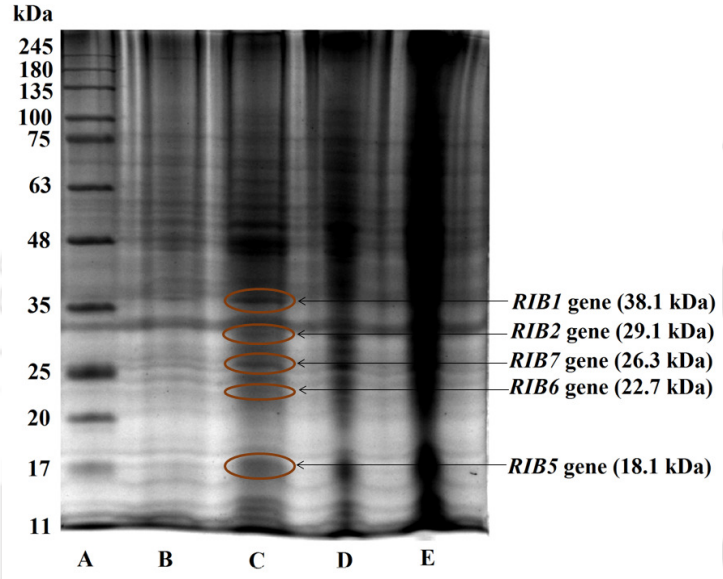

Figure 4.7. Electrophoretic patterns of proteins of *Debaryomyces hansenii var. hanseii* on SDS-PAGE gel. Lane A: Protein ladder; Lane B: Pellet free extract (control fermentation); Lane C: Pellet free extract (test fermentation); Lane D: Cell pellet (control fermentation); Lane E: Cell pellet (test fermentation)

4.3.4 Examinations of morphological changes and yeast cell viability

Flow cytometry analysis was performed to ascertain about morphological changes in the cells obtained after ultrasound-assisted fermentation. The results of which are shown in Fig. 4.8. SSC (side scatter) is a measure roughness of cell surface induced by stress conditions, while FSC (forward scatter) is a measure of the size of the cells, i.e. the higher the FSC greater will be the cell size. Figs. 4.8A and B show acquisition dot plots for control and test samples respectively. As per results shown in Fig. 4.8, no significant change in FSC and SSC is observed for the cells from control

and test fermentations. This is indicated by the presence of majority of cells in the lower left quadrant in control fermentation (99.93 %), and test fermentation (98.63 %). Also, histogram plots showed similar pattern in both samples as M1 in both cases is almost same (99.93% and 98.71% for control and test fermentation, respectively). Therefore, there is no morphological change in *D. hansenii var. hansenii* cells induced due to exposure to sonication.

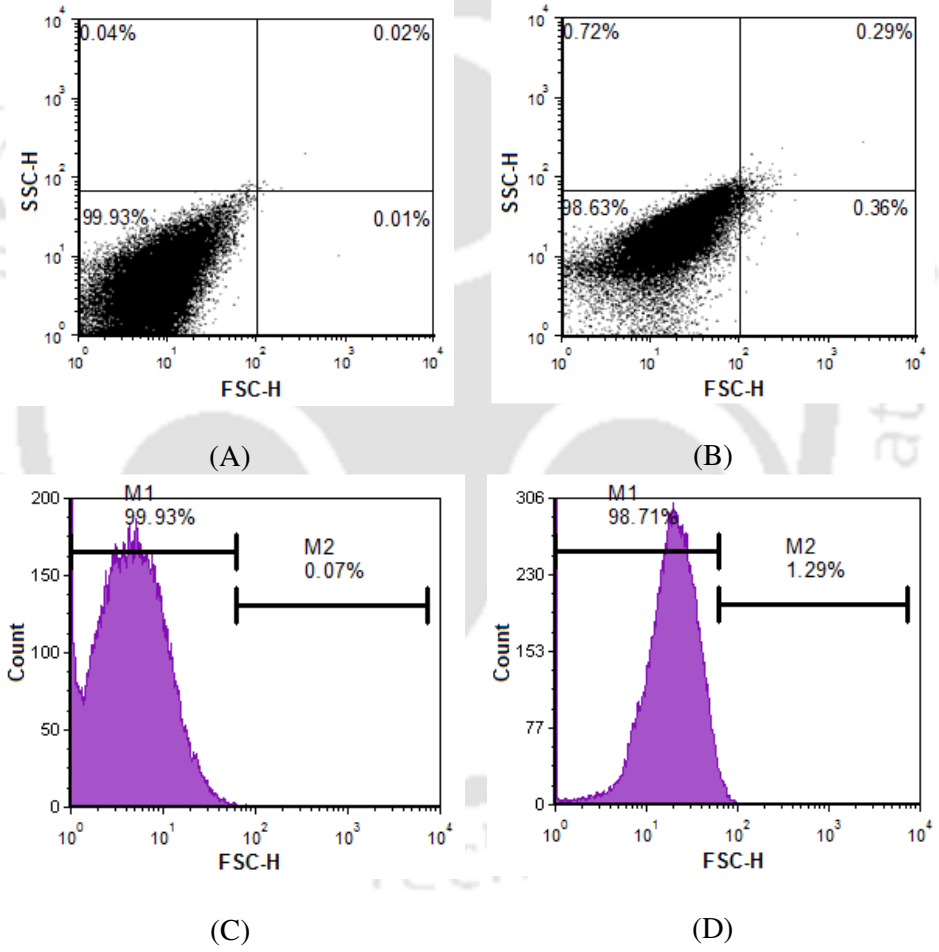

Figure 4.8. Flow cytometric analysis for detecting morphological changes in *Debaryomyces hansenii var. hansenii* cells under the influence of ultrasound. (A) and (B) Acquisition dot plots (FSC vs. SSC) of control and test samples, respectively, (C) and (D) Histogram plots (Count vs. FSC) of control and test samples, respectively.

4.4 CONCLUSION

This chapter has demonstrated the influence of sonication on drastic enhancement of riboflavin production through glucose fermentation and has also provided mechanistic insight into this effect. Riboflavin yield after statistical optimization of medium composition and fermentation parameters was 1.8 mg/g cell, which increased to 4.1 mg/g cell after supplementation of medium with glycine and transition metal cations (Fe, Co, and Zn). Sonication of the fermentation broth in the final 12 h log phase boosted this yield 5× to 20 mg/ g cell. Kinetic analysis of control and test fermentations using Monod growth model revealed sharp rise in maximum specific growth rate (μ_{max}) from 0.09 to 0.3 h^{-1} with concurrent fall in Monod constant (K_S) from 13.2 to 5.67 g/L. More than 3× rise in μ_{max} revealed enhanced metabolism in cells of *D. hansenii var. hansenii*, while reduction in Monod constant also indicated rise in enzyme-substrate affinity. Finally, the SDS-PAGE analysis of cellular proteins (in pellets and pellet free extract) in test fermentation revealed overexpression of all five proteins in riboflavin metabolism, viz. GTP cyclohydrolase II, HTP reductase, dimethylribityllumazine synthase, dihydroybutanone phosphate synthase, and riboflavin synthase. This is yet another confirmation of enhancement of metabolism of cells of *D. hansenii var. hansenii* due to sonication. These effects are essentially attributed to faster cellular transport induced by microturbulence generated by sonication. In summary, this study has demonstrated (on laboratory scale) the efficacy of sonication in intensification of the fermentative production of riboflavin, which could form useful basis for studies on higher production scale.

REFERENCES

Ahmed, S., Bharali, S., Purama, R.K., Majumder A., Fontes, C.M.G.A., Goyal, A., 2009. Structural and biochemical properties of lichenase from *Clostridium thermocellum.* Indian J. Microbiol. 49, 72–76.

Aslam, J.. Mohajir, M.S., Khan, S.A., Khan, A.Q., 2008. HPLC analysis of water-soluble vitamins (B_1, B_2, B_3, B_5, B_6) in *in vitro* and *ex vitro* germinated chickpea (*Cicer arietinum* L.). Afr. J. Biotechnol. 7 (14), 2310–2314.

Avhad, D.N., Rathod, V.K., 2015. Ultrasound assisted production of a fibrinolytic enzyme in a bioreactor. Ultrason. Sonochem. 22, 257–264.

Bhasarkar, J.B., Dikshit, P.K., Moholkar, V.S., 2015. Ultrasound Assisted Biodesulfurization of Liquid Fuel using Free and Immobilized Cells of *Rhodococcus rhodochrous* MTCC 3552: A Mechanistic Investigation. Bioresour. Technol. 187, 369–378.

Boretsky, Y. R.; Pynyaha, Y. V.; Boretsky, V. Y.; Fedorovych, D. V.; Fayura, L. R.; Protchenko, O.; Philpott, C. C.; Sibirny, A. A., 2011. Identification of the genes affecting the regulation of riboflavin synthesis in the flavinogenic yeast *Pichia guilliermondii* using insertion mutagenesis. FEMS Yeast Res. 11 (3), 307–314.

Chaudhuri, S., Batabyal, S., Polley, N., Pal., S.K., 2014. Vitamin B_2 in Nanoscopic Environments under Visible Light: Photosensitized Antioxidant or Phototoxic Drug? J. Phys. Chem. A. 118, 3934–3943.

Choi, E.J., Ahn, H., Kim, M., Han, H., Kim, W.J., 2015. Effect of ultrasonication on fermentation kinetics of beer using six-row barley cultivated in Korea. J. Inst. Brew. 121, 510–517.

Dikshit, P.K., Moholkar, V.S., 2016. Optimization of 1,3–dihydroxyacetone production from crude glycerol by immobilized *Gluconobacter oxydans* MTCC 904. Bioresour. Technol. 216, 1058−1065.

Dmytruk, K., Lyzak, O., Yatsyshyn, V., Kluz, M., Sibirny, V., Puchalski, C., Sibirny, A., 2014. Construction and fed-batch cultivation of *Candida famata* with enhanced riboflavin production. J. Biotechnol. 172, 11−17.

Dmytruk, K.V., Sibirny, A.A., 2012. *Candida famata* (*Candida flareri*). Yeast 29, 453−458.

Dmytruk, K.V., Yatsyshyn, V.Y., Sybirna, N.O., Fedorovych, D.V., Sibirny, A., 2011. Metabolic engineering and classic selection of the yeast *Candida famata* (*Candida flareri*) for construction of strains with enhanced riboflavin production. Metab. Eng. 13, 82−88.

Hassan, O., Chee, M.J., 2001. Sensitivity of UV detection in simultaneous separation and detection of B-vitamins using HPLC. MJAS 7, 251−255.

Heefner, D.L., Boyts, A., Burdzinski, L., Yarus, M. Efficient riboflavin production with yeast. Patent number: 5231007, Patent date: July 27, 1993.

Hu, J., Lei, P., Mohsin, A., Liu, X., Huang, M., Li, L., Hu, J., Hang, H., Zhuang, Y., Guo, M., 2017. Mixomics analysis of *Bacillus subtilis*: effect of oxygen availability on riboflavin production. Microb. Cell Fact. 16:150.

Jiménez, A., Santos, M.A., Pompejus, M., Revuelta, J.L., 2005. Metabolic engineering of the purine pathway for riboflavin production in *Ashbya gossypii.* Appl. Environ. Microbiol. 71 (10), 5743−5751.

Kurtzman, C.P., Robnett, C.J., 2013. Relationships among genera of the *Saccharomycotina* (*Ascomycota*) from multigene phylogenetic analysis of type species. FEMS Yeast Res. 13, 23−33.

Ledesma-Amaro, R., Serrano-Amatriain, C., Jiménez, A., Revuelta, J.L., 2015. Metabolic engineering of riboflavin production in *Ashbya gossypii* through pathway optimization. Microb. Cell Fact. 14:163.

Levine, H., Oyaas J.E., Wasserman, L., Hoogerheide, J.C., Stern R.M., 1949. Riboflavin production by *Candida* yeasts. Ind. Eng. Chem. 41 (8), 1665−1668.

Mateos, L., Jimenez, A., Revuelta, J., Santos, M.A., 2006. Purine biosynthesis, riboflavin production, and trophic-phase span are controlled by a myb-related transcription factor in the fungus *Ashbya gossypii*. Appl. Environ. Microbiol. 72 (7), 5052−5060.

Moholkar, V.S., Huitema, M., Rekveld, S., Warmoeskerken, M.M.C.G., 2002. Characterization of an ultrasonic system using wavelet transforms. Chem. Eng. Sci. 57, 617−629.

Moholkar, V.S., Sable, S.P., Pandit, A.B., 2000. Mapping the cavitation intensity in an ultrasonic bath using the acoustic emission. AIChE J. 46, 684−694.

National Collection of Yeast Cultures, 2017. Available from: http://www.ncyc.co.uk/

Nikolic, S., Mojovic, L., Rakina, M., Pejinb, D., Pejin, J., 2010. Ultrasound-assisted production of bioethanol by simultaneous saccharificationand fermentation of corn meal. Food Chem. 122 (1), 216−222.

Oraei, M., Razavi, S.H., Khodaiyan, F., 2018. Optimization of Effective Minerals on Riboflavin Production by *Bacillus subtilis subsp. subtilis* ATCC 6051 Using Statistical Designs. Avicenna J. Med. Biotech. 10 (1), 49−55.

Palmer, T., Bonner, P. *Enzymes,* 2nd ed.; Horwood Publishing Limited, 2008.

Plackett, R.L., Burman, J.P., 1946. The design of optimum multifactorial experiments. Biometrika. 33, 305–325.

Plaut G.W., 1954. Biosynthesis of riboflavin. I. Incorporation of C14-labeled compounds into rings B and C. J. Biol. Chem. 208, 513–520.

Roya, D., Mohammad, R., Hossein, N., Gholamreza, G., 2013. Isolation of Two Riboflavin Producer Yeasts from Environment and Optimization of Vitamin Production. J. Appl. Environ. Biol. Sci. 3 (12), 23–29.

Sauer, U., Hatzimanikatis, V., Hohmann, H., Manneberg, M., van Loon, A.P.G.M., Bailey, J.E., 1996. Physiology and metabolic fluxes of wild-type and riboflavin-producing *Bacillus subtilis*. Appl. Environ. Microbiol. 62 (10), 3687–3696.

Sivasankar, T., Paunikar, A.W., Moholkar, V.S., 2007. Mechanistic Approach to Enhancement of the Yield of a Sonochemical Reaction. AIChE J. 53 (5), 1132–1143.

Sulaiman, A.Z., Ajit, A., Yunus, R.M., Chisti, Y., 2011. Ultrasound–assisted fermentation enhances Bioethanol productivity. Biochem. Eng. J. 54, 141–150.

Suzuki, G.T., Macedo, J.A., Macedo, G.A., 2011. Medium composition influence on biotin and riboflavin production by newly isolated *candida* sp. Braz. J. Microbiol. 42, 1093–1100.

Tizazu, B.Z., Moholkar, V.S., 2018. Kinetic and thermodynamic analysis of dilute acid hydrolysis of sugarcane bagasse. Bioresour. Technol. 250, 197–203.

Voronovsky, A.Y., Abbas, C.A., Dmytruk, K.V., Ishchuk, O.P., Kshanovska B.V., Sybirna, K.A., Gaillardin, C., Sibirny, A.A., 2004. *Candida famata* (*Debaryomyces hansenii*) DNA sequences containing genes involved in riboflavin synthesis. Yeast 21, 1307–1316.

Wang, L., Chi, Z., Wang, X., Ju, L., Chi, Z., Guo, N., 2008. Isolation and characterization of *Candida membranifaciens* subsp. *flavinogenie* W14-3, a novel riboflavin-producing marine yeast. Microbiol. Res. 163, 255–266.

Xin, Z., Pu, L., Gao, W., Wang, Y., Wei, J., Shi, T., Yao, Z., Guo, C., 2017. Riboflavin deficiency induces a significant change in proteomic profiles in HepG2 cells. Sci. Rep. 7:45861.

Yaguchi, A., Rives, D., Blenner, M., 2017. New kids on the block: emerging oleaginous yeast of biotechnological importance. AIMS Microbiol. 3 (2), 227–247.

Ultrasound-Assisted Antisolvent crystallization of lactose monohydrate

5.1 INTRODUCTION

Lactose ($C_{12}H_{22}O_{11}$) is a disaccharide consisting of galactose and glucose subunits. Being a sugar (or energy source), lactose finds application as a food and pharmaceutical product (Wong et al., 2012). Solid form of lactose could be amorphous or crystalline. Crystalline lactose generally exists in the form of two anomers, viz. α-lactose and β-lactose, or mixture of both. The prevalent anomer of lactose depends on the technique of crystallization and product recovery. Existence of α-lactose and β-lactose is due to the phenomenon called mutarotation (Haase and Nickerson, 1966; Raghavan et al., 2001; Crisp et al., 2011). Mutarotation is induced by addition of water to lactose, resulting in changes of anomeric form. Mutarotation essentially involves rotation of hydroxyl group available on the C-1 carbon of the

glucose molecule, which allows the opening of the ring available on the first carbon molecule, and spatial arrangement of hydroxyl group that gives either α-lactose or β-lactose (Jawad et al., 2012; Pawar et al., 2018). Industrially, lactose is produced from the whey remained after processing of milk for producing milk products. Refining of lactose from whey solution involves several steps among which crystallization is an important step (Wong and Hartel, 2014; Pandalaneni et al., 2018).

Common techniques for crystallization of lactose are: (1) cooling crystallization, (2) seeded cooling crystallization, and (3) antisolvent crystallization (Figura, 1993). Cooling crystallization suffers from demerit of impractically large induction time for nucleation ranging from days to weeks. This limitation could be overcome with seeded cooling crystallization. This process also provides stability to crystals at ambient temperatures. But the issue with seeded cooling crystallization is generation of fines and varied morphology of the crystal crop that affects downstream processing and final product properties (Zeng et al., 2000; Omar et al., 2015). The technique of antisolvent crystallization overcomes these issues with better control over nucleation, growth rate and morphology (MacFhionnghaile et al., 2017). Antisolvent added to aqueous lactose solution is generally miscible with water, and reduces the lactose solubility in the blended solvent (water + antisolvent) that leads to precipitation of solute (lactose) in the form of crystals. More recently, ultrasound irradiation or sonication has been employed as a tool for enhancement of lactose recovery during crystallization with uniform size and habit of crystals. Several previous authors (Bund and Pandit, 2007; Kougoulos et al., 2010; Gogate and Gajendragadkar, 2017; Pawar et al., 2018) have reported beneficial effects of sonication on lactose crystallization process and recovery. Two distinct merits of ultrasonic crystallization reported in previous literature for lactose recovery are: (1) rapid and consistent nucleation

throughout reaction volume, and (2) higher crystal product with relatively uniform crystal size. The exact physical mechanism of influence of ultrasound on antisolvent crystallization of lactose has remained unexplored. In a previous study (Nalajala and Moholkar, 2011), we had reported mechanistic studies in ultrasound-assisted antisolvent crystallization of KCl. This study clearly showed that both nucleation rate as well as growth rate of crystals was influenced by micro-convection generated by sonication. The dominant crystal size reduced with application of sonication.

In the present study, we have addressed the important matter of establishing physical mechanism of ultrasound assisted antisolvent crystallization of lactose. The basis of present study is to discriminate between individual effects of macro-convection and micro-convection in the systems, which are manifested in terms of overall crystal yield and the crystal size distribution (or the mean crystal size). The approach adopted in this study includes experiments on antisolvent crystallization, determination of kinetic parameters of crystallization with modified-MSMPR model, and analysis of trends in the kinetic parameters vis-à-vis simulations of cavitation bubble dynamics. Macro-convection is induced by mechanical stirring of crystallization magma, while micro-convection is induced by ultrasound and cavitation (which is nucleation, growth and transient collapse of tiny air bubbles). Interestingly, the micro-convection comprises of three components, viz. microstreaming due to ultrasound wave, and microturbulence and acoustic or shock waves due to transient cavitation, each of which has distinct character. This study has also attempted to reveal individual effects of these components on the crystallization process and the resultant average crystal size and yield.

5.2 EXPERIMENTAL

5.2.1 Materials

Lactose monohydrate was procured from Himedia (India) and analytical grade ethanol (antisolvent) of 99.9% v/v was obtained from Jiangsu Huaxi International Trade Co. Ltd, China. Lactose solutions of three concentrations viz. 5% w/v, 10% w/v and 15% w/v were prepared using Millipore water.

5.2.2 Experimental procedure

The experiments were devised to study the effect of three physical parameters on crystal yield and size distribution (or mean size), viz. (1) initial concentration of lactose, (2) rate of ethanol (antisolvent) addition, and (3) application of mechanical stirring and/or sonication of the solution. In order to distinguish between the effect of ultrasound and cavitation, lactose crystallization with sonication was also carried out at elevated static pressure. The rationale underlying raising of static pressure of the system will be explained in next sections. The experiments were carried out in three protocols as shown in Table 5.1

Table 5.1. Experimental protocols for antisolvent crystallization of lactose monohydrate

Experimental protocols	Initial lactose concentration (% w/v)	Ethanol addition rate (mL/min)	Static pressure (atm)
Protocol 1*	5	1	1
	10	2	
	15	3	
Protocol 2#	5	1	1
	10	2	
	15	3	
Protocol 3@	15	1	2

* – mechanical stirring (400 rpm); # – sonication with mechanical stirring;
@ – sonication at elevated static pressure, Sonication (1 min @37 kHz) was applied after every 6 ml ethanol addition.

A three neck round bottom flask of 500 mL capacity was used to carry out crystallization reactions. The necks or ports of the flask were utilized as follows: (1) ethanol addition using syringe pump, (2) mechanical stirrer (for protocols 1 and 2) or pressure gauge (for protocol 3), and (3) connection to a nitrogen cylinder for application of elevated pressure over crystallization magma (for protocol 3). The schematic of the experimental setups in different protocols is given in Figs. 5.1A and B.

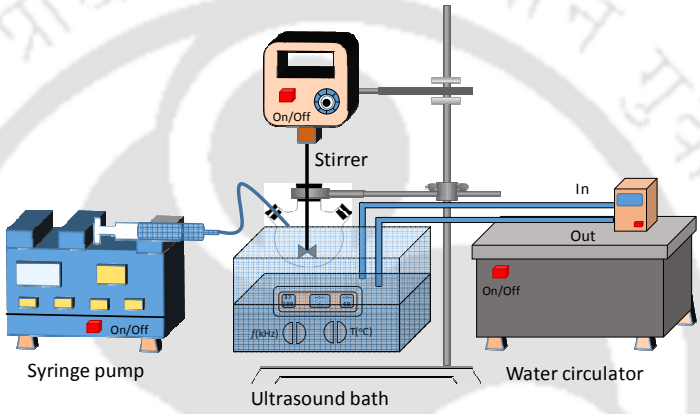

(A)

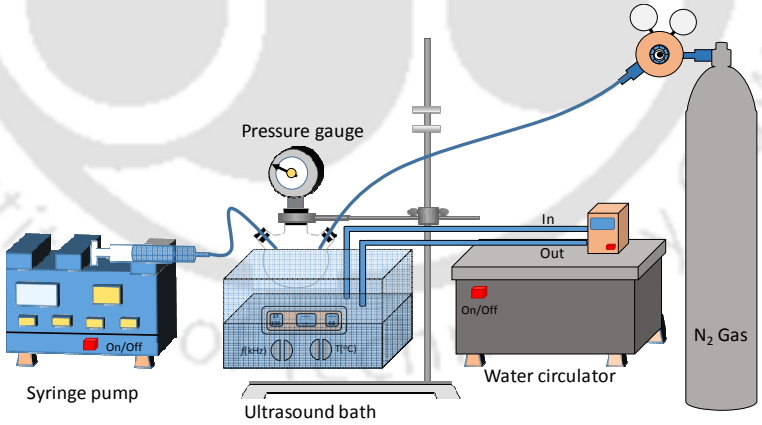

(B)

Figure 5.1. Experimental setup for antisolvent crystallization protocols: (A) Protocol 1 and 2 and (B) Protocol 3. In protocol 1 ultrasound bath was kept on silent mode.

An ultrasound bath (Elmasonic P, Frequency 37 kHz, Rated power 35 W, Volume 2.5 L) was used for the sonication of aqueous lactose solution. The bath was filled with water. The crystallization flask was immersed in the bath at a specific location, which was carefully maintained same in all experiments. The temperature of water in the bath was controlled at 30 ± 2°C through circulation of water. The actual acoustic power dissipation in the bath and the pressure amplitude of the ultrasound waves was determined using the calorimetric technique (Sivasankar et al., 2007). The acoustic pressure amplitude in the bath was determined as 1.5 bar. The pH of lactose solution was maintained at 5.0 ± 0.4. The quantity of ethanol to be added in the lactose solution of different initial concentrations was optimized in preliminary experiments on the basis of lactose crystal yield. In these experiments, no visible crystal formation was seen till the composition of ethanol in the solution reached till 70-80% v/v. In view of this, the final composition of ethanol in the solution was fixed as 90% v/v. Thus, final total volume of crystallization solution was 100 mL, i.e. 10 mL of aqueous lactose solution and 90 mL of ethanol, added at different rates. The rate of ethanol addition into the crystallization flask was controlled using a syringe pump (Make: New Era Pump Systems, Inc., USA, Model: 300). The crystallization magma was subjected to sonication of 1 min duration after every 6 mL ethanol addition. Thus in all experiments, total sonication time corresponding to 90 mL ethanol addition was 15 min. However, depending on the rates of ethanol addition, the total period of crystallization varied. The period of crystallization corresponding to ethanol flow rate of 1, 2 and 3 mL/min was 90, 45 and 30 min, respectively. At the end of experiment, the lactose crystals in the solution were separated by vacuum filtration through 0.45 μm vacuum filter and were dried overnight at 50°C. The

crystals were weighed to determine the yield and the morphology of the crystals was examined using FE-SEM micrographs as explained below.

5.2.3 Lactose characterization

The surface and structural morphology of lactose crystals was assessed using Field emission scanning electron microscope (FESEM, Make: Zeiss, Model: Sigma 300). The machine was operated under vacuum at voltage range 3-5 KV. The samples of the lactose crystals were prepared by adding precisely equal quantities of crystals obtained after drying in ethanol followed by sonication for ~ 5 min so as to break-up the agglomerates. Nearly 50 μL of resultant solution was then placed on an aluminum pin stub. The micrographs of the crystals obtained in the three protocols (with lactose solutions of different initial concentrations) were obtained at similar magnification so as to compare the morphologies. These micrographs were analyzed with ImageJ software for determination of the size distribution of the crystals.

5.2.4 Modeling of batch antisolvent crystallization: Modified MSMPR model

A popular model for kinetics of crystallization is the MSMPR (mixed suspension mixed product removal) model. In this section, we present a modified version of this model for the system of antisolvent batch crystallization of lactose from aqueous solutions. The crystallization system in present study was batch type with no product withdrawal but continuous addition of antisolvent. Thus, the volume of the system was variable.

The crystallization solution was subjected to mechanical stirring as well as sonication (protocol 2), which generated sufficiently strong convection in the solution. Thus, one can assume that the growth rate of crystals in the magma was not only

constant in entire volume, but also independent of crystal size. Thus, the growth rate can be written in differential and discretized form as: $G = dL/dt$ or $\Delta L = G \cdot \Delta t$. The change in number density of crystals in the size range dL can be written as: $d(N/V) = ndL$, where n is crystal population density (N/L, where N is the total number of crystals with size L). Under assumption of strong convection and perfect mixing of the crystallization solution, the rate of change of number density of crystals (in the size range dL) can be assumed to vary linearly in time, which gives:

$$-\frac{\Delta ndL}{ndL} = -\frac{\Delta n}{n} = \frac{\Delta t}{\tau} \tag{5.1}$$

where τ is the total time over which the antisolvent is added to crystallization magma. Equation 5.1 can be written in differential form – with substitution of $\lim_{\Delta t \to 0} \Delta t = dt = dL/G$.

$$-\frac{dn}{n} = \frac{dL}{G\tau} \tag{5.2}$$

Integrating equation 5.2 gives:

$$n = n_0 \exp\ (-L/G\tau) \tag{5.3}$$

Using chain rule, the rate of change of crystal density in the magma can be written as:

$$\frac{d\left(N/V\right)}{dt} = \frac{d\left(N/V\right)}{dL}\left(\frac{dL}{dt}\right) \tag{5.4}$$

where, $\lim_{L \to 0} d(N/V)/dt = B$, $dL/dt = G$ and $\lim_{L \to 0} d\left(N/V\right)/dL = n_0$. This leads to the relation: $B = n_0 G$ (where B is the rate of nucleation). A plot of $\ln n$ against L should give a straight line with slope $m = -1/G\tau$ and an intercept of $\ln n_0$. Knowing the total time of crystallization, the growth rate G can be determined from slope. Using values of n_0 and G, the nucleation rate B can be obtained. The input for the model is the size

distribution of lactose crystals, which was obtained using FESEM micrographs, as noted earlier.

5.2.5 Cavitation bubble dynamics

Ultrasound wave is essentially a longitudinal wave that passes through the medium in the form of compression/rarefaction cycles which generates periodic (or sinusoidal) variation in bulk pressure in the medium. Sonication of the liquid medium also induces phenomenon of cavitation, which is nucleation, growth and implosive transient collapse of gas bubbles driven by bulk pressure variation in the system. These gas bubbles are already present in the liquid medium or could also be contributed by the gas pockets trapped in the crevices of solid boundaries such as reactor wall. For relatively smaller pressure amplitudes of ultrasound wave (typically smaller than static pressure in the system), stable cavitation prevails, in which the volume oscillations of the bubble are in phase with compression/rarefaction cycles of the wave. For ultrasound pressure amplitude higher than static pressure, transient cavitation occurs, in which the volume oscillations of the bubble are dominated by inertial forces. In this case, the bubble undergoes large expansion, followed by extremely rapid transient collapse in few tens of nanoseconds. The compression of the bubble is adiabatic and temperature inside the bubble reaches extreme (~ 5000 K, ~ 500 bar). The rapid compression of the bubble also causes spherical convergence of the fluid elements surrounding it. As the bubble compression comes to halt, these fluid elements are reflected back and give rise to an acoustic wave with high pressure amplitude. The volume oscillations of the bubbles also generates oscillatory velocity field around them known as microturbulence. The magnitudes of pressure amplitude of acoustic wave and velocity of microturbulence can be determined using

simulations of cavitation bubble dynamics. For simulations of cavitation bubble dynamics in the crystallization solution, we have chosen the bubble dynamics equation proposed by Lofstedt et al. (1995) and Hilgenfeldt et al. (1996) given as:

$$R\frac{d^2R}{dt^2}+\frac{3}{2}\left(\frac{dR}{dt}\right)^2=\frac{1}{\rho}\left(p(R,t)-P_0-P(t)\right)+\frac{R}{\rho c}\frac{d}{dt}\left[p(R,t)-P(t)\right]-\frac{4\mu}{\rho R}\frac{dR}{dt}-\frac{2\sigma}{\rho R} \tag{5.5}$$

Using van der Waal's equation, the pressure inside the cavitation bubble is written as:

$$p(R,t)=\left(P_0+\frac{2\sigma}{R_0}-P_v\right)\left(\frac{R_0^3-h^3}{R^3-h^3}\right)^{\nu}+P_v \tag{5.6}$$

The sinusoidal variation of pressure in the medium due to sonication is written as:

$$P(t)=P_A\cos(2\pi ft)=P_A\cos(\omega t) \tag{5.7}$$

Various notations are as follows: R = radius of cavitation bubble at any time t, R_0 = initial radius of the bubble, P_0 = static pressure in the crystallization system, dR/dt = velocity of the bubble wall during radial motion, d^2R/dt^2 = acceleration of the bubble wall during radial motion, f = frequency of ultrasound, ω = angular frequency of ultrasound, P_A = pressure amplitude of the ultrasound wave.

The second order second degree equation of cavitation bubble dynamics can be transformed into two simultaneous ODEs as:

$$\frac{dR}{dt}=s \tag{5.8}$$

$$\frac{ds}{dt}=\frac{1}{R\rho}\left[p(R,t)-P(t)-P_0\right]+\frac{1}{\rho c}\left[\frac{-3\gamma R^2p(R,t)}{(R^3-h^3)}\frac{dR}{dt}\right]+\frac{1}{\rho c}\omega P_A sin(\omega t)$$
$$-\frac{4\mu}{\rho R^2}\frac{dR}{dt}-\frac{2\sigma}{\rho R^2}-\frac{3}{2}\frac{s^2}{R} \tag{5.9}$$

These ODEs can be solved using Runge-Kutta adaptive step size method (Press et al., 1992). Using the solutions of these equations, the magnitude of the convection effects,

viz. velocity of the microturbulence $u(r,t)$ and pressure amplitude of the acoustic waves $P_s(r,t)$ can be calculated using following equations:

$$u(r,t) = \frac{R^2}{r^2}\left(\frac{dR}{dt}\right) \tag{5.10}$$

$$P_s(r,t) = \rho\frac{R}{r}\left[2\left(\frac{dR}{dt}\right)^2 + R\frac{d^2R}{dt^2}\right] \tag{5.11}$$

where r is the distance from bubble centre. A representative value of r can be taken as 1 mm.

***Simulation parameters*:** The composition of the crystallization solution, and hence its physical properties changed continuously during the process due to addition of antisolvent (ethanol). The initial lactose solution is aqueous to which ethanol is added continuously. The seeding of lactose crystals is visible in the solution only after addition of ~ 60 mL ethanol, which grows rapidly as crystallization solution gets enriched in ethanol. The final solution has composition of 90 ml ethanol + 10 ml aqueous lactose solution, which has been considered for simulations. The following properties of 90% v/v ethanol have been used for simulations: vapor pressure (P_v) = 7800 Pa, viscosity (μ) = 0.948×10^{-3} Pa-s, surface tension (σ) = 0.02 N/m, density (ρ) = 781 kg/m^3, sonic velocity (c) = 1127 m/s. A representative value of the initial bubble radius (R_o) is taken as 5 μm. Other physical parameters for simulations are: ultrasound frequency (f) = 37 kHz; ultrasound pressure amplitude (P_A) = 1.4 bar; polytropic constant of bubble contents (γ) = 1/3; van der Waal's hard core radius (h) = R_0/8.86.

Microstreaming: The microconvection created in the medium due to sonication is also contributed by oscillatory motion of liquid elements induced by propagation of ultrasound. This is known as microstreaming. The magnitude of microstreaming

velocity depends on ultrasound or acoustic pressure amplitude, as explained subsequently in the discussion.

5.3 RESULTS AND DISCUSSION

The yields of lactose crystals and the corresponding percentage recoveries in experimental protocol 1 (mechanical stirring at 400 rpm) and protocol 2 (mechanical stirring with sonication) are shown in Table 5.2A. The results of lactose crystallization in protocol 3 (sonication at elevated static pressure of 2 atm) are given in Table 5.2B. The data presented in Tables 5.2A and B depicts influence of three experimental parameters, viz. initial solute (or lactose) concentration in the solution, rate of antisolvent addition and application of sonication on lactose yield. In protocol 3, the rate of antisolvent addition was kept constant at 1 mL/min, and only the initial solute concentration was varied. We discuss below the salient features of the influences of these parameters on lactose yield and plausible rationale for the same.

Table 5.2A. Results of antisolvent crystallization of lactose at atmospheric static pressure (protocols 1 and 2)

Sr. No.	Initial lactose (w/v)	Ethanol flow rate (mL/min)	Final lactose weight (g)		Lactose recovery (%)	
			Protocol 1 (MS)	Protocol 2 (US + MS)	Protocol 1 (MS)	Protocol 2 (US + MS)
1	5%	1	0.368 ± 0.005	0.437 ± 0.003	73.6 ± 2.1	87.4 ± 2.4
		2	0.351 ± 0.002	0.415 ± 0.004	70.3 ± 1.8	83.1 ± 1.9
		3	0.334 ± 0.006	0.401 ± 0.002	66.8 ± 1.4	80.2 ± 1.7
2	10%	1	0.805 ± 0.010	0.913 ± 0.014	80.5 ± 1.9	91.3 ± 1.6
		2	0.761 ± 0.008	0.875 ± 0.012	76.1 ± 1.7	87.5 ± 2.2
		3	0.715 ± 0.012	0.826 ± 0.010	71.5 ± 2.2	82.6 ± 1.8
3	15%	1	1.285 ± 0.072	1.414 ± 0.091	85.6 ± 2.6	94.2 ± 1.7
		2	1.213 ± 0.081	1.360 ± 0.083	80.8 ± 1.8	90.6 ± 2.1
		3	1.117 ± 0.079	1.307 ± 0.076	74.4 ± 2.3	87.1 ± 1.9

Notation: MS – mechanical stirring (400 rpm); US + MS – sonication with mechanical stirring. Sonication (1 min @37 kHz) was applied after every 6 ml ethanol addition.

Table 5.2B. Results of antisolvent crystallization of lactose at elevated static pressure (protocol 3)[#]

Sr. No.	Initial lactose weight (g)	Final lactose weight (g)	Lactose recovery (%)
1	0.5 (5% w/v)	0.400 ± 0.002	92.1 ± 1.9
2	1.0 (10% w/v)	0.875 ± 0.014	95.2 ± 1.8
3	1.5 (15% w/v)	1.346 ± 0.082	98.3 ± 1.7

- ethanol addition rate = 1 mL/min

5.3.1 Effect of initial lactose concentration

In protocols 1 and 2, for given antisolvent addition rate, the percentage yield of lactose increased with initial concentration of the solution – although the rise was marginal. For example, for the highest ethanol addition rate of 3 mL/min, percentage yield for initial concentration of 5% w/v was 80.2%, which marginally increased to 87.1% for 15% w/v lactose. A plausible explanation for this result could be given in terms of prevalent nucleation rate in the magma for different initial concentrations of lactose. The rate of nucleation and (and nuclei population density) increases proportionately with the degree of supersaturation generated in the medium – which in turn depends on the initial concentration of lactose solution. As a consequence of higher nucleation rate in the solution, the yield of lactose crystals increases. Marginal rise in the crystal yield with rising initial solution concentration could be attributed to effective agitation of the solution due to which nuclei grow equally fast, despite higher population.

5.3.2 Effect of rate of antisolvent addition

In protocols 1 and 2, the yield of lactose crystals reduced with rise in antisolvent addition rate for a given initial lactose concentration. The reduction in crystal yield was, however, marginal (~ 8 to 10%). An explanation for this result can

also be given in terms of relative rates of nucleation and growth for varying rates of antisolvent addition. For slower antisolvent addition rate, the instantaneous degree of supersaturation in the solution is low that results in formation fewer nuclei, which grow rapidly and uniformly. As the antisolvent addition rate increases, the nuclei population density and rate of nucleation rises very rapidly. However, not all nuclei grow to form crystals, if the convection in the medium is not strong enough to have effective mass transfer rate of lactose molecules from solution phase to crystal surface. In such situation, the nuclei may redissolve in the solution leading to reduction in the crystal yields.

5.3.3 Effect of sonication

Comparing the percentage lactose recoveries for the protocols 1 and 2 across all combinations of initial lactose concentrations and rates of antisolvent addition, it could be seen that lactose yield for protocol 2 were higher by ~ 10-15%. On relative basis, ultrasound was more effective in enhancing crystal yields for lower initial lactose concentration and higher rate of antisolvent addition. For example, for initial lactose concentration of 5% w/v, sonication enhances crystal yield (or percentage recovery) from 73.6% to 87.4% (a rise of 18.8%) for the slowest ethanol addition rate of 1 mL/min. On the other hand, for ethanol addition rate of 3 mL/min, the rise in crystal yield with sonication is 20.1% (from 66.8% to 80.2%). For same ethanol addition rate but initial lactose concentration of 15% w/v, rise in crystal yield with sonication is relatively smaller (~7% rise from 74.4% to 87.1%). Rise in the crystal yields with sonication is essentially a manifestation of intense micro-convection generated in the medium. As noted earlier, the rate of nucleation in the solution is governed by supersaturation, which in turn is a function of initial solute concentration

and the rate of antisolvent addition. However, growth rate of these nuclei is governed by intensity of convection in the medium. Sonication of the solution induces intense micro-level convection through phenomena of microstreaming, microturbulence and shock waves (or acoustic waves), as noted earlier. This convection drastically enhanced the mass transfer in the system, and transfer of lactose molecules from solution phase to crystal surface. As a result, the growth rate of nuclei increased markedly, causing rise in overall lactose yield.

As revealed from results presented in Table 5.2B, the lactose yields are further enhanced in protocol 3. For all initial concentrations of lactose, the yields are > 90%, and for the highest concentration of 15% w/v, almost complete recovery of lactose (~ 98.3%) is seen. As revealed through kinetic analysis of crystallization presented in next section, the influence of sonication on lactose yield is manifested through two physical factors, viz. nucleation rate and growth rate of crystals. Moreover, the average size of lactose crystals obtained in each protocol is also a manifestation of these factors.

5.3.4 Crystallization kinetics

Figs. 5.2A, B and C show representative FE-SEM micrographs of lactose crystals in the three experimental protocols for initial lactose concentration of 15% w/v and ethanol addition rate of 1 mL/min. The micrographs in Figs. 5.2A and B are obtained at similar magnification of 300 X, while micrograph in Fig. 5.2C is at a higher magnification of 1.5 KX. Figs. 5.2A and B reveal loose clustering and agglomeration between the lactose particles. Fig. 5.2C shows strong congregation between lactose particles with formation of lumps. The crystal size distribution of lactose obtained from FE-SEM micrographs in different protocols was analysed with

modified MSMPR model (presented in section 5.2.4) to obtain the kinetic parameters of crystallization, viz. nuclei population density (n_0), growth rate of crystals (G), the rate of nucleation (B) and average crystal size. Figs. 5.3A, B and C show the plots of ln n vs. L (eqn. 5.3) in the three experimental protocols for different initial lactose concentrations. The rate of antisolvent addition, however, was fixed at 1 mL/min.

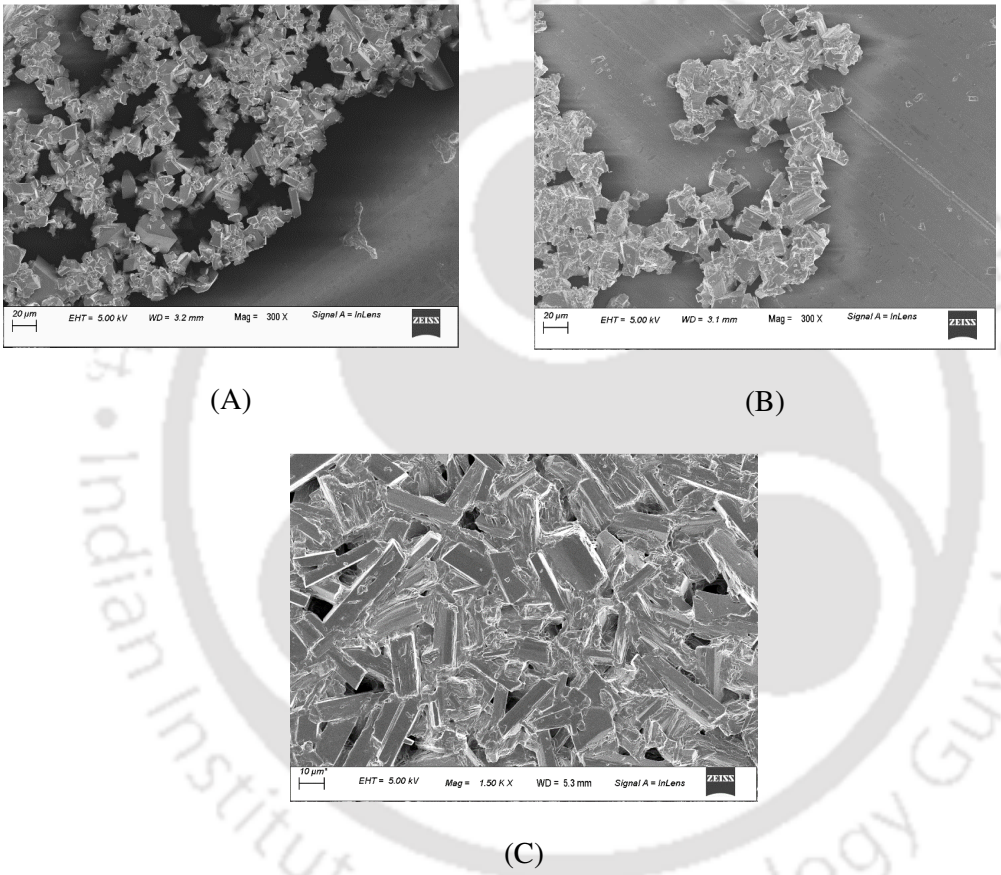

Figure 5.2. FESEM micrographs of lactose crystals obtained from antisolvent crystallization of 15% w/v lactose solution in different experimental protocols. (A) protocol 1; (B) protocol 2; (C) protocol 3.

The salient features of kinetics of crystallization in the three protocols, as evident from the kinetic parameters listed in Table 5.3 for the three experimental protocols, are as follows:

(1) In protocol 1, both nuclei population density and growth rate increased with initial lactose concentration, and as a consequence, the rate of nucleation also augmented. This is obviously attributed to higher level of supersaturation generated in the crystallization magma with increasing initial solute concentration. However, the average crystal size of lactose showed relatively insignificant variation with initial solute concentration (viz. 6.01, 8.09 and 6.52 μm for 5, 10 and 15% w/v lactose).

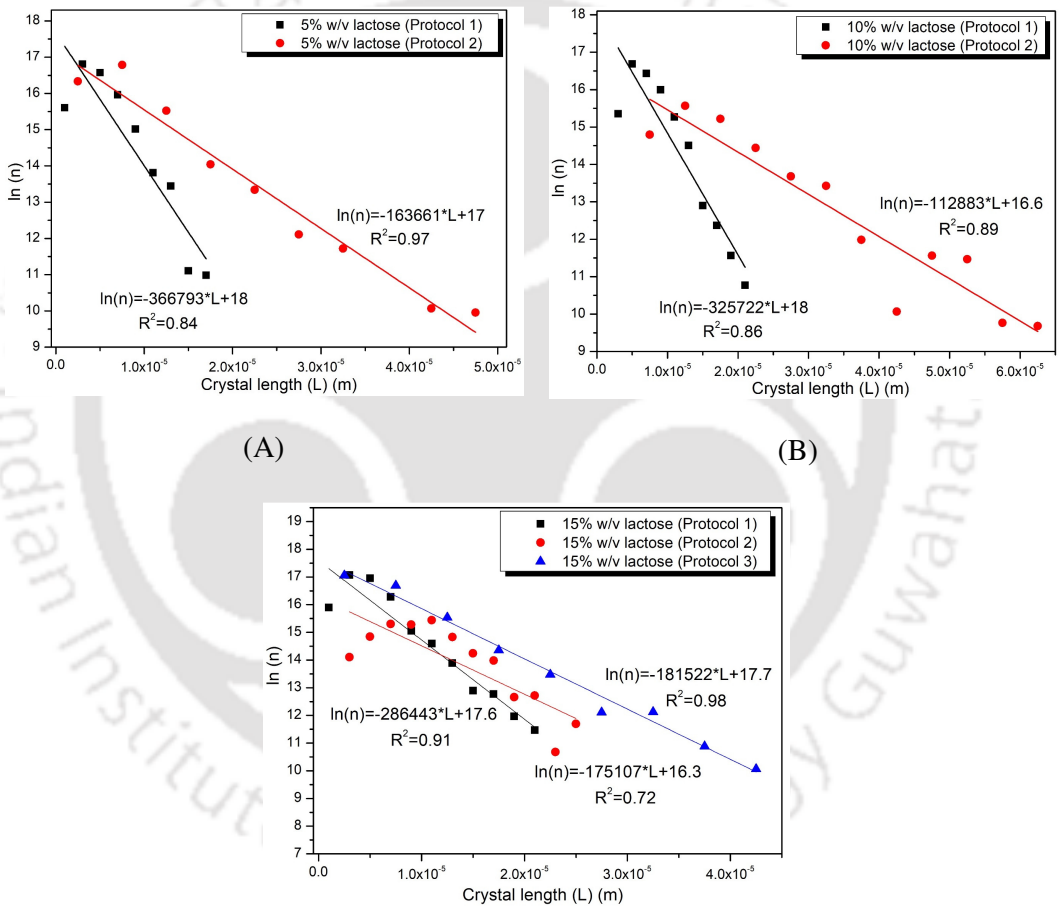

Figure 5.3. Plots of ln n versus L for determination of nuclei population density (n_0) and growth rate of crystals (G) in the three experimental protocols for different initial concentration of lactose: (A) 5% w/v; (B) 10% w/v; (C) 15% w/v.

This could be collective consequence of relatively high rate of mechanical stirring (@ 400 rpm), in addition to simultaneous rise in n_0 and G, which essentially resulted in equal growth of all crystals.

(2) In protocol 2 experiments, where crystallization magma was subjected to intermittent sonication, the nuclei population density reduced as compared to protocol 1 for any initial solute concentration. However, the growth rate of crystals showed significant rise. As a result of these inverse variations in n_0 and G, the rate of nucleation in protocol 2 was smaller than protocol 1. For example, for initial lactose concentration of 10% w/v, n_0 reduced from 7.21×10^7 m^{-4} (protocol 1) to 1.60×10^7 m^{-4} (protocol 2), while G increased from 5.69×10^{-10} m/s to 1.64×10^{-9} m/s. Nucleation rate, however, reduced from 0.0411 to 0.0262 $m^{-3} \cdot s^{-1}$.

Table 5.3. Kinetic analysis (parameters) of antisolvent lactose crystallization in different protocols

Sr. No.	Initial lactose concentration (% w/v)	Average crystal size (μm)	n_o (m^{-4})	G ($m \cdot s^{-1}$)	B ($m^{-3} \cdot s^{-1}$)
1	5 (protocol 1)	6.01	4.73×10^7	5.05×10^{-10}	0.0239
2	5 (protocol 2)	10.65	2.91×10^7	1.13×10^{-9}	0.0329
3	10 (protocol 1)	8.09	7.21×10^7	5.69×10^{-10}	0.0411
4	10 (protocol 2)	10.28	1.60×10^7	1.64×10^{-9}	0.0262
5	15 (protocol 1)	6.52	9.36×10^7	6.46×10^{-10}	0.0605
6	15 (protocol 2)	11.54	1.16×10^7	1.06×10^{-9}	0.0122
7	15 (protocol 3)	20.81	4.74×10^7	1.52×10^{-9}	0.0721

Due to relatively smaller number of nuclei that grew at a higher rate, the average crystal size in protocol 2 was significantly larger than corresponding crystal size in protocol 1. However, in concurrence with protocol 1 experiments, the average crystal size showed minor variation with initial lactose concentration, and almost similar average crystal size was obtained for 5, 10 and 15% w/v initial lactose concentration, viz. 10.65, 10.28 and 11.54 μm, respectively.

(3) A remarkable result was obtained for protocol 3, in which the crystallization solution was subjected to only intermittent sonication (with no mechanical stirring) at elevated static pressure of 2 atm. The initial lactose concentration was 15% w/v. In this case, both nuclei population density (4.74×10^{7} m^{-4}) and growth rate (1.52×10^{-9} m/s) increased as compared to protocol 2 (viz. 1.16×10^{7} m^{-4} and 1.06×10^{-9} m/s). As a result, the nucleation rate showed drastic boost of ~ 6× (from 0.0122 m^{-3} s^{-1} to 0.0721 m^{-3} s^{-1}). The average crystal size (20.81 μm) was nearly double that of the size in protocol 2 (11.54 μm). Due to large number of nuclei that grew at high rate, nearly complete lactose recovery (98.3%) was obtained in protocol 3.

5.3.5 Links with cavitation bubble dynamics

The trends in kinetic parameters of crystallization in the three protocols are essentially manifestations of the nature of convection generated in the medium due to mechanical stirring and sonication. The results of simulations of radial motion of a 5 μm air bubble along with associated physical effects of microturbulence and shock waves (which contribute to microconvection in the solution) are presented in Figs. 5.4 and 5, for the conditions of atmospheric (1 atm) and elevated (2 atm) static pressure, respectively. It could be seen from Fig. 5.4 that at atmospheric static pressure, the cavitation bubble undergoes significant expansion. The radius of the bubble grows to 3 to 4 times original size (thus volume expands as ~R3, i.e. 27 to 64×). This is followed by extremely rapid transient collapse with few afterbounces. The volume oscillations of the bubble generate oscillatory velocity field around the bubble, with average velocity of 0.003 m/s. The transient collapse of the bubble results in generation of shock wave with pressure amplitude of ~ 15 to 20 atm.

As the static pressure in the system is raised, drastic change in seen in behavior of the bubble, as depicted in Fig. 5.5. The growth of the bubble is sharply reduced, as the bubble radius expands to merely 30-40% of the initial size. The magnitude of the shock waves reduces to ~ 1.5 kPa, while microturbulence velocity is ~ 0.5 mm/s. Thus, the contribution of cavitation bubble dynamics to generation of microconvection in the solution practically reduces to zero at elevated static pressure. An important difference in the characteristics or nature of microturbulence and shock waves, as evident from Fig. 5.4 is that shock waves are rather sporadic and intermittent, while microturbulence is continuous phenomenon. Relatively, the intensity of shock waves is far higher than microturbulence.

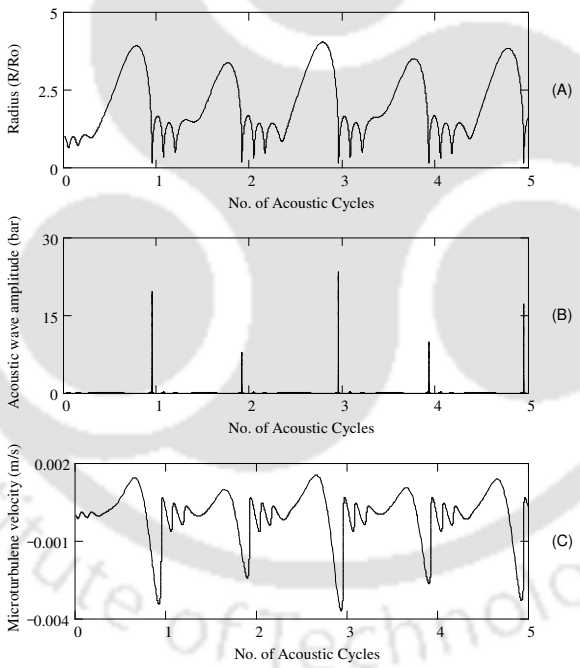

Figure 5.4. Graphical results of simulations of cavitation bubble dynamics in lactose solution at atmospheric static pressure (1 atm). Time profiles of (A) bubble radius (non-dimensional), (B) acoustic (or shock) wave emission from the bubble, (C) microturbulence generated by the bubble

As noted earlier, the microconvection in the medium is also contributed by microstreaming, which is oscillatory motion of fluid elements induced by propagation

of ultrasound wave. The magnitude of the microstreaming velocity (u) is related to acoustic pressure amplitude (P_A) as: $P_A = u\rho c$, where ρ is the density of the liquid and c is the sonic velocity in the liquid. The physical properties of the liquid are relatively insensitive to static pressure (for low to moderate pressure levels), and thus, magnitude of microstreaming stays practically unchanged in protocol 2 and 3. The pressure amplitude of ultrasound wave in the bath was 1.5 bar. The values of density and sonic velocity in 90% v/v ethanol can be taken as 789 kg/m^3 and 1127 m/s, respectively. Thus, the magnitude of microstreaming velocity can be determined as 0.17 m/s. Comparing the velocities of microturbulence and microstreaming reveals that contribution to microconvection by the latter is several orders of magnitude stronger than the former.

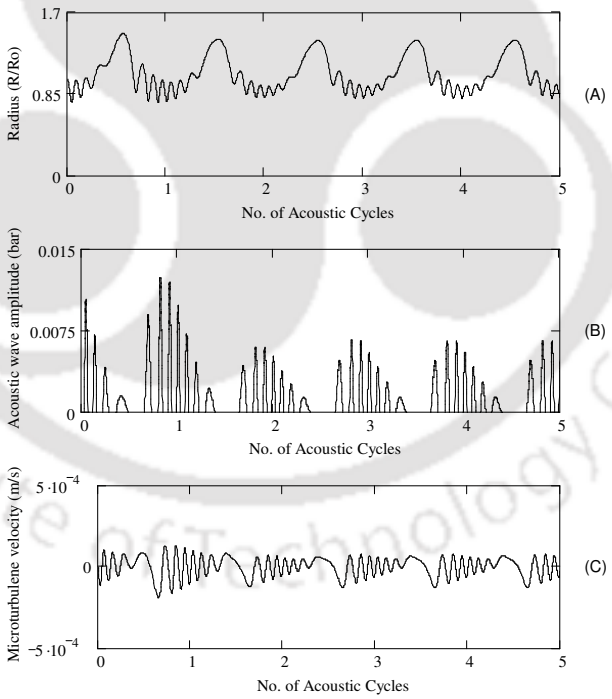

Figure 5.5. Graphical results of simulations of cavitation bubble dynamics in lactose solution at elevated static pressure of 2 atm. Time profiles of (A) bubble radius (non-dimensional), (B) acoustic (or shock) wave emission from the bubble, (C) microturbulence generated by the bubble

The degree of supersaturation produced in the solution depends on initial solute concentration and the rate of antisolvent addition. However, for similar degree of supersaturation, the prevalent nuclei population density, growth rate of crystals, rate of nucleation and average size of crystal crop is a strong function of nature of convection produced in the medium. The convection induced by mechanical stirring is essentially "macro-convection" that produces bulk movement of crystallization solution due to which lactose precipitating out of solution is distributed uniformly in the liquid. However, macroconvection is not so effective in enhancing mass transfer of solute molecules coming out of liquid phase to crystal surface. Thus, the solute molecules end up in forming new nuclei rather than growing already present nuclei in the solution. This is manifested in terms of higher nucleation rate but smaller growth rate. Sonication, on the other hand, produces microscale convection which is effective in enhancing mass transfer of lactose molecules from solution phase to crystal surface. Uniform and faster deposition of solute molecules on to the nuclei leads to higher growth rate and higher average particle size. Concurrently, the nucleation rate also reduces. Another factor that could also contribute to reduction in nucleation rate in protocol 2 is the intermittent shock waves (or acoustic waves) emitted by the transient bubbles. These acoustic waves can cause re-dispersion or disintegration of lactose particles gathered together to form a nucleus.

Individual contributions of microstreaming and acoustic waves to crystallization process are further evident by comparison of kinetic parameters for protocols 2 and 3. Rise in static pressure of the medium in protocol 3 eliminates occurrence of transient cavitation in the medium. This essentially means that phenomena of both microturbulence and shock waves are absent at elevated static pressure. Moreover, no mechanical stirring was provided to solution in protocol 3.

Nonetheless, microstreaming due to sonication stays unaffected. This essentially means that lactose crystallization in protocol 3 occurred only in presence of microconvection. As noted previously, the values of n_0, G and B for protocol 3 are several fold higher than protocol 2. The average crystal size of lactose in protocol 3 is also twice as high than protocol 2. This result clearly shows that transient cavitation in the system acts against nucleation in the solution. On the contrary, the microstreaming due to ultrasound not only assists growth of the crystals the but also nucleation. Formation of lumps of lactose crystals in protocol 3 (as seen in Fig. 5.2C) can also be explained on the basis of absence of macroconvection in the system. Due to absence of mechanical stirring, the lactose precipitating out of solution was not distributed in the bulk volume. Although microstreaming generates intense mixing in the solution, it is highly localized, which doesn't give effective volumetric distribution of solute. Thus, the lactose crystals end up in forming lumps and clusters.

5.4 CONCLUSION

This study has attempted to explore the mechanistic features of sonocrystallization of lactose from aqueous solution. The basic approach adopted in this study was to analyze experimental results using modified MSMPR model for batch crystallization and couple it to simulations of cavitation bubble dynamics. Different experimental protocols adopted in this study varied the nature of convection produced in the system that influenced the kinetic parameters of crystallization. Final manifestation of the influence of convection in the system is yield of lactose and the average crystal size. Mechanical stirring of the solution, which provides macroconvection in the system, was effective in enhancing nucleation rate but not growth rate. The microconvection due to sonication comprised of microstreaming due

to ultrasound waves and shock waves due to transient cavitation. Microstreaming was revealed to enhance both nucleation rate and growth rate, while shock waves reduced the nucleation. The highest lactose yield with the largest average crystal size was obtained in protocol 3, in which crystallization was carried out at elevated static pressure that eliminated transient cavitation – leaving microstreaming intact. The microstreaming, however, was not able to cause bulk mixing of lactose, resulting in formation of lumps of crystals. Thus, the results of this study have clearly demonstrated that lactose crystallization from aqueous solutions is assisted by ultrasound but not cavitation.

REFERENCES

Bund, R.K.; Pandit, A.B., 2007. Rapid lactose recovery from buffalo whey by use of 'anti-solvent, ethanol'. J. Food Eng. 82 (3), 333–341.

Crisp, J.L., Dann, S.E., Blatchford, C.G., 2011. Antisolvent crystallization of pharmaceutical excipients from aqueous solutions and the use of preferred orientation in phase identification by powder X-ray diffraction. Eur. J. Pharm. Sci. 42 (5), 568–577.

Figura, L.O., 1993. The physical modification of lactose and its thermoanalytical identification. Thermochim. Acta. 222 (2), 187–194.

Gogate, P.R., Gajendragadkar, C.N., 2017. Ultrasound assisted intensified recovery of lactose from whey based on antisolvent crystallization. Ultrason. Sonochem. 38, 754–765.

Haase, G., Nickerson, T.A., 1966. Kinetic reactions of alpha and beta lactose. I. Mutarotation. J. Dairy Sci. 49 (2), 127–132.

Hilgenfeldt, S., Lohse, D., Brenner, M.P., 1996. Phase Diagrams for Sonoluminescing Bubbles. Phys. Fluids 8 (11), 2808–2826.

Jawad, R., Elleman, C., Vermeer, L., Drake, A.F., Woodhead, B., Martin, G.P., Royall, P.G., 2012. The measurement of the β/α anomer composition within amorphous lactose prepared by spray and freeze drying using a simple (1)H-NMR method. Pharm. Res. 29 (2), 511–524.

Kougoulos, E., Marziano, I., Miller, P.R., 2010. Lactose particle engineering: Influence of ultrasound and anti-solvent on crystal habit and particle size. J. Cryst. Growth 312, 3509–3520.

Lofstedt, R., Weninger, K., Puttermann, S.J., Barber, B.P., 1995. Sonoluminescing Bubbles and Mass Diffusion. Phys. Rev. E 51 (5), 4400–4410.

MacFhionnghaile, P., Svoboda, V., McGinty, J., Nordon, A., Sefcik, J., 2017. Crystallization Diagram for Antisolvent Crystallization of Lactose: Using Design of Experiments To Investigate Continuous Mixing Induced Supersaturation. Cryst. Growth Des. 17, 2611–2621.

Nalajala, V.S., Moholkar, V.S., 2011. Investigations in the Physical Mechanism of Sonocrystallization. Ultrason. Sonochem. 18, 345–355.

Omar, C.S., Dhenge, R.M., Osborne, J.D., Althaus, T.O., Palzer, S., Hounslow, M.J., Salman, A.D., 2015. Roller compaction: Effect of morphology and amorphous content of lactose powder on product quality. Int. J. Pharm. 496 (1), 63–74.

Pandalaneni, K., Amamcharla, J.K., Marella, C., Metzger, L.E., 2018. Influence of milk protein concentrates with modified calcium content on enteral dairy beverage formulations: Physicochemical properties. J. Dairy Sci. 101 (11), 9714–9724.

Pawar, N., Agrawal, S., Methekar, R., 2018. Modeling, Simulation, and Influence of Operational Parameters on Crystal Size and Morphology in Semibatch Antisolvent Crystallization of α Lactose Monohydrate. Cryst. Growth Des. 18, 4511−4521.

Press, W.H., Teukolsky, S.A., Flannery, B.P., Vetterling, W.T., 1992. Numerical Recipes (2nd Ed.); Cambridge University Press: New York.

Raghavan, S.L., Ristic, R.I., Sheen, D.B., Sherwood, J.N., 2001. The bulk crystallization of α-lactose monohydrate from aqueous solution. J. Pharm. Sci. 90 (7), 823−832.

Sivasankar, T., Paunikar, A.W., Moholkar, V.S., 2007. Mechanistic Approach to Enhancement of the Yield of a Sonochemical Reaction. AIChE J. 53 (5), 1132−1143.

Wong, S.Y., Bund, R.K., Connell, R.K., Hartel, R.W., 2012. Designing a lactose crystallization process based on dynamic metastable limit. J. Food Eng. 111 (4), 642−654.

Wong, S.Y., Hartel, R.W., 2014. Crystallization in Lactose Refining−A Review. J. Food Sci. 79 (3), R257−R272.

Zeng, X.M., Martin, G.P., Marriott, C., Pritchard, J., 2000. The Influence of Crystallization Conditions on the Morphology of Lactose Intended for Use as a Carrier for Dry Powder Aerosols. J. Pharm. Pharmacol. 52 (6), 633−643.

Overview and Suggestions for Future Work

6.1 OVERVIEW

Present thesis has addressed important fundamental issues in ultrasound-assisted food processing of liquid systems. An attempt has been made in this thesis for intensification of product yield in different common food processes by application of sonication to the conventional food processing techniques. Three food processes, viz. extraction, fermentation and crystallization, with three model systems were studied in this thesis work. Research reported in previous literature has already reported beneficial action of ultrasound on these processes for increasing product yield or faster kinetics. However, the missing link was the physical mechanism of the process, that is the links between the physics of the process and physical effects of ultrasound and cavitation. An attempt has been made in this thesis to fulfill this research gap with basic approach of coupling experimental results to simulations. The results of this

thesis research have shed light on intricate links between physics of ultrasound and cavitation, and the physics of the basic process.

A peculiar feature of this thesis is that in all studies, the natural strains and isolates of microbial strains have been used. This is in view of their stability and sturdiness in open natural environment. The genetically engineered species have shown excellent performance in controlled environments (i.e. lab scale studies). However, in large scale or open system, these species are not stable. They do not grow aggressively consuming carbon sources/minerals in competition to other species/contaminations present in large scale open systems. Thus these species are not much suitable for commercial scale processes. A summary of various chapters in the thesis is given below:

- Chapter 1 presents general introduction of the theme of the thesis. A brief description is given about different food processes and their conventional techniques. The demerits of these techniques have been identified where ultrasound (or sonication) can provide potential solution.
- In Chapter 2, we have addressed the importance of optimization of fermentation medium composition and process parameters in the enhancement of astaxanthin yield using statistical optimization technique. Further enhancement in intracellular astaxanthin content was observed when sonication (at 10% duty cycle) was applied during *Phaffia rhodozyma* fermentation at optimized conditions. Astaxanthin yield was enhanced from 1360 μg/g DCW (at optimized conditions) to 1728 μg/g DCW with an assistance of sonication. This enhancement is attributed to intense micromixing induced by sonication, which has several possible implications such as physical maturation of cells, reduction in substrate inhibition and conformational changes in secondary structure of intracellular enzymes. Also,

investigations on morphological changes (using flow cytometry) and viability of yeast cells (using methylene blue staining) for ultrasound treated cells revealed that internal complexity and morphology of yeast cells remains unaltered and no cell death occurred during ultrasound exposure.

- In Chapter 3, we have addressed the importance of solvents for effective extraction of intracellular astaxanthin from *Phaffia rhodozyma* cells. Initially four solvents were screened for maximum astaxanthin yield in different protocols. Acetone was found to be best among all and continued to use in preceding experiments. Microbial cells of *Phaffia rhodozyma* were disrupted using ultrasonic probe. To study the effect of solvent mixture on effective astaxanthin extraction, combination of dimethyl sulphoxide (cell disrupting agent) and acetone at varying composition was used as an extracting solvent. The results were analyzed in concurrence with prediction of astaxanthin solubility using UNIFAC (Universal Quasi-Chemical Functional-Group Activity Coefficients) method and simulations of cavitation bubble dynamics. The highest astaxanthin yield of 1536 ± 3 µg/g DCW was obtained for solvent comprising 33% v/v DMSO + 67% v/v acetone. UNIFAC predicted astaxanthin solubility (1.57 g/L) was also highest for this composition, although the convection intensity predicted by bubble dynamics simulations was relatively low. Experiments using extraction solvent with varying composition of DMSO and acetone, coupled with solubility predictions using UNIFAC and simulations of cavitation bubble dynamics have revealed the relative influence of two factors, viz. saturation solubility and convection intensity, on extraction yield of astaxanthin. Our results have established that saturation solubility of astaxanthin, which decides driving force for extraction, is the dominant factor governing extraction process, as compared to intensity of convection in the extraction mixture – which essentially

governs the mass transfer characteristics of the system.

- In Chapter 4, we have presented a study on riboflavin synthesis from *Debaryomyces hansenii var. hansenii*. In this chapter, it was observed that supplementation of additives (glycine, $FeCl_3$, $ZnCl_2$ and $CoCl_2$) played a major role in enhancement of riboflavin yield than mere optimization of medium components and process parameters. Riboflavin yield was further intensified with the application of sonication (at 10% duty cycle) during log phase (24 to 72 h) of fermentation in the segments of 12 h each. The riboflavin yield after statistical optimization and additive supplementation (4.1 mg/g cell) boosted ~ 5× to 20 mg/g cell with sonication of fermentation broth in the final 12 h of log phase. Kinetic analysis was done using Monod growth model to see the effects of ultrasound on maximum specific growth rate and Monod constant which revealed higher maximum specific growth rate of cells (0.30 h^{-1}) with reduced Monod constant (5.67 g/L), indicating faster cell transport and higher substrate affinity. Finally, the SDS-PAGE analysis of cellular proteins in ultrasound-assisted fermentation revealed overexpression of the proteins in riboflavin metabolism. This is a confirmation of enhancement of metabolism of cells of *D. hansenii var. hansenii* due to sonication.

- In Chapter 5, we have attempted to reveal the mechanistic features of antisolvent crystallization of lactose from aqueous solutions. Experiments were carried out in three protocols, viz. mechanical stirring, mechanical stirring with sonication and sonication at elevated static pressure. These protocols essentially varied the nature of convection in the system. Mechanical stirring provided macroconvection while sonication induced microconvection in the system. Other experimental parameters were initial lactose concentration and rate of antisolvent (ethanol) addition. Basic methodology was to couple kinetic parameters of

crystallization to simulations of bubble dynamics. The nuclei population density, growth rate of crystals, rate of nucleation, average size of crystal crop and total lactose yield in different protocols was analysed against macro- and microconvection in the medium. Macroconvection assisted nucleation but could not give high growth rate. Microconvection comprised of microstreaming due to ultrasound and acoustic (or shock) waves due to transient cavitation. Sonication at atmospheric static pressure enhanced growth rate but reduced nucleation. However, with elimination of cavitation at elevated static pressure, sonication enhanced both nucleation and growth rate resulting in almost complete lactose recovery. These results clearly reveal that lactose crystallization is assisted by ultrasound, but is adversely affected by transient cavitation.

An important outcome of all chapters is the strong influence of mass transfer on the process. Thus, an important key to intensification of these processes is enhancement mass transfer characteristics of the system. Looking at the prevalent mechanics for all processes that has become evident from this thesis, the physical effects of sonication – i.e. generation of intense micro-convection - are relevant for enhancing efficiencies of food processes. This microconvection is able to enhance mass transfer in microscale systems (bacterial cultures or lactose crystals etc.), which is manifested in terms of faster kinetics with higher yield. A key revelation of the thesis (which has not been reported in previous literature) is the intra-cell influence of sonication in terms of overexpressions of genes corresponding to different enzymes in metabolic pathway. This effect is underlying the enhanced productivity of natural isolates of bacterial cultures – at par with genetically modified strains.

6.2 SUGGESTIONS FOR FUTURE WORK

The present thesis aimed at application of ultrasound in food processing of liquid systems viz. extraction (astaxanthin), fermentation (riboflavin) and crystallization (lactose). The results of this thesis can give basic mechanistic guidelines for development of industrial/large scale process. Moreover the methodologies adopted in this thesis can form general framework for further mechanistic studies in similar systems. Some suggestions for future work in these areas can be given as follows:

1. The experimental studies carried out in this thesis were carried out at laboratory scale. Further studies can be carried out to scale up these processes to pilot scale by considering some additional parameters such as aeration, amount of antifoaming agent etc. along with the parameters used in the current study.
2. In the present thesis, we have used commercial purified forms of carbon sources such as glucose and lactose (for crystallization) which can be replaced with waste carbon sources obtained from food waste or agricultural waste to reduce overall production cost.
3. Wild/commercial microbial strains have been used in this thesis for astaxanthin and riboflavin synthesis which can be replaced with stable mutant strains to enhance yield and productivity.
4. An important contribution of this thesis is insight into the actual cellular mechanism for enhanced kinetics and yield. It has been revealed that two possible mechanisms can contribute to the enhanced metabolism, viz. faster cellular transport of nutrients, substrate and products, and enhanced kinetics of metabolic reactions due to higher activity of the enzymes. The latter effect is attributed to changes in

secondary structure of enzymes during sonication leading to unfolding of proteins. As further research in this area, a distinction between the two mechanisms can be made, and individual (or relative) contributions of each mechanism can be identified.

5. The role of ultrasound can be studied in depth by considering various parameters such as varying the frequency and power input of ultrasound in the system. Multi transducer systems can also be introduced in these processes unlike the single transducer system used in the present study.

6. The present thesis has studied antisolvent crystallization of lactose. However, many food processing systems use thermal crystallization. It would be worthwhile to study mechanism of influence of sonication on thermally operated systems. The physical characterization of the solid product can also be carried out. Alternative protocols include continuous sonication of the system under elevated static pressure.

RESEARCH OUTPUT

PAPERS IN PEER REVIEWED INTERNATIONAL JOURNALS

OUT OF THESIS

1. **Amit H. Batghare**, Neha Singh, Vijayanand S. Moholkar. Investigations In Ultrasound–Induced Enhancement of Astaxanthin Production by Wild Strain *Phaffia rhodozyma* MTCC 7536. Bioresource Technology 2018; 254: 166–173.

2. **Amit H. Batghare**, Saiprasad Pati, Kuldeep Roy, Vijayanand S. Moholkar. Mechanistic Investigations in Ultrasound-Assisted Extraction of Astaxanthin from *Phaffia rhodozyma* MTCC 7536. Bioresource Technology Reports 2018; 4: 166–173.

3. **Amit H. Batghare**, Kuldeep Roy, Kaustubh C. Khaire, Vijayanand S. Moholkar. Mechanistic investigations in ultrasound-induced intensification of fermentative riboflavin production. Bioresource Technology Reports 2020; 9, 100380.

4. **Amit H. Batghare**, Kuldeep Roy, Vijayanand S. Moholkar. Investigations in physical mechanism of ultrasound-assisted antisolvent batch crystallization of lactose monohydrate from aqueous solutions. Ultrasonics Sonochemistry 2020, 105127.

OTHER PUBLICATIONS

1. Neha Singh, **Amit H. Batghare**, Bhaskar J. Choudhury, Vijayanand S. Moholkar. Microalgae Based Biorefinery: Assessment of Wild Fresh Water Microalgal Isolate for Simultaneous Biodiesel and β-carotene Production. Bioresource Technology Reports 2020, 100440.

2. Ritesh S. Malani, **Amit H. Batghare**, Jaykumar B. Bhasarkar, Vijayanand S. Moholkar. Engineering and Modeling Aspects of Desulfurization: Review and Analysis. (Under review).

BOOK CHAPTERS

1. **Amit H. Batghare**, Vijayanand S. Moholkar. Production of nutraceutical astaxanthin from waste resources. Waste Biorefinery Vol III, Elsevier (Under review).

CONFERENCE PRESENTATIONS

1. Poster presentation: "Mechanistic Investigations in Ultrasound–Induced Enhancement of Riboflavin Production by *Debaryomyces hansenii var. hansenii* MTCC 3574" at International Conference on Biotechnological Research and Innovation for Sustainable Development (BioSD), CSIR-IICT Hyderabad during November 22 – 25, 2018 (International Conference).

2. Poster presentation: "Optimization and Ultrasound-Assisted Intensification of Astaxanthin Production by *Phaffia rhodozyma* MTCC-7536" at International Conference on Emerging Trends in Biotechnology for Waste Conversion (ETBWC), CSIR-NEERI Nagpur during October 8 – 10, 2017 (International Conference).

3. Poster presentation: "Optimization of astaxanthin production by *Phaffia rhodozyma* using yeast malt media" at Research Conclave, IIT Guwahati during March 16 – 19, 2017 (National Conference).

APPENDIX

A1. Calculation of the acoustic pressure amplitude by the ultrasound bath (Sivasankar et al., 2007)

The pressure amplitude of the acoustic wave produced in the ultrasound bath was determined using calorimetric method. This method is based on the assumption that all acoustic energy delivered to the reaction medium is finally dissipated as heat. The procedure followed for determination of the acoustic pressure amplitude is described below:

The ultrasound bath was filled with 2L water. This was subjected to continuous sonication for 10 min. During this period, the temperature of the water in the bath increased by 2°C. This would mean that the actual rate of energy input to the system was:

$$\frac{mC_p\Delta T}{t} = \frac{2 \times 4180 \times 2}{600}\frac{\text{Joule}}{\text{s}} = 27.87 \text{ W}.$$

The acoustic intensity in the bath can be calculated using the actual area of ultrasound transmission. The sonication in the bath is generated by attaching two transducers of radius 1 in. (approx.). Thus:

$$I = \frac{\text{Actual power (W)}}{\text{Area of transducers (m}^2\text{)}} = \frac{27.87}{2\times\pi\times\left(2.54 \times 10^{-2}\right)^2} = 6875 \text{ W/m}^2.$$

The relation between acoustic intensity and acoustic pressure amplitude is given as:

$I = \frac{P_A^{\,2}}{2\rho c}$, where ρ is the density of the medium and c is the speed of sound in the

medium. With the substitution of ρ = 1000 kg/m^3 and c = 1481 m/s, acoustic pressure amplitude can be calculated as:

$$P_A = \sqrt{2I\rho c} = \sqrt{2 \times 6875 \times 1481 \times 1000} = 142701 \text{ Pa} = 1.427 \text{ bar} \approx 1.4 \text{ bar}.$$

APPENDIX FOR CHAPTER 2

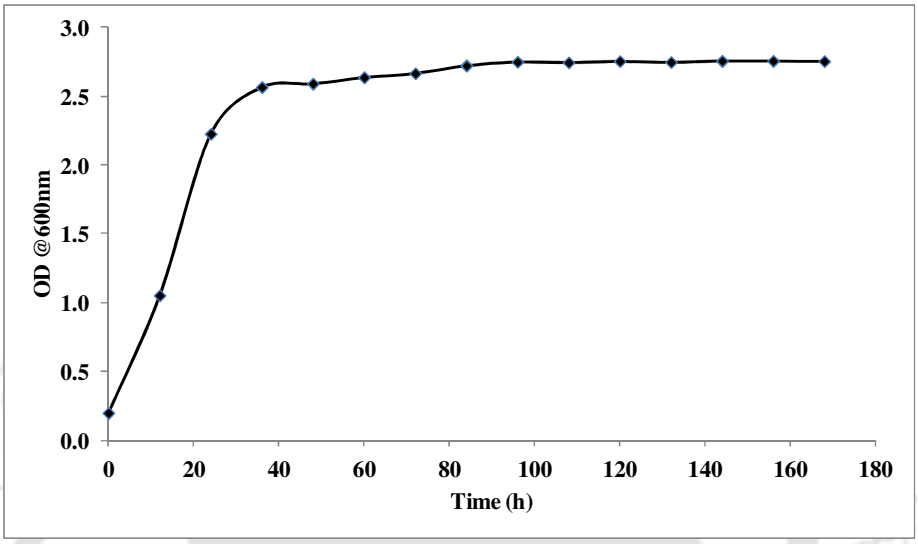

Figure A1. Growth curve of *Phaffia rhodozyma* showing stationary phase reached after 48 h.

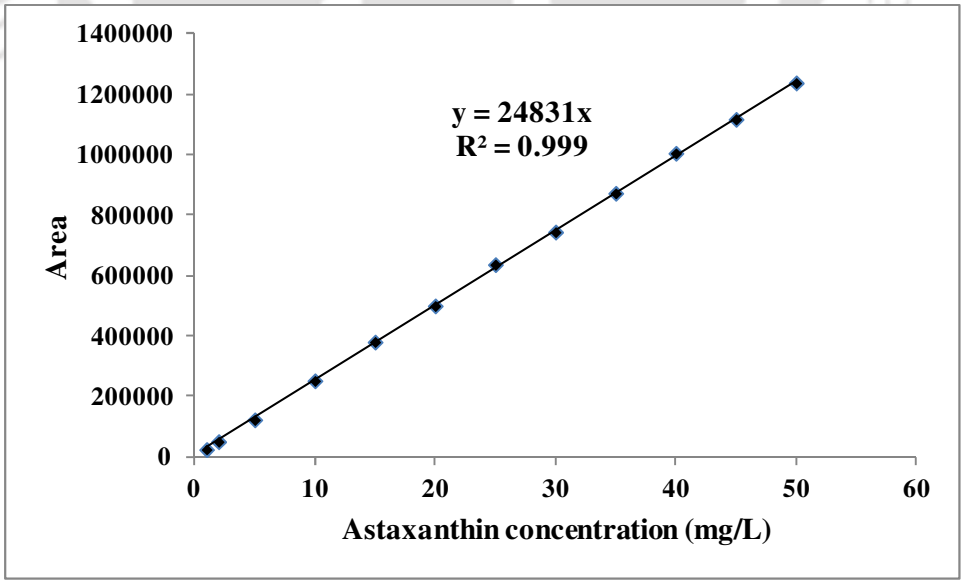

Figure A2. Standard calibration plot by HPLC analysis for astaxanthin

APPENDIX FOR CHAPTER 4

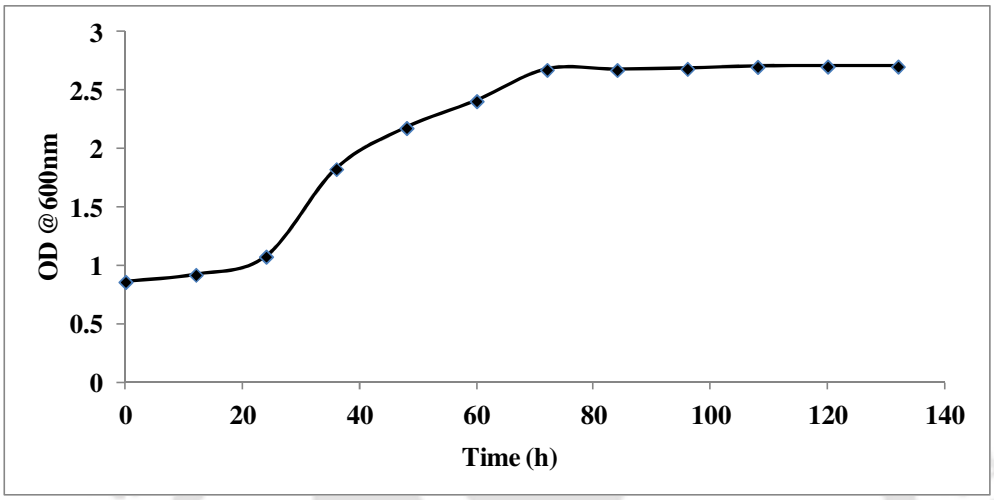

Figure A3. Growth curve of *Debaryomyces hansenii var. hansenii* showing start of log phase at 24 h

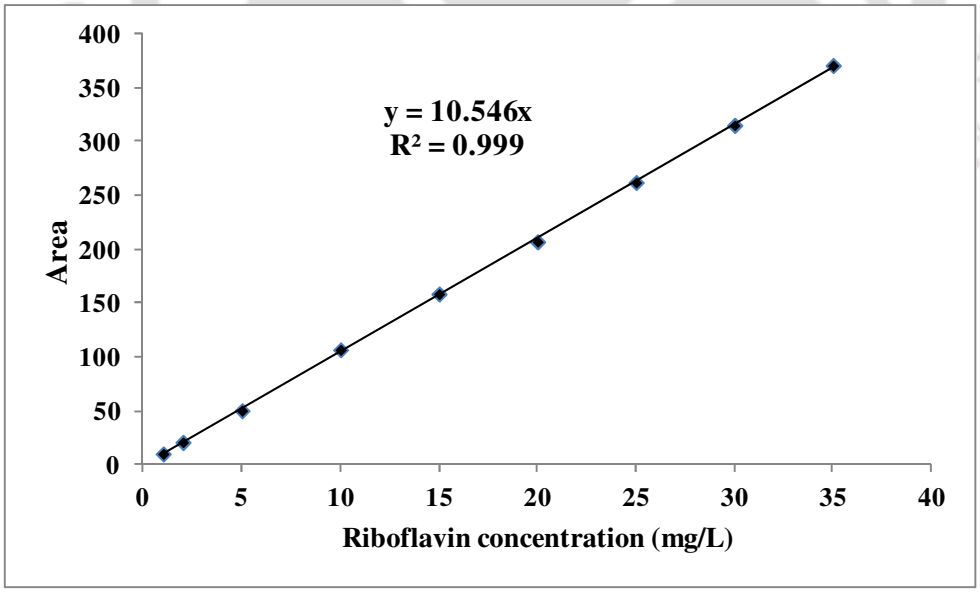

Figure A4. Standard calibration plots by HPLC analysis for riboflavin

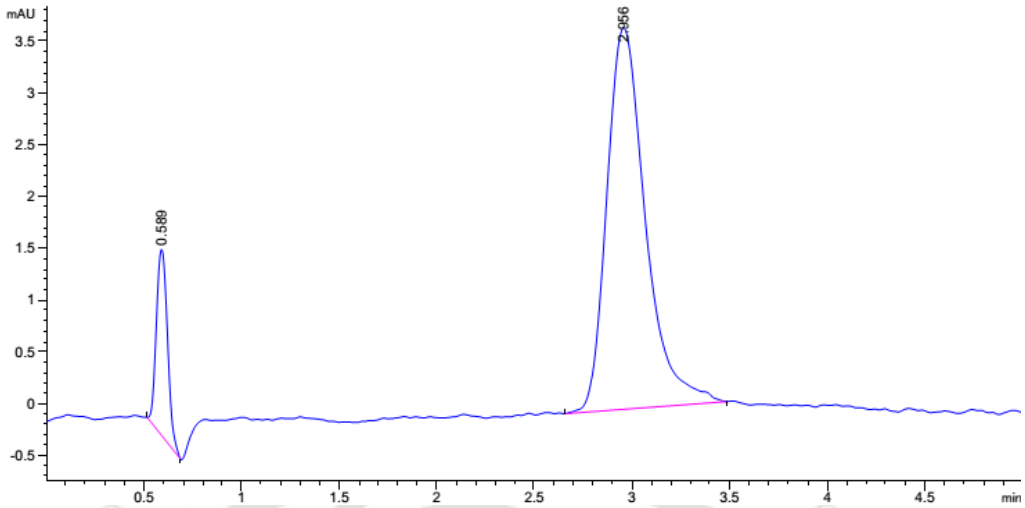

Figure A5. HPLC chromatogram showing riboflavin concentration for a sample at 72 h of fermentation

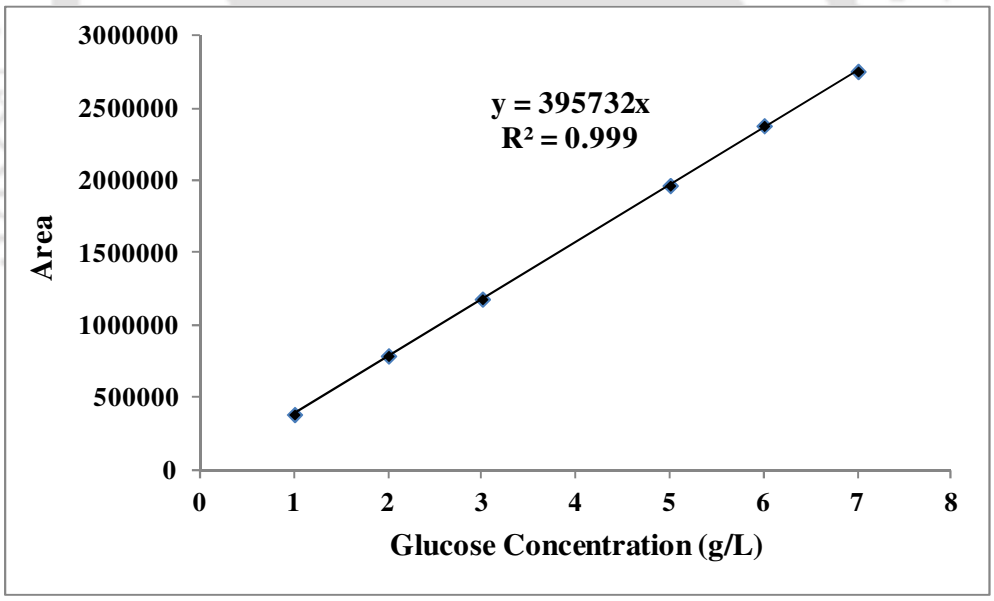

Figure A6. Standard calibration plots by HPLC analysis for glucose

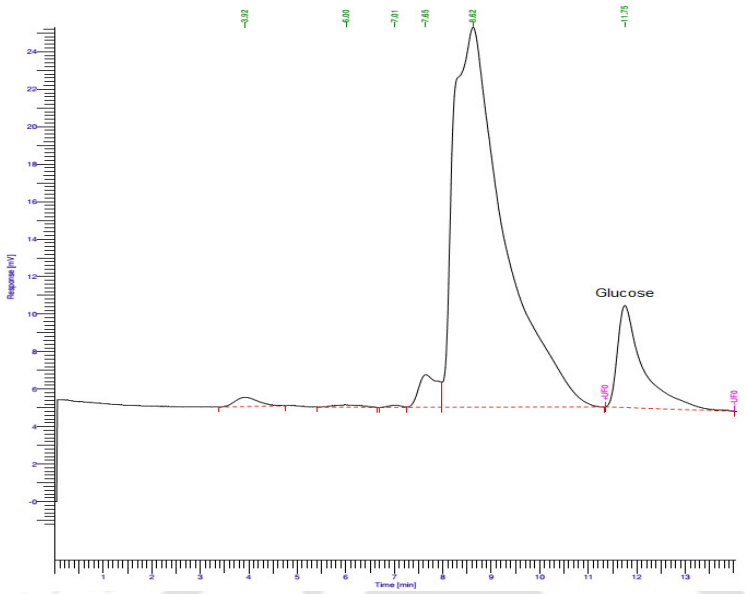

Figure A7. HPLC chromatogram showing glucose concentration for a sample at 72 h of fermentation

Table A1. Statistical analysis of results from Plackett–Burman experimental design for riboflavin synthesis

(A) Coefficient values, *t* and *p* values for each variable

Model term	Coefficient Estimate	Computed *t*-value	*p*-value
Intercept	3.142	15.92	0.000*
$(NH_4)_2SO_4$ (X_1)	1.275	6.46	0.001*
KH_2PO_4 (X_2)	0.057	0.29	0.094
$MgSO_4 \cdot 7H_2O$ (X_3)	0.942	4.77	0.005*
$CaCl_2 \cdot 2H_2O$ (X_4)	–0.407	–2.06	0.786
NaCl (X_5)	0.540	2.74	0.041*
Yeast Extract (X_6)	0.630	3.19	0.024*

*Significant *p* values, $p \leq 0.05$; $R^2 = 0.945$; Predicted $R^2 = 0.685$; Adjusted $R^2 = 0.879$

(B) ANOVA for the model

Term	SS	DF	MS	*F*- value	*p*-value
Constant	40.4334	6	6.7389	14.41	0.005
$(NH_4)_2SO_4$ (X_1)	19.5075	1	19.5075	41.73	0.001
KH_2PO_4 (X_2)	0.0385	1	0.0385	0.08	0.094
$MgSO_4 \cdot 7H_2O$ (X_3)	10.6408	1	10.6408	22.76	0.005
$CaCl_2 \cdot 2H_2O$ (X_4)	1.9845	1	1.9845	4.24	0.786
NaCl (X_5)	3.4992	1	3.4992	7.48	0.041
Yeast Extract (X_6)	4.7628	1	4.7628	10.19	0.024
Residual Error	0.9376	5	0.4675		
Total	41.371	11			

Table A2. Results of statistical (CCD) analysis of medium optimization for riboflavin synthesis

(A) Coefficient values, *t* and *p* values for each variable

Model term	Coefficient Estimate	Computed *t*-value	*p*-value
Intercept	7.709	317.418	0.000*
$(NH_4)_2SO_4$ (X_1)	0.581	48.456	0.000*
$MgSO_4{\cdot}7H_2O$ (X_3)	0.029	2.432	0.029*
NaCl (X_5)	–0.212	–17.725	0.000*
Yeast Extract (X_6)	0.269	22.444	0.000*
$(NH_4)_2SO_4$ (X_1) × $(NH_4)_2SO_4$ (X_1)	–0.536	–47.750	0.000*
$MgSO_4{\cdot}7H_2O$ (X_3) × $MgSO_4{\cdot}7H_2O$ (X_3)	–0.224	–20.016	0.000*
NaCl (X_5) × NaCl (X_5)	–0.121	–10.794	0.000*
Yeast Extract (X_6) × Yeast Extract (X_6)	–0.608	–54.196	0.000*
$(NH_4)_2SO_4$ (X_1) × $MgSO_4{\cdot}7H_2O$ (X_3)	0.140	9.537	0.000*
$(NH_4)_2SO_4$ (X_1) × NaCl (X_5)	0.583	39.679	0.000*
$(NH_4)_2SO_4$ (X_1) × Yeast Extract (X_6)	0.268	18.291	0.000*
$MgSO_4{\cdot}7H_2O$ (X_3) × NaCl (X_5)	0.113	7.718	0.000*
$MgSO_4{\cdot}7H_2O$ (X_3) × Yeast Extract (X_6)	–0.332	–22.590	0.000*
NaCl (X_5) × Yeast Extract (X_6)	–0.174	–11.885	0.000*

* Significant *p* values, $p \leq 0.05$; $R^2 = 0.998$; Predicted $R^2 = 0.994$; Adjusted $R^2 = 0.997$

(B) ANOVA results of statistical analysis for medium optimization

Source	SS	DF	MS	*F*- value	*p*-value
Regression	36.310	14	2.593	751.20	0.000
Linear	10.951	4	2.738	792.94	0.000
Square	15.999	4	3.999	1158.50	0.000
Interaction	9.360	6	1.560	451.85	0.000
Residual (error)	0.048	14	0.003		
Lack of fit	0.038	10	0.004	1.57	0.352
Pure Error	0.010	4	0.002		
Total	38.333	29			

(C) Analysis of contour plots

Parameter space for maximum riboflavin yield

Contour plot	Range of concentration (g/L)				
	$(NH_4)_2SO_4$ (X_1)	$MgSO_4{\cdot}7H_2O$ (X_3)	NaCl (X_5)	Yeast Extract (X_6)	Riboflavin yield (mg/L)
a. (X_3) vs (X_1)	3.32–5.18	0.26–0.48	0.35#	3.5#	8
b. (X_6) vs (X_1)	3.39–5.32	0.35#	0.35#	3.17–4.76	8
c. (X_5) vs (X_1)	3.36–5.44	0.35#	0.17–0.57	3.5#	8
d. (X_6) vs (X_3)	3.5#	0.28–0.41	0.35#	3.41–4.10	8
e. (X_5) vs (X_3)	3.5#	0.23–0.42	0.16–0.37	3.5#	8
f. (X_5) vs (X_6)	3.5#	0.35#	0.122–0.38	3.38–4.65	8

Optimum values of media components:

(1) $(NH_4)_2SO_4$ = 3.59 g/L; (2) $MgSO_4{\cdot}7H_2O$ = 0.25 g/L; (3) Yeast Extract = 4.32 g/L; (4) NaCl = 0.18 g/L

Maximum riboflavin concentration at optimized conditions: 8.21 mg/L (yield = 1.5 mg/g of cells)

Center point values of media components

Table A3. Results of statistical (CCD) analysis of fermentation parameter optimization for riboflavin synthesis

(A) Coefficient values, *t* and *p* values for each variable

Model term	Coefficient	Computed *t*-value	*p*-value
Intercept	8.74965	637.601	0.000*
Medium pH (X_1)	0.05542	8.178	0.000*
Temperature (X_2)	–0.16255	–23.985	0.000*
Inoculum size (X_3)	–0.03311	–4.886	0.000*
Shaking speed (X_4)	0.06207	9.158	0.000*
Medium pH (X_1) × Medium pH (X_1)	–0.11158	–17.601	0.000*
Temperature (X_2) × Temperature (X_2)	–0.22711	–35.825	0.000*
Inoculum size (X_3) × Inoculum size (X_3)	–0.22013	–34.724	0.000*
Shaking speed (X_4) × Shaking speed (X_4)	–0.11267	–17.772	0.000*
Medium pH (X_1) × Temperature (X_2)	0.08487	10.225	0.000*
Medium pH (X_1) × Inoculum size (X_3)	0.08127	9.791	0.000*
Medium pH (X_1) × Shaking speed (X_4)	0.17048	20.539	0.000*
Temperature (X_2) × Inoculum size (X_3)	–0.11985	–14.440	0.000*
Temperature (X_2) × Shaking speed (X_4)	0.02291	2.760	0.015*
Inoculum size (X_3) × Shaking speed (X_4)	0.02278	2.744	0.016*

*Significant *p* values, $p \leq 0.05$; R^2= 0.996; Predicted R^2= 0.985; Adjusted R^2= 0.993

(B) ANOVA results of statistical analysis for fermentation parameters optimization

Source	SS	DF	MS	*F*- value	*p*-value
Regression	4.32201	14	0.30871	280.06	0.000
Linear	0.82662	4	0.20665	187.47	0.000
Square	2.56293	4	0.64073	581.25	0.000
Interaction	0.93246	6	0.15541	140.98	0.000
Residual (error)	0.01543	14	0.00110		
Lack of fit	0.00789	10	0.00079	0.42	0.88
Pure Error	0.00754	4	0.00188		
Total	4.65074	29			

(C)Analysis of contour plots

Parameter space for maximum riboflavin yield

Contour plot	Range of concentration (g/L)				
	Medium pH (X_1)	Temperature (X_2)	Inoculum size (X_3)	Shaking speed (X_4)	Riboflavin yield (mg/L)
a. (X_2) vs (X_1)	3.48–6.73	22.05–26.68	6#	145#	8.5
b. (X_3) vs (X_1)	3.65–6.76	25#	3.68–8.23	145#	8.5
c. (X_4) vs (X_1)	5.54–6.77	25#	6#	158–186	8.8
d. (X_3) vs (X_2)	5#	22.00–26.62	3.72–8.38	145#	8.5
e. (X_4) vs (X_2)	5#	22.10–26.53	6#	112–191	8.5
f. (X_3) vs (X_4)	5#	25#	4.80–6.76	134–170	8.7

Optimum values of media components:

(1) medium pH = 6.1; (2) temperature = 25°C; (3) inoculum size = 6.4 % v/v; (4) shaking speed = 172 rpm

Maximum riboflavin concentartion at optimum conditions: 8.83 mg/L (yield = 1.7 mg/g of cells)